

# **Heel Build-up During Thermal Desorption of VOCs in Presence of Oxygen**

by

Mohammad Feizbakhshan

A thesis submitted in partial fulfillment of the requirements for the degree of

Doctor of Philosophy

in

Environmental Engineering

Department of Civil and Environmental Engineering

University of Alberta

© Mohammad Feizbakhshan, 2020

## ABSTRACT

Oxygen presence during thermal desorption of volatile organic compounds (VOCs) from adsorbent can promote heel build-up and loss of adsorption capacity, which reduces the performance of adsorbent in a cyclic adsorption/desorption process. The heel build-up, in some cases, could be attributed to the chemical reactions between VOCs and the purge gas oxygen impurities that shortens adsorbent's life span, and leads to a more frequent adsorbent replacement, repeated reactivations, and disposal, and imposes high operation and maintenance cost on the industries. Therefore, this research aims to understand the effect of desorption conditions and adsorbent physical properties and material on oxygen-induced reactions and corresponding heel build-up. Several commercially available adsorbents (activated carbon, zeolite, and polymer) were tested and different characterization methods were used to identify the possible mechanisms for heel build-up. Knowing the nature of the oxygen-induced reactions is important as it could help in 1) finding optimal operational parameters, 2) selecting proper material, 3) minimizing heel build-up in the presence of oxygen, 4) investigating potential regeneration methods of spent adsorbents, 5) increasing adsorbent's lifetime, and 6) savings in capital and operational costs associated with adsorbent replacement.

The combined effects of desorption temperature and oxygen impurity on heel build-up in cyclic adsorption/desorption of 1,2,4-trimethylbenzene (TMB) on beaded activated carbon (BAC) was studied (Chapter 2). Three impurity levels of oxygen in the purge gas ( $\leq 5$  ppm, 10,000 ppm, 21% O<sub>2</sub> in N<sub>2</sub>) at two desorption temperatures (200°C and 288°C) were investigated and a new method was proposed to identify heel nature using thermogravimetric analysis. The effect of adsorbent's physical properties (pore size distribution and surface area) on heel build-up was studied using

three commercial activated carbons (Chapter 3). Micropore surface analysis, XPS, Boehm titration, and differential thermogravimetric (DTG) analysis were used to assess differences in the physical and chemical properties of these adsorbents. To understand the effect of adsorbent material on heel build-up, activated carbon, zeolite, and polymer adsorbents were tested under similar conditions and in the presence of oxygen (Chapter 4). It was observed that desorption temperature and oxygen concentration thresholds for heel build-up depended on the adsorbent material. Finally, the mechanism of heel build-up was investigated using three activated carbons (ACs) and one zeolite adsorbent at a severe condition of high oxygen concentration and at temperatures of 150, 200, and 250 °C to analyze and characterize the products of oxygen-induced reactions. In addition to the previously used characterization methods, gas chromatography-mass spectrometry was used to understand the mechanism of heel build-up.

In summary, it was found that 1) combination of desorption temperature and purge gas oxygen increases heel build-up, 2) polymers have limited use in thermal desorption at high concentration of oxygen due to oxidizing reactions, 3) the highly microporous structure of activated carbon promotes heel build-up, while a hierarchy of pores eases the desorption with less heel, 4) confined pore opening of zeolite restrict reactions between VOCs and oxygen in the porous network and therefore, molecular sieve adsorbents are advantageous in the cyclic process of VOC adsorption when high oxygen impurity exists.

## PREFACE

The research completed in this thesis is an original work by myself, Mohammad Feizbakhshan. All or parts of Chapters 2 to 5 have been submitted or ready for submission for peer review and publication. I was responsible for planning, designing, and conducting laboratory experiments, analyzing and interpreting the results, and writing and editing these papers that were fully reviewed and supervised by Dr. Zaher Hashisho in the Department of Civil and Environmental Engineering at the University of Alberta. My co-authors from the Air Quality Characterization Lab in the Department of Civil and Environmental Engineering at the University of Alberta, and collaborators from our industrial sponsor, Ford Motor Company, were responsible for conducting part of laboratory tests, reviewing the manuscript drafts, and providing useful comments and discussions.

Chapter 2 has been submitted (under review) as M. Feizbakhshan, B. Amdebrhan, Z. Hashisho, J. H. Phillips, D. Crompton, J. E. Anderson, M. Nichols (2020). Effects of oxygen impurity and desorption temperature on heel build-up in activated carbon. *Journal of Hazardous Material*.

Chapters 3 to 5 are ready for submission for peer review and publication.

## **DEDICATIONS**

Dedicated to my beloved parents, Soraya and Mohammadreza

&

My lovely wife, Sara

## ACKNOWLEDGMENTS

While the title page of this thesis contains my name alone, the research found herein would not have been possible without the guidance, wisdom, and support of many.

My supervisor, Prof. Zaher Hashisho, introduced me to air pollution control and showed me what it means to be a serious scholar. I would not be where I am today without his patience, training, and encouragement.

Over my graduate career, I benefitted from financial support from Ford Motor Company and the Natural Sciences and Engineering Research Council (NSERC) of Canada, Air & Waste Management Association (Air Quality Study and Research Scholarship) as well as Westmoreland Coal Company (Graduate Scholarship in Environmental Engineering).

My Parents, Mohammadreza and Soraya, have always supported me in everything that I have ever done. Thank you for always pushing me to do more and do better.

My wife, Sara has always been my strongest supporter and confidant. Her encouragement (and patience!) allowed me to do the sort of embedded research that I love doing. This thesis is as much yours as it is mine. I love you.

I appreciate my colleagues for their valuable help and contributions: Biniyam Amdebrhan, Weimin Chen, Saeed Niknaddaf, Seyed Mojtaba Hashemi, Arman Peyravi, and Guangxin Zhang.

I also acknowledge my defense committee members, Dr. Rajender Gupta, Dr. Lexuan Zhong, Dr. Charles Jia, Dr. Bipro Dhar, and Dr. Leila Hashemian for their contributions to this work.

# TABLE OF CONTENTS

<b>ABSTRACT.....</b>	<b>II</b>
<b>PREFACE.....</b>	<b>IV</b>
<b>DEDICATIONS .....</b>	<b>V</b>
<b>ACKNOWLEDGMENTS .....</b>	<b>VI</b>
<b>TABLE OF CONTENTS .....</b>	<b>VII</b>
<b>LIST OF TABLES .....</b>	<b>XI</b>
<b>LIST OF FIGURES .....</b>	<b>XII</b>
<b>GLOSSARY OF ACRONYMS .....</b>	<b>XVI</b>
<b>CHAPTER 1: INTRODUCTION AND RESEARCH OBJECTIVE.....</b>	<b>1</b>
1.1 GENERAL OVERVIEW OF VOCs AND THE ABATEMENT TECHNIQUES.....	1
1.2 ADSORPTION .....	3
1.3 DESORPTION .....	4
1.4 HEEL BUILD-UP .....	5
1.5 RESEARCH MOTIVATION .....	10
1.6 RESEARCH OBJECTIVES.....	10
1.7 ORGANIZATION OF THESIS .....	11
1.8 REFERENCES .....	14
<b>CHAPTER 2: EFFECTS OF OXYGEN IMPURITY AND TEMPERATURE ON HEEL BUILD-UP .....</b>	<b>19</b>

2.1 CHAPTER OVERVIEW .....	19
2.2 INTRODUCTION.....	19
2.3 MATERIALS AND METHODS .....	22
2.3.1 Adsorbent and Adsorbate .....	22
2.3.2 Experimental Setup & Methodology .....	22
2.3.3 Adsorbent Characterization Methods.....	25
2.4 RESULTS & DISCUSSION.....	26
2.4.1 Desorption Profiles and Duration .....	26
2.4.2 Heel Build-up and Adsorption Capacity Reduction.....	27
2.4.3 Characterization of adsorbents after the 5-cycle tests .....	31
2.5 CONCLUSIONS .....	39
2.6 REFERENCES .....	41
<b>CHAPTER 3: EFFECTS OF AC PORE SIZE DISTRIBUTION ON OXYGEN INDUCED HEEL BUILD-UP .....</b>	<b>46</b>
3.1 CHAPTER OVERVIEW .....	46
3.2 INTRODUCTION.....	46
3.3 EXPERIMENTAL .....	49
3.3.1 Adsorbent and Adsorbate .....	49
3.3.2 Experimental Setup and Methodology.....	50
3.3.3 Characterization techniques .....	54
3.4 RESULTS & DISCUSSION.....	55
3.4.1 Adsorption capacity and heel build-up.....	55



3.4.2 Reversible and irreversible heel formation .....	59
3.4.3 Surface area and pore size analysis.....	62
3.4.4 X-ray photoelectron spectroscopy (XPS) .....	66
3.4.5 Boehm Titration.....	66
3.5 CONCLUSIONS .....	70
3.6 REFERENCES .....	72
<b>CHAPTER 4: EFFECTS OF ADSORBENTS MATERIAL ON OXYGEN INDUCED HEEL BUILD-UP; COMPARISON OF ACTIVATED CARBON, ZEOLITE, AND POLYMER ADSORBENTS.....</b>	<b>76</b>
4.1 CHAPTER OVERVIEW .....	76
4.2 INTRODUCTION.....	76
4.3 EXPERIMENTAL .....	79
4.3.1 Adsorbent and Adsorbate .....	79
4.3.2 Experimental setup and Methodology .....	79
4.3.3 Characterization techniques .....	82
4.4 RESULTS & DISCUSSION.....	83
4.4.1 Adsorption/Desorption at 200 °C .....	83
4.4.2 Adsorption/Desorption at 288 °C .....	90
4.4.3 Surface analysis results.....	94
4.4.4 Thermogravimetric analysis results .....	97
4.5 CONCLUSIONS .....	98
4.6 REFERENCES .....	100

## **CHAPTER 5: MECHANISM OF VOC'S HEEL BUILD-UP THROUGH OXYGEN**

<b>INDUCED REACTIONS .....</b>	<b>104</b>
5.1 CHAPTER OVERVIEW .....	104
5.2 INTRODUCTION.....	104
5.3 MATERIALS AND METHODS .....	106
5.3.1 Adsorbate and Adsorbents .....	106
5.3.2 Experimental setup and Methods .....	108
5.3.3 Characterization Methods.....	109
5.4 RESULTS & DISCUSSION.....	111
5.5 CONCLUSIONS .....	125
5.6 REFERENCES .....	126
<b>CHAPTER 6: CONCLUSIONS AND RECOMMENDATIONS.....</b>	<b>131</b>
6.1 DISSERTATION OVERVIEW .....	131
6.2 CONCLUSIONS .....	131
6.3 RECOMMENDATIONS .....	134
<b>BIBLIOGRAPHY .....</b>	<b>136</b>
<b>APPENDIX A: SUPPLEMENTARY INFORMATION.....</b>	<b>147</b>

## LIST OF TABLES

Table 1-1 Classification of volatile organic compounds (from WHO [2]).....	1
Table 2-1. Comparison of the changes in the physical properties of the samples to the adsorption capacity reduction and heel build-up. Values are reported as mean $\pm$ standard deviation of at least two runs. ....	36
Table 3-1. The surface chemical composition (atomic %) of virgin activated carbons obtained from XPS analysis .....	49
Table 3-2. BET surface area, micropore volume, total pore volume, and surface chemical composition of virgin activated carbons obtained by N <sub>2</sub> adsorption at -195.8 °C.....	49
Table 3-3. Adsorption capacity and heel build-up of activated carbons (Wt%).....	58
Table 3-4. Removable heel percentage (%) by heating to 850 °C.....	60
Table 3-5. BET surface area, micropore volume, meso-macropore volume, and the total pore volume of the tested activated carbons .....	65
Table 3-6. The surface atomic composition of virgin and regenerated activated carbons .....	66
Table 3-7. Boehm titration analysis based on the molecular weight of the lightest possible molecules .....	68
Table 3-8. Wt% of the total added SOFGs, cumulative heel (H <sub>T</sub> ), and removable heel (H <sub>R-850</sub> ). .....	69
Table 5-1. Physical and chemical properties of the selected adsorbents .....	107
Table 5-2 BET surface area, micropore volume, meso-macropore volume, and the total pore volume of the tested adsorbent .....	116
Table 5-3. Properties of organic compounds identified using GC-MS analysis.....	123

## LIST OF FIGURES

Figure 2-1. Schematic diagram of the adsorption-desorption setup. ....	25
Figure 2-2. Desorption profile of TMB-loaded G-70R at 200°C and 288°C .....	27
Figure 2-3. Adsorption capacity ( $q_i$ ) and heel build-up ( $H_i$ ) per cycle for G-70R samples desorbed at 200°C and 288°C: (a/b) desorbed in $\leq 5$ ppm $O_2$ in $N_2$ , (c/d) desorbed in 10,000 ppm $O_2$ in $N_2$ , (e/f) desorbed in 21% $O_2$ in $N_2$ . Error bars indicate the standard deviation of the arithmetic mean of two sets of data. ....	29
Figure 2-4. TGA analysis of 5-cycle G-70R samples desorbed at 200°C and 288°C using $N_2$ purge gas containing (a/b) $\leq 5$ ppm $O_2$ , (c/d) 10,000 ppm $O_2$ , (e/f) 21% $O_2$ .....	32
Figure 2-5. Percentage of the absolute cumulative heel ( $H_T = Heel_{<430} + Heel_{430-850} + Heel_{>850}$ ) obtained from DTG analysis.....	35
Figure 2-6. Pore size distribution (PSD) of G-70R after the 5-cycle adsorption/desorption of TMB using oxygen impurity of (a) $\leq 5$ ppm, (b) 10.000 ppm, (c) 21% (Air).....	38
Figure 3-1. The pore size distribution of virgin activated carbons .....	50
Figure 3-2. Schematic diagram of the adsorption-desorption setup .....	52
Figure 3-3. Breakthrough curves of TMB on ACFC-20, G-70R, and B-100777. N and A after the adsorbent name refers to ultra-pure nitrogen ( $\leq 5$ ppm <sub>v</sub> $O_2$ ) and air ( $\sim 21\%$ $O_2$ ) as desorption gas, respectively .....	56
Figure 3-4. Temperature and desorption profile of TMB-loaded G-70R, B-100777, ACFC-20 for the 1 <sup>st</sup> cycle using $N_2$ .....	59
Figure 3-5. TGA of virgin and tested activated carbons.....	61

## List of Figures

Figure 3-6. DTG of virgin and tested activated carbons.....	62
Figure 3-7. The pore size distribution of virgin and regenerated activated carbons.....	64
Figure 3-8. Boehm titration results for virgin and tested samples .....	67
Figure 3-9. The lightest molecules representing SOFGs on the ACs' surface from TMB and O <sub>2</sub> reactions .....	68
Figure 4-1, Schematic diagram of the adsorption-desorption setup .....	81
Figure 4-2. Adsorption breakthrough curves for TMB on G-70R samples desorbed at 200°C with different oxygen content in the purge gas.....	84
Figure 4-3. Adsorption breakthrough curves for TMB on V503 samples desorbed at 200°C with different oxygen content in the purge gas.....	85
Figure 4-4. Adsorption breakthrough curves for TMB on HSZ-385 samples desorbed at 200°C with different oxygen content in the purge gas.....	86
Figure 4-5. Adsorption capacity and heel build-up for activated carbon G-70R desorbed at 200 °C. Error bars indicate the standard deviation of the arithmetic mean of two sets of data...	88
Figure 4-6. Adsorption capacity and heel build-up for polymer adsorbent Dowex V503 desorbed at 200 °C. Error bars indicate the standard deviation of the arithmetic mean of two sets of data.....	89
Figure 4-7. Adsorption capacity and heel build-up for zeolite HSZ-385 samples desorbed at 200 °C. Error bars indicate the standard deviation of the arithmetic mean of two sets of data...	90
Figure 4-8. Adsorption breakthrough curves for TMB on G-70R samples desorbed at 288°C with different oxygen impurities.....	91

## List of Figures

Figure 4-9. Adsorption breakthrough curves for TMB on HSZ-385 samples desorbed at 288°C with different oxygen impurities.....	92
Figure 4-10. Adsorption capacity and heel build-up for G-70R desorbed at 200 °C (error bars obtained from duplicated results).....	93
Figure 4-11. Adsorption capacity and heel build-up of 5-cycle on HSZ-385 samples desorbed at 288 °C (error bars obtained from duplicated results) .....	94
Figure 4-12. N <sub>2</sub> adsorption isotherm on virgin and regenerated G-70R.....	95
Figure 4-13. N <sub>2</sub> adsorption isotherm on virgin, regenerated, and control samples of Dowex V503 .....	96
Figure 4-14. N <sub>2</sub> adsorption isotherm on virgin and regenerated HSZ-385.....	97
Figure 4-15. DTG analysis of samples desorbed by air at 200 °C and 288 °C compared to virgin ones: a) activated carbon G-70R, b) zeolite HSZ-385.....	98
Figure 5-1. Schematic of the experimental setup.....	109
Figure 5-2. Adsorption breakthrough curves at 150, 200, and 250°C, based on FID measurements .....	112
Figure 5-3. Breakthrough time (min) and the weight gain percentage ( $\Delta W\%$ ) of adsorbents in different test temperatures .....	114
Figure 5-4. Pore size distribution (PSD) of the of adsorbents tested at the adsorption temperatures of 150, 200, and 250 °C .....	115
Figure 5-5. Weight losses calculated from TGA results.....	117
Figure 5-6. DTG results of adsorbents tested .....	119

## List of Figures

Figure 5-7. Chromatogram of the effluent condensate for the samples tested at 150, 200, and 250 °C .....	122
Figure A-1. Adsorption breakthrough curves for TMB on G-70R samples desorbed at 200/288°C with different oxygen impurities.....	148
Figure A-2. Chromatogram of 98% purity TMB (Y-axis is truncated to zoom the spectra).....	149

## GLOSSARY OF ACRONYMS

AC	Activated Carbon
ACFC	Activated Carbon Fiber Cloth
BAC	Beaded Activated Carbon
BET	Brunauer-Emmett-Teller
DAC	Data Acquisition and Control
DFT	Density Functional Theory
DO	Dissolved Oxygen
DTG	Derivative Thermo-Gravimetric
EPA	Environmental Protection Agency
GAC	Granular Activated Carbon
GC-MS	Gas Chromatography-Mass Spectrometry
MFC	Mass Flow Controller
MS	Mass Spectrometry
PSA	Pressure Swing Adsorption
PSD	Pore Size Distribution
QSDFT	Quenched Solid Density Functional Theory
SCCM	Standard Cubic Centimeter per Minute
SFG	Surface Functional Group
SOFG	Surface Oxygen Functional Group
TGA	Thermo-Gravimetric Analysis
TMB	1,2,4-trimethylbenzene
TSA	Temperature Swing Adsorption
VOC	Volatile Organic Compounds
VSA	Vacuum Swing Adsorption
XPS	X-ray Photoelectron Spectroscopy



# CHAPTER 1: INTRODUCTION AND RESEARCH OBJECTIVE

## 1.1 General Overview of VOCs and the Abatement Techniques

Volatile organic compounds (VOCs) are defined as “organic chemical compounds whose composition makes it possible for them to evaporate under normal indoor atmospheric conditions of temperature and pressure” by the US Environmental Protection Agency (EPA) [1]. In more detail, VOCs are a large family of carbon-based chemicals that the World Health Organization (WHO) categorizes them, based on their initial boiling points, into three groups of very volatile organic compounds (VOCs), volatile organic compounds (VOCs), and semi-volatile inorganic compounds (SVOCs) (Table 1-1).

Table 1-1 Classification of volatile organic compounds (from WHO [2])

VOCs Category	Boiling Point Range (°C)	Example Compounds
VVOC	<0 to 50-100	Propane, butane, methyl chloride
VOC	50-100 to 240-260	Formaldehyde, d-Limonene, toluene, acetone, ethanol (ethyl alcohol) 2-propanol (isopropyl alcohol), hexanal
SVOC	240-260 to 380-400	Pesticides (DDT, chlordane, plasticizers (phthalates), fire retardants (PCBs, PBB))

VOCs negatively impact human health and the environment by their toxicity, carcinogenicity, and their ability to create photochemical smog [3]. VOCs are emitted from various industries including fuel storage, transportation, and consumption, organic chemical manufacturing, agricultural

activities, and solvent uses [4-7]. VOCs contribute to the formation of ground-level ozone, and fine particulate matter that could lead to adverse health impacts such as respiratory and cardiac symptoms. Therefore, in 2009, Canada established VOCs concentration limits in automotive refinishing products like paint solvents and coating [8].

VOCs emission control techniques can be generally categorized into destruction and recovery methods based on whether the VOCs can be recovered. In the destruction methods, VOCs are mainly converted to H<sub>2</sub>O and CO<sub>2</sub> by using techniques such as incineration [9], photocatalytic oxidation [10, 11], and ozone catalytic oxidation [12], which inevitably may produce some toxic by-products and usually require a vast amount of energy. The recovery methods including adsorption [13], condensation [9], absorption [14], and membrane separation [15] could be more economic particularly in applications where VOCs are a necessary and an expensive component of operation such as painting and coating. Amongst these techniques, adsorption is widely used in removing VOCs from air and water streams because of its high removal efficiency and low energy and maintenance cost [16-20]. Speaking of adsorbents, activated carbon (AC) is the most common industrially used adsorbent due to its low cost and high adsorption efficiency. Activated carbon has a porous carbonaceous skeleton with a large network of pores with various size ranges that provide a large adsorption capacity for contaminants [5, 19]. However, there are other considerations such as desorption efficiency, bed fires, and adsorption affinity or adsorption isotherm that one may select other adsorbents over AC such as zeolite or polymer [21].

## 1.2 Adsorption

Adsorption takes place when an adsorbent is in contact with the surrounding media of a compound (an adsorbate) and occurs as a result of interaction between the field of forces of the solid surface and fluid phase [22]. Physical adsorption (also known as physisorption) occurs through relatively weak intermolecular attractive forces such as van der Waals, while chemical adsorption (also known as chemisorption) involves the formation of a chemical bond between the adsorbate and the surface of the adsorbent [18].

The adsorption capacity of a certain adsorbent after a sufficiently long time is known as “adsorption equilibrium” and is a function of temperature and the concentration of adsorbate [23]. In fact, at a given temperature, the relation between the amount adsorbed and concentration of the adsorbate is called “adsorption isotherm”. The adsorption isotherm is a function of adsorbate concentration and the amount of available adsorption area that molecules of the adsorbate can reach, hence adsorption isotherm depends on temperature and is different for each type of adsorbent and adsorbate [24]. Most commercial adsorbents are porous particles with a large surface area. The external pores of adsorbents allow mass transfer to the interior pores, where most of the adsorption takes place.

Having a large internal surface area, activated carbon, zeolite, and polymer adsorbents have each been used to control VOCs emissions. Activated carbon is vastly used to adsorb VOCs owing to its low cost and high removal efficiency [25-27]. The use of zeolites and polymers have more recently emerged in control of VOC's emission [28, 29]. Activated carbons are characterized with wide range of pore sizes from larger pores (macropores > 50 nm) leading to smaller pores (50 nm

> mesopores > 2 nm), which lead to even smaller pores (micropores > 2nm) [30]. Polymers have a range of pore sizes as well, but usually less narrow micropores compared to activated carbons [21]. However, zeolites with regular crystalline structures have pores of uniform size [31].

### 1.3 Desorption

To reuse adsorbents, desorption is needed. Desorption is a reverse process of adsorption used to remove the accumulated substances and to restore the adsorption capacity. Desorption process can be done by different techniques including thermal treatment [26], pressure variation [32], chemical extraction [33], and bio-regeneration [34]. Selecting the desorption method depends on various parameters including the properties of adsorbents and adsorbates but commonly, thermal desorption is the most economical compared to the other methods especially when VOCs have lower vapor pressures [23, 35].

Thermal desorption involves heat transfer to the adsorption media and diffusion of desorbed VOCs to the mobile phase [24]. Desorption rate depends on temperature and concentration of adsorbates. Logically, temperature should exceed the boiling point of adsorbed VOCs to completely desorb them at atmospheric pressure. Elevated temperatures facilitate desorption but must not be too high that damages the adsorbent. Accordingly, thermal desorption is widely used for activated carbon and zeolite adsorbents [14], however, for polymers that have low-temperature tolerance, pressure swing adsorption (PSA) is the most often used technology. Yet TSA can be a favorable method for polymers regeneration due to its simplicity and high removal efficiency but it must be assured that the desorption temperature does not lead to bed fires [21] or denature of the polymer.

The success of the desorption process can be measured by the “removal efficiency” (RE) that is the ratio of the desorbed amount to the adsorbed amount of VOCs in each cycle. Monitoring RE in a cyclic process is related to the adsorption capacity of adsorbent over time. In physical adsorption and under suitable conditions, an ideal desorption (regeneration) process should be able to remove VOCs from the adsorbent pores with no impact on the physical or chemical properties of the adsorbent, or the chemical composition of the adsorbate. In this case, the adsorption is “reversible”. On the other hand, “irreversible” adsorption is attributed to chemical bonds of strongly or permanently adsorbed species [5, 36-39]. Gradual deterioration of adsorbent usually occurs in a repeated adsorption/desorption process due to incomplete desorption, unwanted reactions or impurities, and structural changes of adsorbent [19, 37]. This irreversibility can constantly decrease the adsorption capacity of the adsorbent and contribute to heel build-up that eventually results in adsorbents with a low working capacity [5, 38]. Heel build-up may also occur through the gradual accumulation of non-desorbed VOCs or other impurities due to improper desorption conditions (i.e. insufficient temperature).

#### **1.4 Heel build-up**

To better control and prevent heel build-up, quantitative and qualitative studies are required to identify the nature and mechanism of the heel. Effective parameters in heel build-up can be classified into three categories [40]:

- Adsorbent properties (e.g. surface functional group, and pore size distribution)
- Adsorbate properties (e.g. molecular dimensions, chemical reactivity, thermal stability)
- Adsorption/desorption conditions (e.g. temperature, purge gas impurity)

Chemical reactions of adsorbates 1) with each other, 2) with purge gas impurities, or 3) with the adsorbent can contribute to heel build-up (chemisorption). Products of these reactions can be larger molecules trapped in the micropores or chemisorbed onto the adsorbent surface, or sometimes a deposited carbon on the adsorbent surface resulting from the decomposition of adsorbates. To identify the nature of the heel build-up, one should understand the mechanism of adsorption. Several studies have focused on the reasons for heel formation [41-47]. Suzuki et al. [44], Urano et al. [43], and Liu et al. [46] in three different studies tried to classify adsorbates based on their responses during thermal desorption. The classifications can be unified as below:

- Vaporization type: volatile adsorbates that can be removed in a single step by simple physical desorption.
- Decomposition type: desorption in three steps: 1-initial physical desorption, 2-thermal cracking, and 3- desorption of decomposition products (Adsorption energy and thermal stability of the compound determine whether if it is desorbed in its original form or not).
- Carbonization type: adsorbates are decomposed but form a charred residue on the adsorbent. The accumulation of this charred residue causes adsorbent activity loss.

In the common practice, following adsorption, recycling of saturated adsorbent is required to recover the adsorbent's capacity to be economically and environmentally acceptable for cyclic use [19]. According to the above-mentioned classification, adsorbates can be removed in different ways depending on their response during thermal desorption. The vaporization type adsorbates can be removed in a single step through shifting the adsorption equilibrium by applying heat, vacuum, or using other pathways such as solvent extraction; however, thermal desorption is the most

commonly used technique [18, 19]. On the other hand, removal of the decomposition type adsorbates requires more effort or higher energy to break down the chemically formed bonds. Not all of the decomposed adsorbates can leave the pores, and some may form a charred residue on the surface (carbonization type) which leads to adsorbent activity loss. To recover the lost adsorption capacity due to carbonization, a very high temperature along with a proper oxidizing agent (e.g. CO<sub>2</sub>, H<sub>2</sub>O) is required to remove the charred residue and to develop new pores.

Desorption conditions (e.g., temperature, heating rate, purge gas impurity) impact heel build-up in different ways. A temperature greater than the adsorbate's boiling point is required to completely desorb the adsorbed species at atmospheric pressure. Previous studies showed that increasing desorption temperature reduces the process time and improves desorption efficiency by facilitating mass transfer and diffusion particularly for heavy adsorbates adsorbed in narrow pores of the adsorbent [47-49]. Even though increasing temperature improves desorption rate, if there is any chemical reaction occurring between adsorbed species and purge gas or adsorbent, increasing the temperature may promote this reaction and result in a greater heel build-up before adsorbates escape adsorbent's pores [45].

During thermal desorption, inert gas (usually N<sub>2</sub>) is used to purge adsorbent beds to avoid bed fires and any unfavorable reactions [50]. However, impurities in the purge gas (mostly oxygen) can react with the adsorbate species or the adsorbent surface. These reactions are unfavorable and may result in heel build-up. However, purifying nitrogen impacts operational costs of N<sub>2</sub> generation and consequently the operational cost of adsorption/desorption process. Limited studies reported the impact of oxygen content in the purge gas on heel build-up during desorption [51, 52] and they

attributed this heel formation to a chemical reaction between oxygen and VOCs (mostly aromatics compound). In the liquid phase and during adsorption, several studies reported irreversible adsorption of VOCs in the presence of dissolved oxygen [41, 42, 53, 54]. Various methods, such as oxygen uptake measurement and GC analysis of adsorbent extracts, have been employed to indirectly prove the reaction of phenolic compounds with oxygen. Musso [55] discussed that oxidative coupling occurs through reactions between phenolate radicals. These radicals are formed from phenol by the loss of a hydrogen ion and an electron in reaction with an oxygen molecule in the aqueous phase. Because of the high activation energy of the radical formation, an elevated temperature (180-210 °C) and pressure (35 atm) are required. Although Zogorski et al. [56] reported that adsorption of 2,4-dichlorophenol on activated carbon is reversible and can be desorbed by distilled water, Yonge [14] et al. found that only a small portion of phenolic compounds ( $\leq 15\%$ ) adsorbed from aqueous solution could be desorbed by water. Similarly, Suzuki et al. [44] found that phenol and phenolic derivatives were poorly desorbed from activated carbon by thermal desorption. Grant and King [57] explained this conflict by introducing oxidative reactions to activated carbon surfaces. These reactions produce polymeric products that are adsorbed so strongly on the carbon that they are “irreversibly adsorbed”. They named four effective parameters to promote oxidative coupling reactions: (a) longer contact times, (b) higher pH values, (c) higher temperatures, (d) the presence of dissolved oxygen, and (e) the nature of the phenolic compound. Also, the presence of a metallic catalyst as well as activated carbon surface acting as a catalyst was found to promote the oxidative coupling reactions at room temperature. By studying the mechanism of irreversible adsorption of phenolic compounds on activated carbon, Grant et al. reported that carbon catalyzes oxidation reactions [57].



Vidic and Suidan [42] have shown that the presence of oxygen (oxic conditions) in the aqueous phase can increase the adsorption capacity of granular activated carbon for phenolic compounds up to three times compared to anoxic conditions. They tested adsorption of o-cresol, phenol, o-chlorophenol, m-ethylphenol, and natural organic matter during a two-week contacting period. The adsorption capacity enhancement was attributed to the polymerization of adsorbates due to the presence of oxygen. They also reported that reaction products (formed polymers) are extremely difficult to desorb in any significant quantity. Later studies examined the kinetics of oxidative coupling in the aqueous phase and showed that this reaction is catalyzed by activated carbon and the presence of oxygen-containing basic groups [41, 42, 53, 54].

Previous studies exhaustively investigated the effect of oxygen during the adsorption of organic compounds on activated carbon in the aqueous phase. However, limited studies have evaluated the effect of oxygen on heel build-up during cyclic adsorption/desorption of VOCs on activated carbon. Lashaki et al. [47] and Hashemi et al. [37] showed that the presence of oxygen in the purge gas increases heel build-up during the desorption process of VOCs. Since there is always an impurity of oxygen in the purge gas, heel build-up due to the oxygen-induced reactions seems inevitable but it can be minimized if the mechanism is known. The current method to mitigate the effect of oxygen in heel build-up is through ultra-purification of the purge gas to remove the oxygen impurity. However, nitrogen purification to this higher level increases the operational costs of the process in terms of power consumption for the N<sub>2</sub> generation.

### **1.5 Research Motivation**

Heel build-up reduces adsorption capacity and subsequently the performance of adsorbent in the cyclic process of adsorption. As a result, the life span of adsorbent will be shortened and frequent replacement of adsorbent is needed, which increases the demand for more materials, repeated reactivation and disposal, and therefore, imposes high operation and maintenance cost. While the influence of oxygen on heel build-up during desorption of VOCs has been observed and reported, the impacts of operational conditions (temperature and oxygen concentration) and adsorbent characteristics (physical properties and material) on the extent of this type of heel have not been studied. Besides, limited information is available on the formation mechanism of this type of heel in the porous structure of different adsorbents. Therefore, this research aims to fill this knowledge gap by understanding the effect of operational conditions and adsorbent type (material) and physical properties on heel build-up. Different commercially available adsorbent material (activated carbon, zeolite, and polymer) were tested and different characterization methods were used to identify the possible mechanisms for heel build-up. Knowing the nature of the oxygen-induced reactions is important as it could help in 1) finding optimal operational parameters, 2) selecting proper material, 3) minimizing heel build-up in the presence of oxygen, 4) investigating potential regeneration methods of spent adsorbents, 5) increasing adsorbent's lifetime, and 6) savings in capital and operational costs associated with adsorbent replacement.

### **1.6 Research Objectives**

The goal of this research is to maximize the lifespan of activated carbon in the cyclic adsorption/desorption process of organic compounds. In this regard, the nature of oxygen-induced

reactions between organic compounds and oxygen/carbon surface was investigated. The impact of various operational parameters such as adsorbent material and porosity, desorption temperature, and purge gas oxygen impurity were studied as well. Therefore, the objectives of this research can be summarized as follows:

- Objective 1: To quantify the combined effect of purge gas O<sub>2</sub> impurity and temperature on heel build-up
- Objective 2: To investigate the effect of physical properties of adsorbents (i.e. pore size distribution and specific surface area) on the extent of heel build-up
- Objective 3: To evaluate the impacts of adsorbents material (activated carbon, zeolite, polymer) on heel build-up in the presence of various O<sub>2</sub> impurities and temperatures
- Objective 4: To study the mechanism and impacts of heel build-up associated with oxygen-induced reactions and on different adsorbents.

## **1.7 Organization of Thesis**

This work is divided into 6 chapters. Chapter 1 gives a general overview of the topics discussed in the dissertation; chapters 2 to 5 support the objectives elaborated in chapter 1 and cover experimental methodologies, results and discussions; and finally, chapter 6 provides key conclusions and recommendations.

Chapter 1 provides an introduction about the VOCs and adsorption process, commercial desorption techniques, drawbacks of oxygen presence in thermal desorption, and the influential parameters of

heel build-up. A literature review of available studies on the oxygen-induced reactions is presented in this chapter and in the end, the research motivation and objectives are presented.

Chapter 2 investigates the effect of temperature and oxygen concentration on heel build-up during thermal desorption. Samples of a commercial activated carbon were tested for 5 consecutive adsorption/desorption cycles using 1,2,4-trimethylbenzene. This chapter also examines the changes in physical properties of the activated carbon samples using thermo-gravimetric analysis (TGA) and micropore surface analysis and suggests a new method to identify heel nature using thermogravimetric analysis.

Chapter 3 follows the subject of chapter 2 and focuses mainly on the effect of adsorbent's physical properties (pore size distribution and surface area) on heel build-up. It examines the adsorption performance of three commercial activated carbons using ultra-pure nitrogen versus air as the purge gas. Micropore surface analysis, XPS, Boehm titration, and DTG analysis were used to assess differences in the physical and chemical properties of these adsorbents.

Chapter 4 compares the performance of activated carbon, zeolite, and polymer adsorbents in presence of oxygen. The effect of two desorption temperatures (200 ° C and 288° C) and three desorption purge gas oxygen concentrations ( $\leq 5$  ppm, 10,000 ppm, and 21%) on heel build-up and adsorption capacity of each adsorbent was investigated. Based on the results of this chapter, temperature and oxygen concentration thresholds are introduced for different adsorbents.

Chapter 5 explores the mechanism of heel build-up using a severe condition of high oxygen concentration to analyze and characterize the products of oxygen-induced reactions. three

activated carbons (ACs) and one zeolite are tested using at 3 different temperatures (150, 200, and 250 °C). In addition to the characterization methods used in the previous chapters, GC-MS analysis is performed on the effluent gases to understand the mechanism of heel build-up.

Chapter 6 provides a dissertation overview, a summary of findings, key conclusions of the research, and proposes some recommendations for future studies.

## 1.8 References

- [1] Tsuji M., Koriyama C., Ishihara Y., Vogel C. F. A., and Kawamoto T., "Association between bisphenol A diglycidyl ether-specific IgG in serum and food sensitization in young children," *European Journal of Medical Research*, vol. 23, no. 1, pp. 61, 2018.
- [2] Indoor air quality: organic pollutants: report on a WHO meeting, Berlin, West, 23-27 August 1987, Copenhagen: World Health Organization, Regional Office for Europe, 1989.
- [3] Wang L. K., Pereira N. C., and Hung Y.-T., *Handbook of environmental engineering*, Totowa, N.J.: Humana Press, 2004.
- [4] Roelant G. J., Kemppainen A. J., and Shonnard D. R., "Assessment of the Automobile Assembly Paint Process for Energy, Environmental, and Economic Improvement," *Journal of Industrial Ecology*, vol. 8, no. 1 - 2, pp. 173-191, 2004.
- [5] Popescu M., Joly J. P., Carré J., and Danatoiu C., "Dynamical adsorption and temperature-programmed desorption of VOCs (toluene, butyl acetate and butanol) on activated carbons," *Carbon*, vol. 41, no. 4, pp. 739-748, 2003.
- [6] Papisavva S., Kia S., Claya J., and Gunther R., "Characterization of automotive paints: an environmental impact analysis," *Progress in Organic Coatings*, vol. 43, no. 1, pp. 193-206, 2001.
- [7] "Air Pollutant Emission Inventory (APEI) Report," <http://www.ec.gc.ca/pollution/default.asp?lang=En&n=A17452DA-1&offset=8&toc=show>.
- [8] "Volatile organic compound emissions by source," <https://www.canada.ca/en/environment-climate-change/services/environmental-indicators/air-pollutant-emissions.html#VOCs>.
- [9] Luengas A., Barona A., Hort C., Gallastegui G., Platel V., and Elias A., "A review of indoor air treatment technologies," *Reviews in Environmental Science and Bio/Technology*, vol. 14, no. 3, pp. 499-522, 2015.
- [10] Yokosuka Y., Oki K., Nishikiori H., Tatsumi Y., Tanaka N., and Fujii T., "Photocatalytic degradation of trichloroethylene using N-doped TiO<sub>2</sub> prepared by a simple sol-gel process," *Research on Chemical Intermediates*, vol. 35, no. 1, pp. 43-53, 2009.
- [11] Shiraishi F., and Ishimatsu T., "Toluene removal from indoor air using a miniaturized photocatalytic air purifier including a preceding adsorption/desorption unit," *Chemical Engineering Science*, vol. 64, no. 10, pp. 2466-2472, 2009.

- [12] "Effects of an ozone - generating air purifier on indoor secondary particles in three residential dwellings," *Indoor Air*, vol. 15, no. 6, pp. 432-444, 2005.
- [13] Zhang X., Gao B., Creamer A., Cao C., and Li Y., "Adsorption of VOCs onto engineered carbon materials: A review," *Journal of Hazardous Materials*, vol. 338, 2017.
- [14] Schnelle K. B., Dunn R. F., and Ternes M. E., *Air Pollution Control Technology Handbook*: CRC Press, 2015.
- [15] Huang B., Lei C., Wei C., and Zeng G., "Chlorinated volatile organic compounds (Cl-VOCs) in environment — sources, potential human health impacts, and current remediation technologies," *Environment International*, vol. 71, pp. 118-138, 2014.
- [16] Khan F. I., and Kr. Ghoshal A., "Removal of Volatile Organic Compounds from polluted air," *Journal of Loss Prevention in the Process Industries*, vol. 13, no. 6, pp. 527-545, 2000.
- [17] Kolta T., "Selecting Equipment to Control Air Pollution from Automotive Painting Operations," 1992.
- [18] Ruthven D. M., *Principles of Adsorption and Adsorption Processes*: Wiley, 1984.
- [19] Suzuki M., *Adsorption engineering*. Published by Kodansha; Elsevier, 1990.
- [20] Singh S. P., DePaoli D. W., Begovich J. M., Ashworth R. A., and Heyse E. C., "Review of methods for removing VOCs (volatile organic compounds) from the environment," 1987.
- [21] "Choosing an Adsorption System for VOC: Carbon, Zeolite, Or Polymers" *The Clean Air Technology Center, EPA Technical Bulletin*, 1999.
- [22] Ruthven D. M., "Principles of adsorption and adsorption processes," Wiley, 1984.
- [23] Bandosz T. J., "Gas Adsorption Equilibria: Experimental Methods and Adsorptive Isotherms," *Journal of the American Chemical Society*, vol. 127, no. 20, pp. 7655-7656, 2005.
- [24] Do D. D., *Adsorption Analysis: Equilibria and Kinetics*: Published by Imperial College Press and distributed by World Scientific Publishing Co., 1998.
- [25] Bansal R. C., Goyal M., *Activated Carbon Adsorption*: Published by CRC Press, 2005.
- [26] Hemphill L., and Robert S. Kerr Environmental Research Laboratory A., Okla, *Thermal Regeneration of Activated Carbon*: National Technical Information Service, 1978.
- [27] Ruhl M. J., "Recover VOCs via adsorption on activated carbon," *Chemical Engineering Progress*, 89(7), 1993.

- [28] Cruciani G., “Zeolites upon heating: Factors governing their thermal stability and structural changes,” *Journal of Physics and Chemistry of Solids*, vol. 67, no. 9, pp. 1973-1994, 2006.
- [29] Ghafari M., and Atkinson J. D., “Impact of styrenic polymer one-step hyper-cross-linking on volatile organic compound adsorption and desorption performance,” *Journal of Hazardous Materials*, vol. 351, pp. 117-123, 2018.
- [30] Rouquerol J., Avnir D., Fairbridge C. W., Everett D. H., Haynes J. M., Pernicone N., Ramsay J. D. F., Sing K. S. W., and Unger K. K., “Recommendations for the characterization of porous solids (Technical Report),” *Pure and Applied Chemistry*, vol. 66, no. 8, pp. 1739-1758, 1994.
- [31] Breck W. D., *Zeolite Molecular Sieves: Structure, Chemistry, and Use*: Wiley, 1974.
- [32] Ruthven D. M., Farooq S., and Knaebel K. S., *Pressure Swing Adsorption*: Wiley, 1993.
- [33] Rydberg J., *Solvent Extraction Principles and Practice, Revised and Expanded*: Taylor & Francis, 2004.
- [34] Cecen F., and Aktas Ö., *Activated Carbon for Water and Wastewater Treatment: Integration of Adsorption and Biological Treatment*: Wiley, 2011.
- [35] Thomas W. J., and Crittenden B., "5 -Processes and cycles," In *Adsorption Technology & Design*, pp. 96-134, Oxford: Butterworth-Heinemann, 1998.
- [36] Yun J.-H., Choi D.-K., and Moon H., “Benzene adsorption and hot purge regeneration in activated carbon beds,” *Chemical Engineering Science*, vol. 55, no. 23, pp. 5857-5872, 2000.
- [37] Hashemi S. M., Lashaki M. J., Hashisho Z., Phillips J. H., Anderson J. E., and Nichols M., “Oxygen impurity in nitrogen desorption purge gas can increase heel buildup on activated carbon,” *Separation and Purification Technology*, vol. 210, pp. 497-503, 2019.
- [38] Dąbrowski A., Podkościelny P., Hubicki Z., and Barczak M., “Adsorption of phenolic compounds by activated carbon—a critical review,” *Chemosphere*, vol. 58, no. 8, pp. 1049-1070, 2005.
- [39] Aktaş Ö., and Çeçen F., “Effect of type of carbon activation on adsorption and its reversibility,” *Journal of Chemical Technology & Biotechnology*, vol. 81, no. 1, pp. 94-101, 2006.
- [40] Lashaki M. J., *Understanding and improving gas phase capture of organic vapors by carbonaceous adsorbents*, Ph.D. Thesis, University of Alberta, 2016.



- [41] Vidic R. D., Tessmer C. H., and Uranowski L. J., "Impact of surface properties of activated carbons on oxidative coupling of phenolic compounds," *Carbon*, vol. 35, no. 9, pp. 1349-1359, 1997.
- [42] Vidic R. D., Suidan M. T., and Brenner R. C., "Impact of oxygen mediated oxidative coupling on adsorption kinetics," *Water Research*, vol. 28, no. 2, pp. 263-268, 1994.
- [43] Urano K., Yamamoto E., and Takeda H., "Regeneration Rates of Granular Activated Carbons Containing Adsorbed Organic Matter," *Industrial and Engineering Chemistry Process Design and Development*, vol. 21, no. 1, pp. 180-185, 1982.
- [44] Suzuki M., Misic D. M., Koyama O., and Kawazoe K., "Study of thermal regeneration of spent activated carbons: Thermogravimetric measurement of various single component organics loaded on activated carbons," *Chemical Engineering Science*, vol. 33, no. 3, pp. 271-279, 1978.
- [45] Niknaddaf S., Atkinson J. D., Shariaty P., Lashaki M. J., Hashisho Z., Phillips J. H., Anderson J. E., and Nichols M., "Heel formation during volatile organic compound desorption from activated carbon fiber cloth," *Carbon*, vol. 96, pp. 131-138, 2016.
- [46] Liu P. K. T., Feltch S. M., and Wagner N. J., "Thermal Desorption Behavior of Aliphatic and Aromatic Hydrocarbons Loaded on Activated Carbon," *Industrial and Engineering Chemistry Research*, vol. 26, no. 8, pp. 1540-1545, 1987.
- [47] Lashaki M. J., Fayaz M., Wang H., Hashisho Z., Phillips J. H., Anderson J. E., and Nichols M., "Effect of Adsorption and Regeneration Temperature on Irreversible Adsorption of Organic Vapors on Beaded Activated Carbon," *Environmental Science & Technology*, vol. 46, no. 7, pp. 4083-4090, 2012.
- [48] Ferro-García M. A., Joly J. P., Rivera-Utrilla J., and Moreno-Castilla C., "Thermal desorption of chlorophenols from activated carbons with different porosity," *Langmuir*, vol. 11, no. 7, pp. 2648-2651, 1995.
- [49] Kim K.-J., Kang C.-S., You Y.-J., Chung M.-C., Woo M.-W., Jeong W.-J., Park N.-C., and Ahn H.-G., "Adsorption-desorption characteristics of VOCs over impregnated activated carbons," *Catalysis Today*, vol. 111, no. 3, pp. 223-228, 2006.
- [50] Hofelich T. C., LaBarge M. S., and Drott D. A., "Prevention of thermal runaways in carbon beds," *Journal of Loss Prevention in the Process Industries*, vol. 12, no. 6, pp. 517-523, 1999.
- [51] Lashaki M. J., Atkinson J. D., Hashisho Z., Phillips J. H., Anderson J. E., Nichols M., and Misovski T., "Effect of desorption purge gas oxygen impurity on irreversible adsorption of organic vapors," *Carbon*, vol. 99, pp. 310-317, 2016.

- [52] Sabio E., González-Martín M. L., Ramiro A., González J. F., Bruque J. M., Labajos-Broncano L., and Encinar J. M., “Influence of the Regeneration Temperature on the Phenols Adsorption on Activated Carbon,” *Journal of Colloid and Interface Science*, vol. 242, no. 1, pp. 31-35, 2001.
- [53] Vidic R. D., Suidan M. T., Traegner U. K., and Nakhla G. F., “Adsorption isotherms: illusive capacity and role of oxygen,” *Water Research*, vol. 24, no. 10, pp. 1187-1195, 1990.
- [54] Suidan M., “Role of dissolved oxygen on the adsorptive capacity of activated carbon for synthetic and natural organic matter,” 1991.
- [55] Musso H., “Phenol Oxidation Reactions,” *Angewandte Chemie International Edition*, vol. 29, no. 12, pp. 723-735, 1963.
- [56] Zogorski J. S., Algeier G. D., and Mullins R. L., *Removal of Chloroform from Drinking Water*, Final report to Kentucky Water Resources Research Institute, 1978.
- [57] Grant T. M., and King C. J., “Mechanism of Irreversible Adsorption of Phenolic Compounds by Activated Carbons,” *Industrial and Engineering Chemistry Research*, vol. 29, no. 2, pp. 264-271, 1990.

# **CHAPTER 2: EFFECTS OF OXYGEN IMPURITY AND TEMPERATURE ON HEEL BUILD-UP**

## **2.1 Chapter Overview**

This chapter summarizes the information related to the effect of oxygen presence during thermal desorption of volatile organic compounds from activated carbon. The simultaneous effect of desorption temperature (200°C and 288°C) and oxygen concentration ( $\leq 5$ , 10,000, and 21,000 ppmv) on heel build-up was studied using 5-cycle adsorption/desorption tests of 1,2,4-trimethylbenzene on a microporous activated carbon. Thermal gravimetric analysis (TGA), was used to assess the thermal stability of the heels formed on the samples. The porous structure of the samples was also studied using nitrogen sorption analysis and the BET method.

## **2.2 Introduction**

Volatile organic compounds (VOCs) are emitted from many industrial processes including vehicle painting booths [1-3]. Adsorption onto activated carbon is a widely used VOC emission control technique because of its high removal efficiency and low cost [4-8]. However, during the cyclic adsorption/desorption process; the adsorption capacity of activated carbon can gradually decrease due to heel build-up [2, 9-11].

In discussing the heel build-up, it is useful to understand the fundamentals of adsorption and distinguish between physical and chemical adsorption processes [8]. Physical adsorption (also known as physisorption) is reversible, as it occurs through relatively weak intermolecular attractive forces such as van der Waals, while chemical adsorption (also known as chemisorption) is difficult

to reverse, as it involves the formation of chemical bonds between the adsorbate and the surface of the adsorbent. In physical adsorption, under suitable conditions, desorption process should be able to remove the adsorbates from the adsorbent pores without negative impacts on the physical or chemical properties of the adsorbent or the chemical composition of the adsorbate. On the other hand, chemical adsorption is attributed to chemical bonds of strongly or permanently adsorbed species resulting in heel build-up [2, 9-12]. Heel build-up may also occur through the gradual accumulation of non-desorbed physisorbed adsorbates due to improper desorption conditions (i.e. insufficient temperature).

Understanding parameters that contribute to heel build-up is beneficial to avoid or limit heel formation and to extend the adsorbent's lifespan, which can result in savings in capital and operational costs of adsorbent replacement. Suzuki et al. [13] found that phenol and phenolic derivatives were poorly desorbed from activated carbon by thermal desorption. Similarly, Yonge et al. [14] reported that only a small portion of phenolic compounds ( $\leq 15\%$ ) adsorbed on activated carbon from an aqueous solution could be desorbed. Grant and King [15] explained this adsorption irreversibility by the occurrence of oxidative reactions on the activated carbon surfaces. These reactions produce polymeric products that are adsorbed very strongly on the carbon and are "irreversibly adsorbed." They named five factors that promote these oxidative coupling reactions: (a) long contact time, (b) high pH values, (c) high temperature, (d) the presence of dissolved oxygen, and (e) the nature of the organic compound. Besides, the presence of a metallic catalyst was found to promote the oxidative coupling reactions at room temperature. Although these factors have been extensively studied for aqueous phase adsorption [9, 10, 16-20], there is little

information about their effect on heel build-up during the desorption process in both gas and aqueous phases [21-25].

During thermal desorption, inert gas (usually N<sub>2</sub>) is commonly used to purge an adsorbent bed to avoid bed fires and any unfavorable reactions [26]; however, unavoidable impurities in the purge gas (mostly oxygen) can react with the adsorbate species or the adsorbent surface which may result in heel build-up. Although the purification of nitrogen can diminish this type of heel, it increases the operational costs of nitrogen generation and consequently the cost of the adsorption/desorption process [27, 28].

Logically, a temperature higher than the adsorbate's boiling point is required to completely desorb adsorbates at atmospheric pressure. Previous studies showed that increasing desorption temperature reduces the process time and improves the desorption efficiency by facilitating mass transfer and diffusion, specifically for high molecular weight adsorbates in micropores [16, 29, 30]. Although increasing temperature facilitates the desorption process, it may also promote chemical reactions between the adsorbed species and purge gas or adsorbent and result in a greater heel build-up before the adsorbates can escape from the adsorbent's pores [31]. In addition to these competing temperature effects on heel buildup, the simultaneous effects of purge gas oxygen content and desorption temperature have not been studied.

The objective of this study is to explain the effect of temperature and purge gas oxygen content on heel build-up during the desorption process. For this purpose, 5-cycle experiments involving adsorption of 1,2,4-trimethylbenzene (TMB) on a microporous and low catalytic activated carbon adsorbent were completed at different desorption temperatures and oxygen concentrations. The

adsorbent was analyzed for the amount of heel build-up and changes in adsorption capacity, specific surface area, and pore size distribution. Thermogravimetric analysis was also used to assess the thermal stability of the heel.

## **2.3 Materials and Methods**

### **2.3.1 Adsorbent and Adsorbate**

The adsorbent used in this study was petroleum pitch-based beaded activated carbon (BAC, G-70R Kureha Corporation, Japan). The G-70R has high microporosity (>85%) and low catalytic activity (ash content <0.1%) [32]. Prior to the adsorption experiments, G-70R was oven-dried at 120°C for 24 h to remove any adsorbed water and then stored in a desiccator until it reached room temperature.

Aromatic compounds are commonly used in industrial applications as solvents [33, 34]. TMB, an aromatic hydrocarbon commonly found in paint solvents, was selected as a surrogate for VOCs present in automotive painting booth air. TMB has been shown in previous studies to have a high tendency to form heel in the presence of oxygen [25]. TMB (98% purity, Sigma-Aldrich) was used as adsorbate for all the adsorption tests.

### **2.3.2 Experimental Setup & Methodology**

The experimental setup (Figure 2-1) consisted of five main components: an adsorption/desorption tube, an organic vapor generation system, an organic vapor detection system, a heat application module, and a data acquisition and control (DAC) system (Figure 2-1). The adsorption/desorption tube consisted of a stainless steel tube (10.2 mm inner diameter, 160.4 mm long) with quartz wool

at the bottom and top as a support for the adsorption bed ( $1.0 \pm 0.05$  g of dried G-70R). The organic vapor generation system consisted of a syringe pump (KD Scientific, KDS-220) to inject liquid TMB into a 10 standard liter per minute (SLPM) air stream controlled using a mass flow controller (Alicat Scientific). The organic vapor generation system provided a constant TMB inlet concentration of 500 ppm<sub>v</sub>. The organic vapor detection system consisted of a flame ionization detector (FID; Series 9000, Baseline-Mocon Inc.) that was set to monitor TMB concentrations at constant time intervals (every 30 sec). The power application module used for regeneration included a heating and insulation tape (Omega) wrapped around the adsorption/regeneration tube. A DAC system controlled the applied power to the heating tape to maintain the bed temperature at the target temperature (200°C or 288°C) during regeneration.

Each adsorption cycle lasted 60 min, allowing full saturation of the G-70R as determined by equal inlet and outlet VOC concentrations (500 ppm<sub>v</sub>). Desorption purge gases with different concentrations of oxygen impurities ( $\leq 5$  ppm, 10,000 ppm, and 21%) were generated by mixing compressed air (99.999% pure, Praxair) and N<sub>2</sub> (99.9984% pure, Praxair). Since the compressed N<sub>2</sub> contained a maximum of 5 ppm O<sub>2</sub>, it was solely (i.e. without mixing) used as the purge gas for the  $\leq 5$  ppm O<sub>2</sub> case. Similarly, for the 21% O<sub>2</sub> case, compressed air was solely used as the purge gas. To generate 10,000 ppm oxygen impurity, compressed air, and N<sub>2</sub> were mixed at the appropriate ratio using mass flow controllers. Thermal desorption was performed using a flow rate of 1 SLPM for 6 hours. The desorption duration was determined by monitoring the concentration of TMB in the outlet. The adsorption capacity and heel build-up were calculated from a mass balance in each adsorption/desorption cycle as follows:

$$q_i (\%) = \frac{MAA_i - MBA_i}{MI} \times 100$$

$$H_i (\%) = \frac{MAD_i - MBA_i}{MI} \times 100$$

Where  $q_i$  is the adsorption capacity and  $H_i$  is the heel build-up.  $MBA$  (g) and  $MAA$  (g) are the adsorbent mass before and after adsorption, respectively, and  $MAD$  (g) is the adsorbent mass after desorption. Subscript “i” is the cycle number, and  $MI$  stands for the initial mass of dry adsorbent.

Cumulative heel ( $H_T$ ), which is the total accumulated mass percentage after 5 successive adsorption/regeneration cycles, is calculated by adding the heel build-up over the 5 cycles:

$$H_T (\%) = \sum_{i=1}^5 H_i (\%)$$

Adsorption/desorption experiments were duplicated, and average values are reported herein.



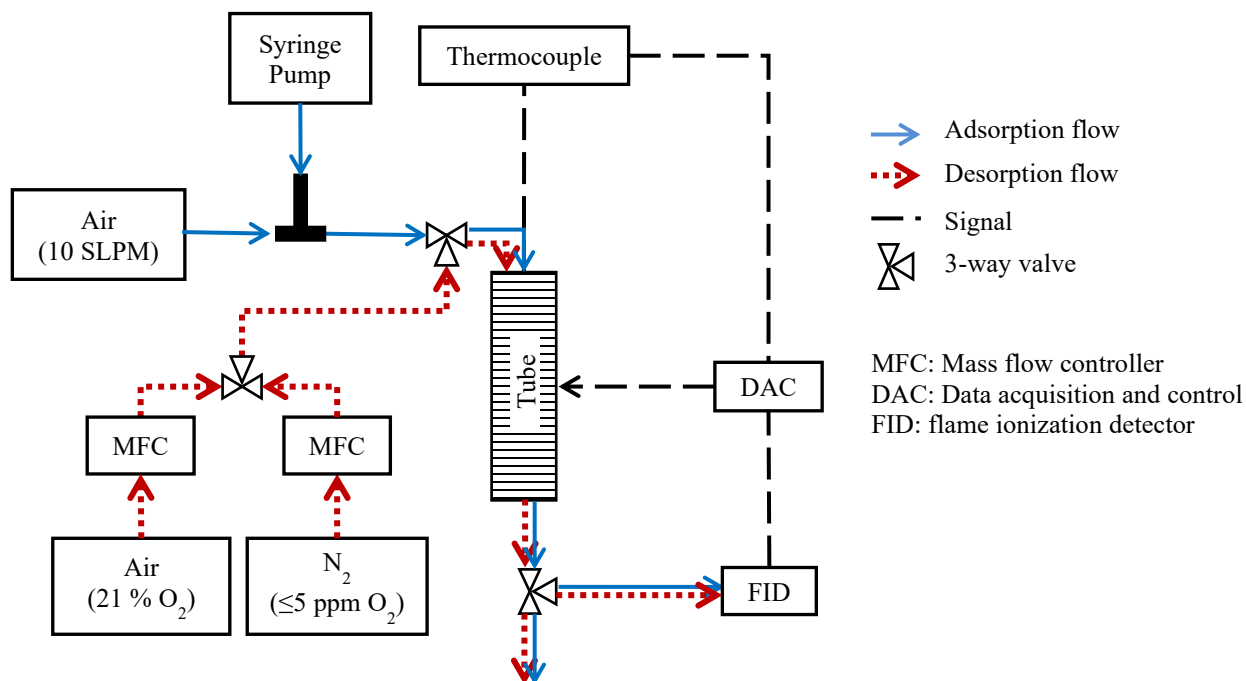


Figure 2-1. Schematic diagram of the adsorption-desorption setup.

### 2.3.3 Adsorbent Characterization Methods

The pore size distribution of virgin and regenerated adsorbents was examined by  $N_2$  adsorption using a surface area analyzer (Autosorb iQ2MP, Quantachrome) at the  $N_2$  boiling point (77 K). Prior to any analysis, the adsorbent (40-50 mg) was degassed at 150 °C for 6 hours to remove contaminants such as moisture and low molecular weight physisorbed hydrocarbons. The specific surface area was calculated from the slope and intercept of the isotherms' curve using the Brunauer, Emmet, and Teller (BET) model at a relative pressure range of 0.01 to 0.1 [28, 35]. The Quenched Solid Density Functional Theory (QSDFT) method provided pore size distributions and micropore volumes (pore width  $<20\text{Å}$ ). The total pore volume was also obtained from the  $N_2$  isotherm at  $P/P_0 = 0.995$ .

The thermal stability of the formed heel on the adsorbents was assessed using a thermogravimetric analyzer (TGA/DSC 1, Mettler Toledo). The weight of the sample was measured as it was heated from 25 to 800 °C at 2 °C /min, in 50 standard cm<sup>3</sup>/min of N<sub>2</sub> (99.999% pure). The relatively slow heating rate was selected to minimize the potential for mass transfer resistance during desorption, and consequently, to obtain high peak resolutions with differential thermogravimetric (DTG) analysis.

## **2.4 Results & Discussion**

### **2.4.1 Desorption Profiles and Duration**

The desorption of TMB from TMB-saturated adsorbent at 200°C and 288°C was monitored to determine the duration needed to reach a threshold of  $\leq 5$  ppm<sub>v</sub> TMB in the purge gas, which is 1% of adsorption concentration. During desorption at 288°C, the desorption outlet concentration peaked at a higher concentration and reached 5 ppm<sub>v</sub> sooner than that at 200°C (Figure 2-2). The desorption time for all the experiments was therefore selected as 6 hours, which corresponded to both temperatures having  $\leq 5$  ppm<sub>v</sub> TMB in the outlet.

Desorption rates increase as the temperature increases due to both higher heat and mass transfer. However, the desorption efficiency is not necessarily improved at higher temperatures. Although desorption at 288°C shortens the process by driving adsorbates out of the pores faster than that of 200°C (Figure 2-2), the potential for the occurrence of any unfavorable reactions at 288°C is higher due to the increased reaction kinetics as will be discussed later.

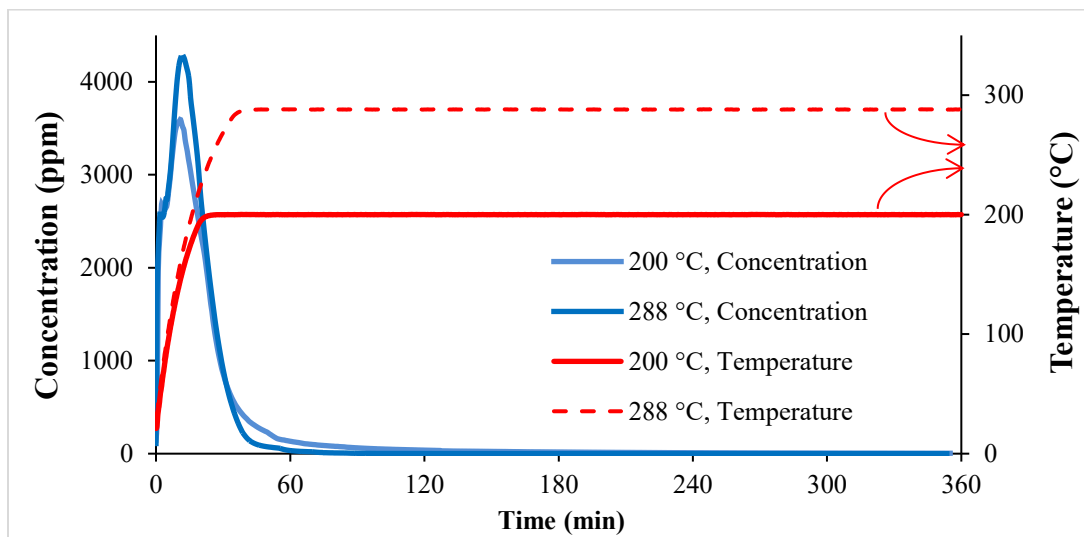


Figure 2-2. Desorption profile of TMB-loaded G-70R at 200°C and 288°C

#### 2.4.2 Heel Build-up and Adsorption Capacity Reduction

Figure 2-3 presents a summary of adsorption capacities and heel build-up for all samples after 5 cycles of adsorption/desorption. More details on the breakthrough curves of the 5-cycle tests are provided in Appendix A. In the case of the purge gas with  $\leq 5\text{ppm}_v$   $\text{O}_2$  impurity, desorption at 288°C showed a cumulative heel build-up of  $0.5\pm 0.1\%$  after 5-cycles, consistent with a small reduction in the adsorption capacity ( $0.3\pm 0.1\%$ ). Desorption at the same level of oxygen impurity at 200°C showed a higher cumulative heel ( $1.6\pm 0.1\%$ ) and consequently, higher adsorption capacity loss ( $1.6\pm 0.1\%$ ); however, the majority of the heel and capacity loss occurred in the first cycle,  $1.5\pm 0.1\%$  and  $1.4\pm 0.1\%$ , respectively, and the other cycles minimally contributed to the heel build-up ( $\sim 0.1\%$ ) and the adsorption capacity loss ( $\sim 0.2\%$ ) (Figure 2-3a & Figure 2-3b). This indicates the inability of thermal desorption at 200°C to completely drive TMB out of all the BAC pores, even though the boiling point of TMB is only 169°C. At 200°C, a portion of TMB is left behind in the narrow micropores, since more energy is required to drive TMB out of the smaller

pores. However, once the narrow micropores were filled by the non-desorbed TMB in the first cycle, a limited amount of heel was formed in the next 4 cycles. Apart from the first cycle, desorption at both 200°C and 288°C by purge gas with  $\leq 5$  ppm O<sub>2</sub> impurity had very limited effects on heel build-up and adsorption capacity, showing less than a 0.2% change. This result has important implications on the operational cost of the cyclic adsorption process. Based on the 5 cycles tests, lowering the desorption temperature from 288°C to 200°C slightly decreases the adsorption capacity by a one-time heel in the first cycle, but would considerably reduce the operational (energy) costs associated with adsorbent heating.

Desorption at 288°C with 10,000 ppm O<sub>2</sub> purge gas had a considerably greater impact than with  $\leq 0.5$  ppmv O<sub>2</sub>. The heel increased during every cycle ( $1.3 \pm 0.1\%$  per cycle) and cumulatively reached  $6.6 \pm 0.2\%$  after the 5-cycle test (Figure 2-3.c). Adsorption capacity also steadily decreased from  $44.2 \pm 0.2\%$  to  $41.2 \pm 0.2\%$  over 5 cycles ( $0.6 \pm 0.1\%$  per cycle). However, desorption at 200°C with 10,000 ppm oxygen impurity showed relatively small changes in the amount of heel build-up compared to the  $\leq 5$  ppm O<sub>2</sub> impurity at 200°C. In both cases, the largest portion of the heel was formed in the first cycle ( $1.5 \pm 0.1\%$ ). The cumulative heel after the 5-cycle test was 2.1% (vs.  $1.6 \pm 0.1\%$  for  $\leq 5$  ppm O<sub>2</sub>) and the total adsorption capacity reduction was  $1.7 \pm 0.1\%$  (vs.  $1.6 \pm 0.1\%$  for  $\leq 5$  ppm O<sub>2</sub>). These results indicate that at 200°C, the effect of oxygen concentration up to 10,000 ppm on heel build-up during desorption is minimal, while at 288°C the presence of oxygen at the same impurity level can significantly reduce the desorption efficiency.

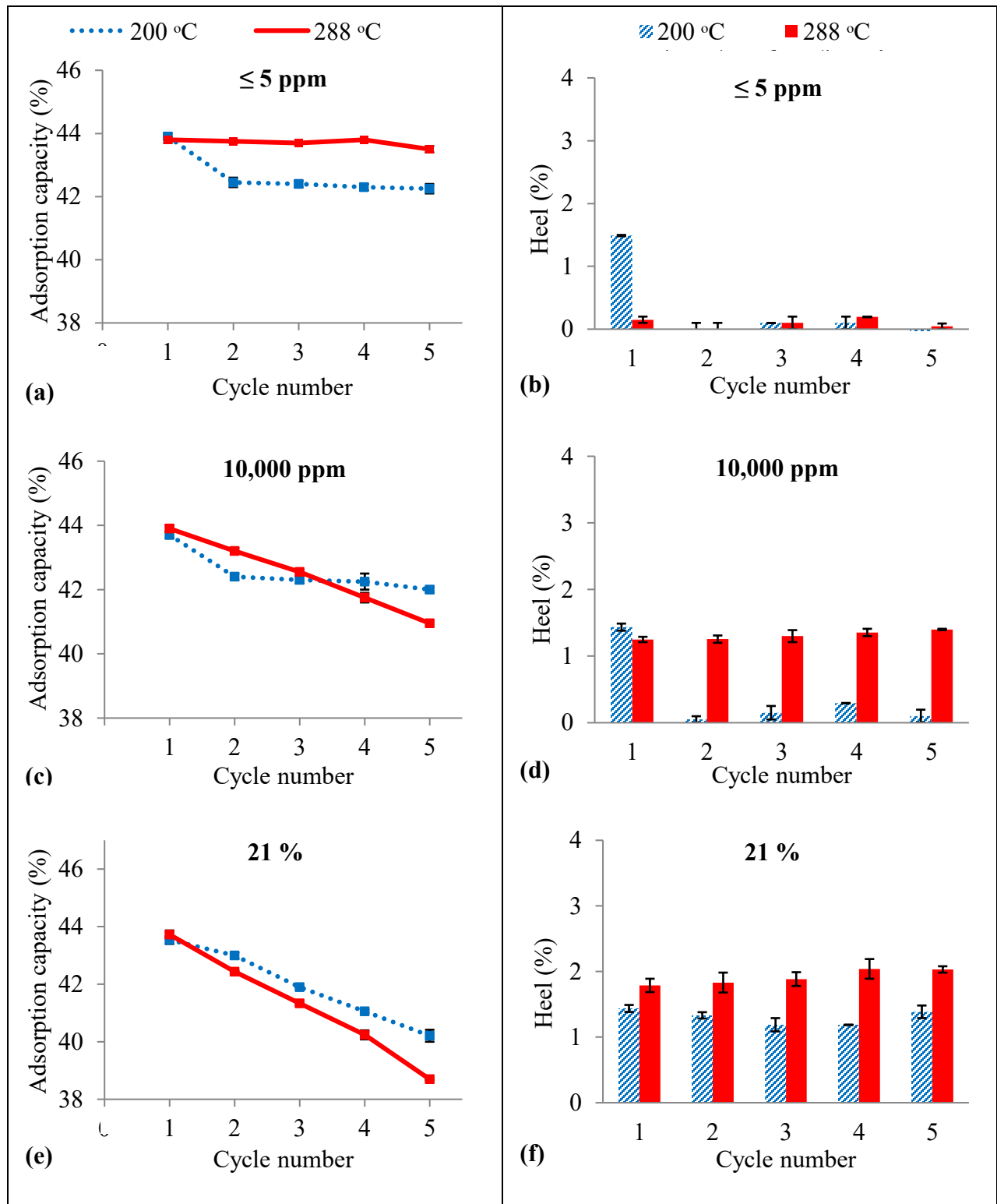


Figure 2-3. Adsorption capacity ( $q_i$ ) and heel build-up ( $H_i$ ) per cycle for G-70R samples desorbed at 200°C and 288°C: (a/b) desorbed in  $\leq 5$  ppm  $O_2$  in  $N_2$ , (c/d) desorbed in 10,000 ppm

O<sub>2</sub> in N<sub>2</sub>, (e/f) desorbed in 21% O<sub>2</sub> in N<sub>2</sub>. Error bars indicate the standard deviation of the arithmetic mean of two sets of data.

The last set of experiments was completed using 21% O<sub>2</sub> in the N<sub>2</sub> desorption purge gas (air) at 200°C and 288°C. The cumulative heel at 200°C and 288°C were 6.4±0.2% and 9.6±0.3% respectively, and the total adsorption capacity reduction was 3.3±0.2% and 5.2±0.2%, respectively. The amount of heel at both temperatures progressively increased in each cycle which led to corresponding reductions in adsorption capacity. In contrast to the cases with ≤5 ppm and 10,000 ppm O<sub>2</sub>, an oxygen concentration of 21% led to rapid heel build-up even at the lower temperature of 200°C.

These results suggest that at a certain desorption temperature, 200°C in the current study, increasing oxygen impurity up to a certain concentration, 10,000 ppm, won't tangibly reduce the performance of the adsorbent in the cyclic use, however, it would significantly reduce the operational cost associated with purifying nitrogen [32]. Apart from the heel in the first cycles at 200 °C that was related to the insufficient desorption temperature, the formation of heel in other cases can be attributed to the reactions owing to the presence of oxygen (oxygen-induced reaction). According to the collision theory, the rate of this oxygen-induced reaction, similar to any other reactions, would depend on the number of collisions between the reactants (closely related to the concentration of O<sub>2</sub> and TMB) and the kinetic energy of molecules (related to the desorption temperature) at the moment of impact [36]. This explains the minimal heel build-up observed in the case of ≤5ppm<sub>v</sub> oxygen due to the insufficient O<sub>2</sub> molecules and the maximum cumulative heel with 21% oxygen impurity at 288°C. This also explains the higher heel build-up at 288°C compared to 200°C in the case of 10,000 ppm O<sub>2</sub> impurity, where the higher temperature of 288°C

supplied the activation energy and provided suitable conditions for successful collisions to form the heel.

### **2.4.3 Characterization of adsorbents after the 5-cycle tests**

Heel build-up can be attributed to physisorption or chemisorption. Physisorbed heel occurs when the desorption condition is insufficient to disrupt the intermolecular interactions between the adsorbed species (TMB) and the adsorbent (G-70R). In contrast to physisorption, chemisorbed species form chemical bonds and considerably more energy is needed (than the heat of desorption) to break the chemical bonds or degrade the chemically adsorbed species. To differentiate between physisorbed and chemisorbed heel, all the samples in the current study were analyzed by thermogravimetry (heating to 850°C in N<sub>2</sub>) to assess the strength of adsorbate-adsorbent interactions (Figure 2-4). The weight change of the virgin G-70R under these conditions, from degradation or/and decomposition, was measured and included when calculating the thermogravimetric analysis (TGA) weight loss of each tested G-70R.

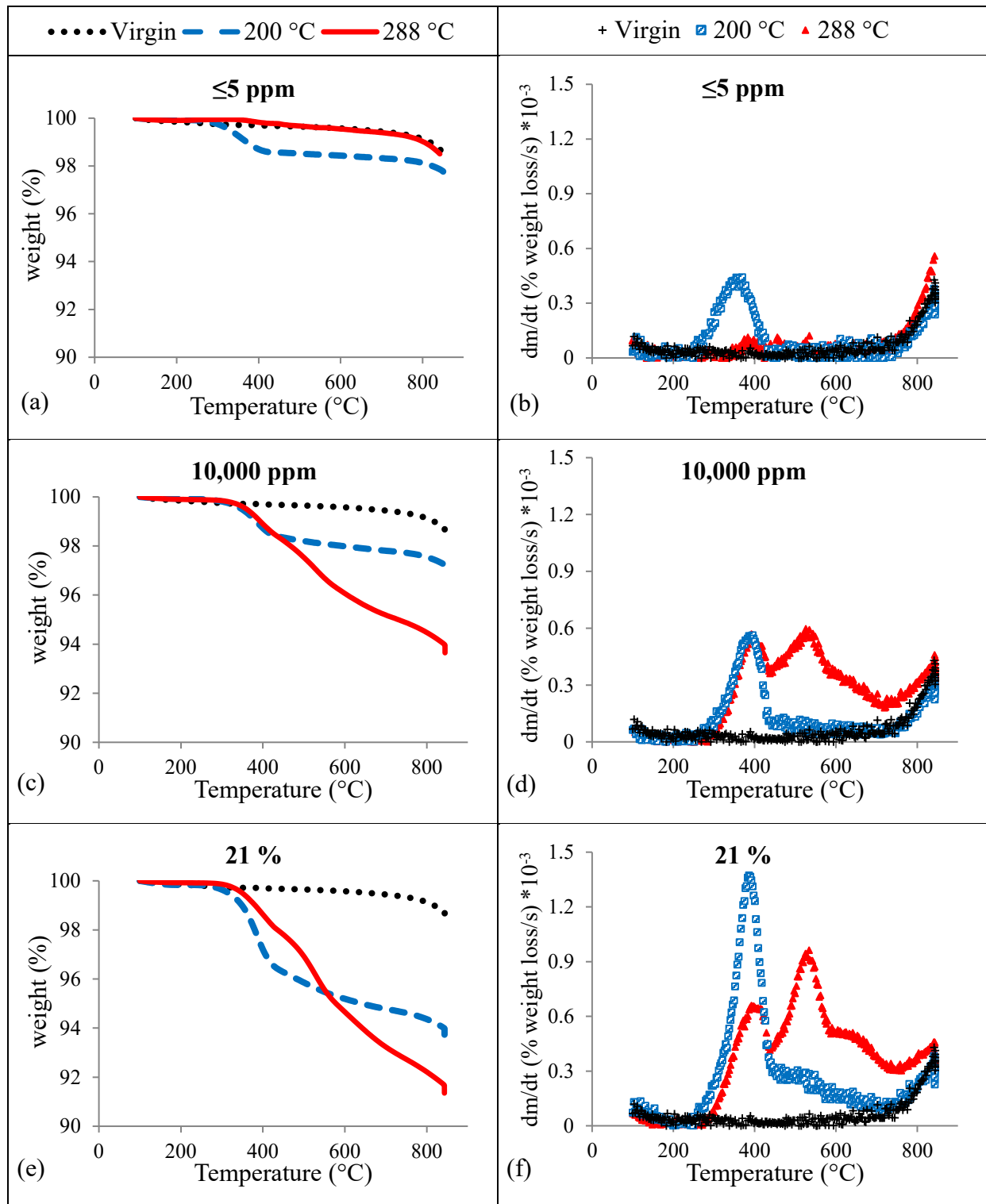


Figure 2-4. TGA analysis of 5-cycle G-70R samples desorbed at 200°C and 288°C using N<sub>2</sub> purge gas containing (a/b) ≤5ppm O<sub>2</sub>, (c/d) 10,000 ppm O<sub>2</sub>, (e/f) 21% O<sub>2</sub>



Based on peaks observed at different temperatures during TGA and the excess heel remaining after TGA, the heel can be divided into 3 categories (Figure 2-4): “Heel<sub><430</sub>”, the portion of the heel associated with strong physisorption which was completely removed by heating to 430°C (physisorbed heel); “Heel<sub>430-850</sub>”, the portion of the heel removed by decomposition through heating at temperatures from 430°C to 850°C (chemically formed heel); “Heel<sub>>850</sub>”, the portion of the heel non-removable by heating to 850°C that was either permanently deposited or its removal required temperatures higher than 850°C (non-desorbable heel due to combination of chemisorbed heel and carbon deposition). Heel<sub><430</sub> and Heel<sub>430-850</sub> percentages can be obtained from the DTG results normalized to the initial mass of virgin adsorbent, and Heel<sub>>850</sub> can be calculated by subtracting the total TGA weight loss from the cumulative heel build-up.

$$Heel_{<430} (\%) = \Delta WS_{430^\circ C} (\%) * \left( 1 + \frac{H_T(\%)}{100} \right) - \Delta WV_{430^\circ C} (\%)$$

$$Heel_{<430} (\%) = \Delta WS_{430-850^\circ C} (\%) * \left( 1 + \frac{H_T(\%)}{100} \right) - \Delta WV_{430-850^\circ C} (\%)$$

$$Heel_{>850} (\%) = H_T(\%) - Heel_{<430} (\%) - Heel_{430-850} (\%)$$

$\Delta WS_{430^\circ C}$  and  $\Delta WV_{430^\circ C}$  are the weight losses (%) of the tested samples and virgin adsorbent, respectively, after TGA heating to 430°C, and the  $\Delta WS_{430-850^\circ C}$  and  $\Delta WV_{430-850^\circ C}$  are the corresponding weight losses by heating from 430 to 850°C. The samples were labeled based on the desorption conditions, designated as “x\_y”, where “x” represents the temperature (200°C or 288°C) and “y” represents oxygen concentration (5 ppm, 10,000 ppm, or 21%). For instance, 288\_21 refers to the sample desorbed at 288°C using 21% oxygen in the N<sub>2</sub> purge gas.

For the samples desorbed at 200°C, DTG analysis confirmed the minimal effect of oxygen in the  $\leq 5$  ppm and 10,000 ppm tests by showing similar peaks at approximately 350°C and no other peaks at higher temperatures (Figure 2-4.b and Figure 2-4.d), while for the 200\_21 sample (Figure 2-4.f), a sharper peak at the same temperature (Heel<sub><430</sub>) was observed along with a broad peak starting from 430°C (Heel<sub>430-850</sub>). In fact, it can be said that for the 200\_21 sample, the formation of Heel<sub>430-850</sub> may contribute to the growth of Heel<sub><430</sub> through restricting the desorption pathways (i.e. pore blockage), which increases the diffusion resistance, decreases the desorbability of TMB at 200°C and hence, leads to additional Heel<sub><430</sub> accumulation on this sample.

For the sample desorbed at 288°C with  $\leq 5$  ppm O<sub>2</sub> impurity no clear peak was detected due to the negligible heel build-up at this condition. However, the presence of oxygen during desorption for both 288\_10 and 288\_21 resulted in two distinct peaks at around 350°C and 550°C. The earlier peak (at ~350°C) for both 288\_10 and 288\_21 was similar to the 200°C desorption experiments, in which the physisorption heel was presumed to have desorbed. However, this low-temperature peak was not seen in the DTG curve of 288\_5. This may be explained by the narrowing of the micropores by the Heel<sub>430-850</sub> fraction, as discussed later, and supported by the pore size distribution analysis.

Considering the high thermal stability of Heel<sub>>850</sub>, resistant to removal even at 850°C, the prevention of its formation is economically and environmentally desirable as it shortens the life span of adsorbents and makes regeneration of the spent adsorbent problematic. The amount of Heel<sub>>850</sub> in both the 200-5 and 288-5 tests was measured as  $\leq 0.3\%$  (Figure 2-5), which suggests that using high purity purge gas ( $\leq 5$  ppm O<sub>2</sub>) prevents the formation of this thermally stable heel at both desorption temperatures. Conversely, temperature plays an important role in the desorption

with 10,000 ppm O<sub>2</sub> in N<sub>2</sub>. For desorption at 200°C, Heel<sub>>850</sub> amounts were minimal for O<sub>2</sub> impurity up to 10,000 ppm but increased to 1.5% at 288°C at this O<sub>2</sub> level. Increasing the O<sub>2</sub> to ~21% increased Heel<sub>>850</sub> at both temperatures, with larger impacts at the higher desorption temperature (1.3% at 200°C and 1.8% at 288°C).

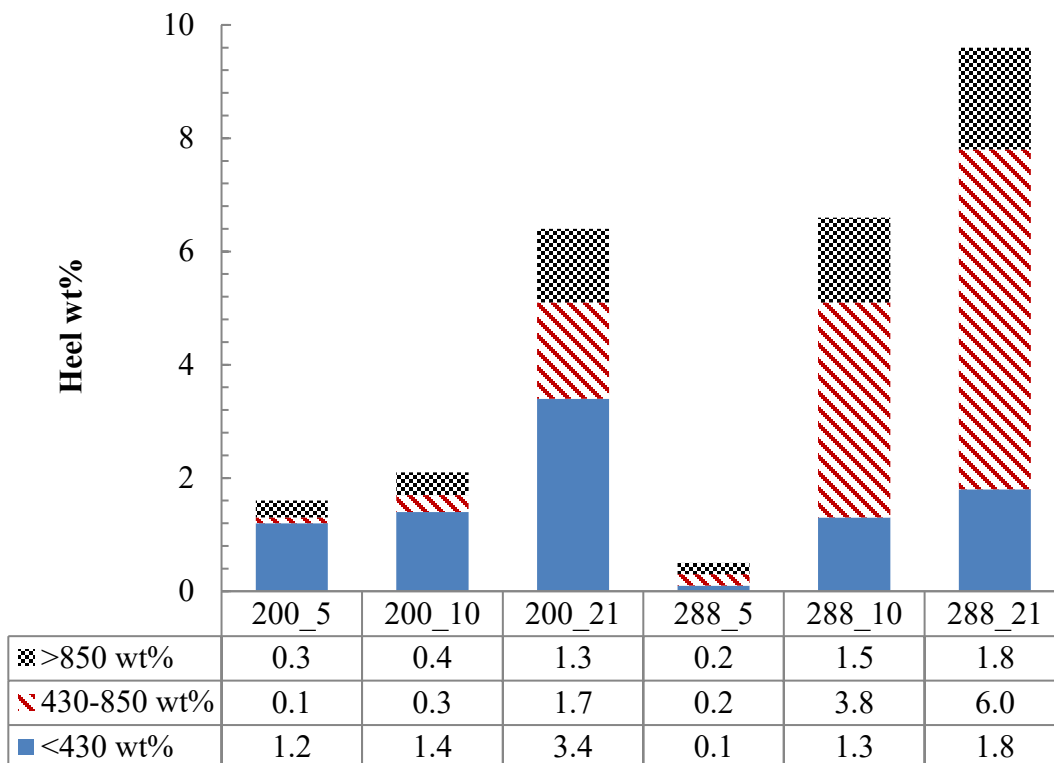


Figure 2-5. Percentage of the absolute cumulative heel ( $H_T = \text{Heel}_{<430} + \text{Heel}_{430-850} + \text{Heel}_{>850}$ ) obtained from DTG analysis

To quantify the effect of heel formation on the physical properties of the adsorbents, all the tested G-70R samples, as well as the virgin one, were examined using N<sub>2</sub> adsorption. The obtained values for the BET surface area, micropore volume, and total pore volume are reported in Table 2-1. Available pore volume was reduced (mostly micropore volume), as was the specific surface area compared to virgin G-70R. As the amount of heel increases, the reduction in pore volume and the

surface area also increases. The pore size distributions (PSD) of all samples are depicted in Figure 2-6.

Table 2-1. Comparison of the changes in the physical properties of the samples to the adsorption capacity reduction and heel build-up. Values are reported as mean  $\pm$  standard deviation of at least two runs.

Carbon sample	Adsorption capacity reduction %	Cumulative Heel %	BET surface area (m <sup>2</sup> /g)	Micropore volume (cm <sup>3</sup> /g)	Mesopore Volume (cm <sup>3</sup> /g)	Total pore volume (cm <sup>3</sup> /g)
Virgin G-70R	NA*	NA*	1380 $\pm$ 9	0.53 $\pm$ 0.01	0.04 $\pm$ 0.00	0.62 $\pm$ 0.01
200_5	1.6 $\pm$ 0.1	1.6 $\pm$ 0.0	1255 $\pm$ 12	0.51 $\pm$ 0.01	0.04 $\pm$ 0.00	0.59 $\pm$ 0.01
288_5	0.3 $\pm$ 0.0	0.5 $\pm$ 0.0	1325 $\pm$ 10	0.52 $\pm$ 0.00	0.04 $\pm$ 0.00	0.60 $\pm$ 0.01
200_10	1.7 $\pm$ 0.0	2.1 $\pm$ 0.1	1286 $\pm$ 14	0.50 $\pm$ 0.00	0.03 $\pm$ 0.00	0.58 $\pm$ 0.00
288_10	3.0 $\pm$ 0.1	6.6 $\pm$ 0.2	1167 $\pm$ 21	0.45 $\pm$ 0.01	0.04 $\pm$ 0.01	0.54 $\pm$ 0.00
200_21	3.3 $\pm$ 0.2	6.4 $\pm$ 0.3	1104 $\pm$ 17	0.44 $\pm$ 0.01	0.05 $\pm$ 0.00	0.53 $\pm$ 0.01
288_21	5.2 $\pm$ 0.2	9.6 $\pm$ 0.4	1071 $\pm$ 25	0.41 $\pm$ 0.02	0.04 $\pm$ 0.01	0.48 $\pm$ 0.02

\* Not applicable

Comparison of the PSDs among the samples 200\_5, 288\_5, and the virgin G-70R (Figure 2-6.a) shows a greater pore volume reduction for sample 200\_5 in the narrow micropore region up to about 7 Å. The loss of volume in the narrow micropore region of 200\_5 can be related to the kinetic diameter of TMB (6.1 to 6.7 Å). The interaction between the adsorbate and adsorbent surface is intensified with higher adsorption energy in these narrow micropores; hence, TMB molecules in these pores are tightly held and influenced by surrounding pore walls and require temperatures

higher than 200°C to be removed. Formation of Heel<sub>430-850</sub> in the G-70R pores constricts the adsorbent interior channels and further hampers desorption of physically-adsorbed TMB. This limits the ability of thermal desorption even at 288°C from driving out the physically-adsorbed TMB trapped in the narrow micropores. Comparing 288\_10 and 288\_21 in terms of amounts of Heel<sub><430</sub> and Heel<sub>430-850</sub> (Figure 2-5) shows that the G-70R pore sizes undergo more changes as the amount of Heel<sub>430-850</sub> increases, leaving greater amounts of adsorbate after desorption (Heel<sub><430</sub>). Another possibility for the simultaneous growth of Heel<sub><430</sub> and Heel<sub>430-850</sub> at high O<sub>2</sub> can be the reaction of TMB and O<sub>2</sub> to form larger molecules due to oxidative coupling and polymerization. If so, these larger molecules could be physically adsorbed in the G-70R pores requiring higher temperatures for removal (Heel<sub><430</sub>), and/or they might be chemisorbed onto the surface of G-70R (Heel<sub>430-850</sub>).

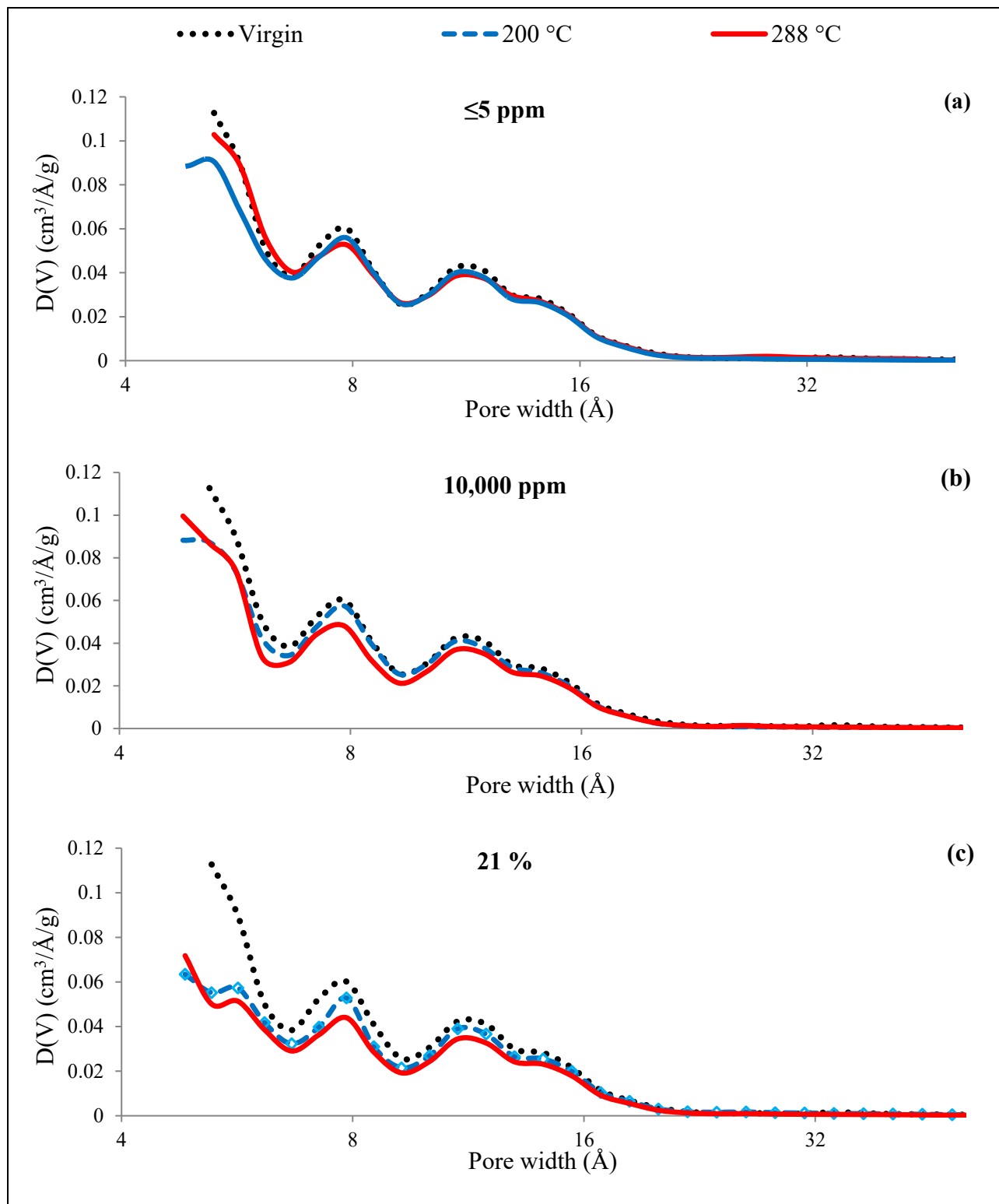


Figure 2-6. Pore size distribution (PSD) of G-70R after the 5-cycle adsorption/desorption of TMB using oxygen impurity of (a)  $\leq 5$  ppm, (b) 10,000 ppm, (c) 21% (Air)

Figure 2-6.b shows a noticeable pore volume reduction for 288\_10 relative to 200\_10, although both were desorbed with the same oxygen impurity of 10,000 ppm. Similar to the 200\_5 sample, 200\_10 showed a slight pore volume reduction due to non-desorbed species in the narrow micropore region ( $\leq 7 \text{ \AA}$ ) as a result of insufficient temperature to completely overcome the strong physisorption. However, oxygen impurity of 10,000 ppm at 288°C resulted in heel build-up (Heel<sub>430-850</sub> & Heel<sub>>850</sub>) over all of the micropore region ( $\leq 20 \text{ \AA}$ ) that can be attributed to the chemical reactions associated with the presence of oxygen. As discussed earlier, these reactions can cause either chemisorption of TMB onto activated carbon surface promoted by the oxygen's presence or can form larger molecules trapped in the narrow micropores as a result of the oxygen-induced reactions. To remove Heel<sub>430-850</sub>, a comparably higher temperature than the desorption temperatures used here are required to either reverse the chemisorption or decompose the polymerized molecules. However, to completely recover the adsorption capacity of activated carbon it may require further steps to gasify the deposited carbon (Heel<sub>>850</sub>) using an oxidizing agent such as water vapor or carbon dioxide [37].

Figure 2-6.c shows reductions in the pore volume for samples 200\_21 and 288\_21 throughout the micropore region, which further confirms the negative impacts of using air or desorption purge gas with a high level of O<sub>2</sub> impurity, particularly at higher desorption temperature (288°C).

## 2.5 Conclusions

The combined effects of desorption temperature and oxygen impurity on heel build-up in cyclic adsorption/desorption of TMB on G-70R was studied. Three impurity levels of oxygen in the purge

gas ( $\leq 5$  ppm, 10,000 ppm, 21% O<sub>2</sub> in N<sub>2</sub>) at two desorption temperatures of 200°C and 288°C were investigated.

At the lowest oxygen impurity condition ( $\leq 5$  ppm O<sub>2</sub> in N<sub>2</sub>), the 5-cycle adsorption/desorption test showed similar results at both 200°C and 288°C, except for the first cycle at 200°C in which the amount of heel was higher compared to 288°C because of the non-desorbed physisorbed adsorbate remaining in the narrow micropores. This was attributed to the insufficient temperature to overcome strong adsorbate/adsorbent interactions in the narrow micropores ( $\leq 7$  Å).

The effect of temperature on heel build-up was observed in the case of 10,000 ppm O<sub>2</sub> where minimal heel build was formed at 200°C (similar to the  $\leq 5$  ppm), but substantial heel build-up and adsorption capacity loss were observed at 288°C. TGA and N<sub>2</sub> adsorption tests performed on these samples suggested a noticeable contribution of apparently oxygen-induced reactions leading to the formation of heel at 288°C, even though higher temperature generally improves desorption by assisting heat and mass transfer.

At the highest oxygen impurity (21% O<sub>2</sub> in N<sub>2</sub>), the oxygen-induced reaction was observed at both 200°C and 288°C, indicating that even at the lower temperature (200°C), exposure of TMB to a relatively large number of oxygen molecules stimulates the reaction between O<sub>2</sub> and TMB. It was concluded that desorption efficiency is a multivariable function that the combined effect of purge gas O<sub>2</sub> impurity and temperature should be taken into account when optimizing desorption conditions. The results suggest several optimization opportunities to enhance the desorption efficiency, to reduce the operational costs, and to increase G-70R life-span in cyclic adsorption processes.



## 2.6 References

- [1] Roelant G. J., Kemppainen A. J., and Shonnard D. R., "Assessment of the Automobile Assembly Paint Process for Energy, Environmental, and Economic Improvement," *Journal of Industrial Ecology*, vol. 8, no. 1-2, pp. 173-191, 2004.
- [2] Popescu M., Joly J. P., Carré J., and Danatoiu C., "Dynamical adsorption and temperature-programmed desorption of VOCs (toluene, butyl acetate and butanol) on activated carbons," *Carbon*, vol. 41, no. 4, pp. 739-748, 2003.
- [3] Papisavva S., Kia S., Claya J., and Gunther R., "Characterization of automotive paints: an environmental impact analysis," *Progress in Organic Coatings*, vol. 43, no. 1, pp. 193-206, 2001.
- [4] Khan F. I. and Kr. Ghoshal A., "Removal of Volatile Organic Compounds from polluted air," *Journal of Loss Prevention in the Process Industries*, vol. 13, no. 6, pp. 527-545, 2000.
- [5] Kolta T., "Selecting Equipment to Control Air Pollution from Automotive Painting Operations," 1992. Available: <http://dx.doi.org/10.4271/920189>.
- [6] Suzuki M., *Adsorption Engineering*, Tokyo. Chemical Engineering Monographs, Elsevier Science Publishers, Amsterdam and New York, 1989.
- [7] Singh S. P., Depaoli D. W., Begovich J. M., Ashworth R. A., and Heyse E. C., "Review of methods for removing VOCs (volatile organic compounds) from the environment," ed, 1987.
- [8] Ruthven D. M., *Principles of Adsorption and Adsorption Processes*. Wiley, 1984.
- [9] Aktaş Ö. and Çeçen F., "Effect of type of carbon activation on adsorption and its reversibility," *Journal of Chemical Technology & Biotechnology*, vol. 81, no. 1, pp. 94-101, 2006.

- [10] Dąbrowski A., Podkościelny P., Hubicki Z., and Barczak M., "Adsorption of phenolic compounds by activated carbon—a critical review," *Chemosphere*, vol. 58, no. 8, pp. 1049-1070, 2005.
- [11] Yun J. H., Choi D. K., and Moon H., "Benzene adsorption and hot purge regeneration in activated carbon beds," *Chemical Engineering Science*, vol. 55, no. 23, pp. 5857-5872, 2000.
- [12] Ruthven D. M., "Principles of adsorption and adsorption processes," ed. New York: Wiley, 1984.
- [13] Suzuki M., Misic D. M., Koyama O., and Kawazoe K., "Study of thermal regeneration of spent activated carbons: Thermogravimetric measurement of various single component organics loaded on activated carbons," *Chemical Engineering Science*, vol. 33, no. 3, pp. 271-279, 1978.
- [14] Yonge D. R., Keinath T. M., Poznanska K., and Jiang Z. P., "Single-solute irreversible adsorption on granular activated carbon," *Environmental Science & Technology*, vol. 19, no. 8, pp. 690-694, 1985.
- [15] Grant T. M. and King C. J., "Mechanism of Irreversible Adsorption of Phenolic Compounds by Activated Carbons," *Industrial and Engineering Chemistry Research*, Article vol. 29, no. 2, pp. 264-271, 1990.
- [16] Lashaki M. J., Fayaz M., Wang H., Hashisho Z., Philips J. H., Anderson J. E., and Nichols M., "Effect of Adsorption and Regeneration Temperature on Irreversible Adsorption of Organic Vapors on Beaded Activated Carbon," *Environmental Science & Technology*, vol. 46, no. 7, pp. 4083-4090, 2012.
- [17] Leng C. C. and Pinto N. G., "Effects of surface properties of activated carbons on adsorption behavior of selected aromatics," *Carbon*, vol. 35, no. 9, pp. 1375-1385, 1997.

- [18] Vidic R. D., Suidan M. T., and Brenner R. C., "Impact of oxygen mediated oxidative coupling on adsorption kinetics," *Water Research*, vol. 28, no. 2, pp. 263-268, 1994.
- [19] Vidic R. D., Tessmer C. H., and Uranowski L. J., "Impact of surface properties of activated carbons on oxidative coupling of phenolic compounds," *Carbon*, vol. 35, no. 9, pp. 1349-1359, 1997.
- [20] Zeid N. A., Nakhla G., Farooq S., and Osei-Twum E., "Activated carbon adsorption in oxidizing environments," *Water Research*, vol. 29, no. 2, pp. 653-660, 1995.
- [21] Lashaki M. J., Atkinson J. D., Hashisho Z., Phillips J. H., Anderson J. E., Nichols M., and Misovski T., "Effect of desorption purge gas oxygen impurity on irreversible adsorption of organic vapors," *Carbon*, vol. 99, pp. 310-317, 2016.
- [22] Sabio E., González-Martín M. L., Ramiro A., González J. F., Bruque J. M., Labajos-Broncano L., and Encinar J. M., "Influence of the Regeneration Temperature on the Phenols Adsorption on Activated Carbon," *Journal of Colloid and Interface Science*, vol. 242, no. 1, pp. 31-35, 2001.
- [23] Urano K., Yamamoto E., and Takeda H., "Regeneration rates of granular activated carbons containing adsorbed organic matter," *Industrial & Engineering Chemistry Process Design and Development*, vol. 21, no. 1, pp. 180-185, 1982.
- [24] Lukomskaya A. Y., Tarkovskaya I. A., and Strelko V. V., "Chemisorption of o-xylene on activated carbons," *Theoretical and Experimental Chemistry*, journal article vol. 22, no. 3, pp. 357-360, 1986.
- [25] Hashemi S. M., Lashaki M. J., Hashisho Z., Phillips J. H., Anderson J. E., and Nichols M., "Oxygen impurity in nitrogen desorption purge gas can increase heel buildup on activated carbon," *Separation and Purification Technology*, vol. 210, pp. 497-503, 2019.

- [26] Hofelich T. C., Labarge M. S., and Drott D. A., "Prevention of thermal runaways in carbon beds," *Journal of Loss Prevention in the Process Industries*, vol. 12, no. 6, pp. 517-523, 1999.
- [27] Flowe M. The Energy Costs Associated with Nitrogen Specifications [Online]. Available: <https://www.airbestpractices.com/system-assessments/air-treatmentn2/energy-costs-associated-nitrogen-specifications>
- [28] Do D. D., *Adsorption Analysis: Equilibria and Kinetics* (Series on Chemical Engineering, no. Volume 2). Published by Imperial College Press and distributed by World Scientific Publishing Co., p. 916, 1998.
- [29] Ferro-García M. A., Joly J. P., Rivera-Utrilla J., and Moreno-Castilla C., "Thermal desorption of chlorophenols from activated carbons with different porosity," *Langmuir*, Article vol. 11, no. 7, pp. 2648-2651, 1995.
- [30] Kim K. J., Kang C. S., You Y. J., Chung M. C., Woo M. W., Jeong W. J., Park N. C., and Ahn H. G., "Adsorption-desorption characteristics of VOCs over impregnated activated carbons," *Catalysis Today*, vol. 111, no. 3, pp. 223-228, 2006.
- [31] Niknaddaf S., Atkinson J. D., Shariaty P., Lashaki M. J., Hashisho Z., Phillips J. H., Anderson J. E., and Nichols M., "Heel formation during volatile organic compound desorption from activated carbon fiber cloth," *Carbon*, vol. 96, pp. 131-138, 2016.
- [32] BAC Product Specifications [Online]. Available: <http://www.kurehacarbonproducts.com/bac.html>
- [33] Yuan B., Shao M., Lu S., and Wang B., "Source profiles of volatile organic compounds associated with solvent use in Beijing, China," *Atmospheric Environment*, vol. 44, no. 15, pp. 1919-1926, 2010.
- [34] Godish T., Davis W. T., and Fu J. S., *Air Quality*. CRC Press, 2014.

- [35] ISO 9277:2010, Determination of the specific surface area of solids by gas adsorption - BET method, 2010.
- [36] Leffler J. E. and Grunwald E., Rates and Equilibria of Organic Reactions: As Treated by Statistical, Thermodynamic and Extrathermodynamic Methods. Dover Publications, 2013.
- [37] Chen W., Wang X., Hashisho Z., Feizbakhshan M., Shariaty P., Niknaddaf S., and Zhou X., "Template-free and fast one-step synthesis from enzymatic hydrolysis lignin to hierarchical porous carbon for CO<sub>2</sub> capture," *Microporous and Mesoporous Materials*, vol. 280, pp. 57-65, 2019.

# **CHAPTER 3: EFFECTS OF AC PORE SIZE DISTRIBUTION ON OXYGEN INDUCED HEEL BUILD-UP**

## **3.1 Chapter Overview**

It was shown in chapter 2 that the desorption efficiency of volatile organic compounds (VOCs) from activated carbon (AC) is negatively affected by the presence of oxygen during thermal desorption. As a result, heel builds up and the adsorption capacity of AC diminishes in cyclic use. In this chapter, the contribution of the physical properties of AC (specific surface area, micropore volume, and total pore volume) to heel build-up was investigated. Three commercial ACs were tested through cyclic adsorption/desorption of 1,2,4-trimethylbenzene (TMB) using ultra-pure nitrogen ( $\leq 5$  ppm<sub>v</sub> O<sub>2</sub>) as the purge gas during thermal desorption. Each set of experiments was repeated with dry air ( $\sim 21\%$  O<sub>2</sub>) to evaluate the effect of O<sub>2</sub> on heel build-up. Pore size distribution (PSD) analysis, thermogravimetric analysis (TGA), and X-ray photoelectron spectroscopy (XPS) analysis, as well as Boehm titration method, were used to understand heel build-up mechanism in the presence of oxygen.

## **3.2 Introduction**

Volatile organic compounds (VOCs) are commonly used and emitted from a wide range of industrial processes including coating and painting activities [1, 2]. To control VOCs emission, activated carbon (AC) has been widely used owing to its excellent adsorption capacity and low cost [3]. Partially or fully saturated AC can be recycled through desorption, which is attainable commonly by pressure or vacuum swing adsorption (PSA/VSA), or temperature swing adsorption (TSA) processes. While PSA and VSA are more suitable for adsorbates with high volatility [4],

TSA is preferred for a wide range of adsorbates with moderate to low volatility [5] and has been effectively applied in the cyclic adsorption of VOCs [6]. However, even during the TSA cyclic process, not all the adsorbates are removed, consequently decreasing the adsorption capacity, shortening the life span of AC, and increasing the operational costs associated with AC replacement [7].

Several studies have been focused on the reasons for AC adsorption capacity loss in the cyclic TSA process [8-12]. Urano et al., Suzuki et al., and Liu et al., in three separate studies, tried to classify adsorbate behavior during the desorption process concerning. Their classifications can be unified as follows: 1) “vaporization type” corresponding to volatile adsorbates that can be removed in a single step by simple physical desorption; 2) “decomposition type” corresponding to strongly physisorbed or chemisorbed adsorbates that require thermal cracking followed by desorption; and 3) “carbonization type” corresponding to decomposed adsorbates that form a charred residue in the adsorbent.

According to the above-mentioned classification, adsorbates can be removed in different ways depending on their behavior during thermal desorption. The vaporization type of adsorbates can be removed in a single step through shifting the adsorption equilibrium by heating, vacuum, or other pathways such as solvent extraction. However, removal of the decomposition type adsorbates requires higher energies to break down the chemically formed bonds. Not all of the decomposed adsorbates can leave the pores and some may form a charred residue on the surface. This leads to permanent activity loss of adsorbent that is also known as non-desorbable heel. Therefore, physiochemical properties of both adsorbate and adsorbent, as well as operational conditions should be taken to the account when heel build-up is studied.

Oxygen impurity in the purge gas can increase heel build-up during thermal desorption of VOCs from activated carbon [13, 14]. Further, it was shown in our previous study [15] that in a certain level of oxygen content, increasing temperature promotes heel build-up. Although the effects of physical properties (e.g. pore size distribution and surface area) [16] and chemical properties (e.g. surface functional groups) [12, 17] of activated carbon on heel build-up have been previously reported, limited information is available regarding the effect of activated carbon physical properties on heel build-up when oxygen is present during thermal desorption of VOCs. Moreover, although the effect of oxygen on heel build-up has been proved [15], the nature of this heel and its thermal stability have never been reported. Therefore, the objective of this study is to bridge this gap by evaluating three activated carbons with distinct physical properties but similar chemical properties. The effect of oxygen presence during desorption was studied using air (~21% O<sub>2</sub>) as the desorbing purge gas against high purity nitrogen ( $\leq 5$  ppm O<sub>2</sub>) in cyclic adsorption/desorption. Thermogravimetric analysis (TGA), Surface area analysis by Nitrogen adsorption, and X-ray photoelectron spectroscopy (XPS) methods were used to analyze the physical and chemical characteristics of the virgin and tested activated carbons. Furthermore, Boehm titration was employed to assess the surface oxygen functional groups of virgin and tested ACs. The experimental results were used to investigate and identify the role of oxygen in the formation of heel during desorption.



### 3.3 Experimental

#### 3.3.1 Adsorbent and Adsorbate

Three activated carbons, B100777 supplied by Blucher GmbH, G-70R supplied by Kureha Corporation, and ACC-5092-20 (ACFC-20) supplied by Nippon Kynol Company were used as the adsorbents in this study. These adsorbents have similar surface chemical compositions (Table 3-1) with no or negligible ash content ( $< 0.1\%$  [18-20]) but different physical properties (specific surface area, micropore volume, and total pore volume, Table 3-2 and Figure 3-1). The characteristics of these adsorbents are useful when studying the effect of surface area and pore size distribution on heel build-up by ruling out other contributing parameters. Prior to the 5-cycle adsorption tests, all adsorbents were air dried at  $120\text{ }^{\circ}\text{C}$  for 24 h and then stored in a desiccator until they reached room temperature. In this study, letters of V, N, and A were used to indicate virgin AC, and AC desorbed using high purity nitrogen or air ( $\sim 21\%$   $\text{O}_2$ ) purge gas, respectively.

Table 3-1. The surface chemical composition (atomic %) of virgin activated carbons obtained from XPS analysis

Sample	Carbon (%)	Oxygen (%)	Nitrogen (%)	Sulfur (%)
ACFC-20-V	92.8	4.8	1.2	1.2
G-70R-V	90.8	6.1	1.4	1.7
B-100777-V	92.1	5.9	1.1	0.9

Table 3-2. BET surface area, micropore volume, total pore volume, and surface chemical composition of virgin activated carbons obtained by  $\text{N}_2$  adsorption at  $-195.8\text{ }^{\circ}\text{C}$

Sample	Specific surface area ( $\text{m}^2/\text{g}$ )	Total pore volume ( $\text{cc}/\text{g}$ )	Micropore volume ( $\text{cc}/\text{g}$ )	Microporosity (%)
--------	---	--	---	-------------------

ACFC-20-V	1940±14	0.73±0.01	0.71±0.01	97.2±0.5
G-70R-V	1380±13	0.62±0.01	0.53±0.01	85.5±0.8
B-100777-V	1745±9	1.78±0.02	0.66±0.01	37.1±0.4

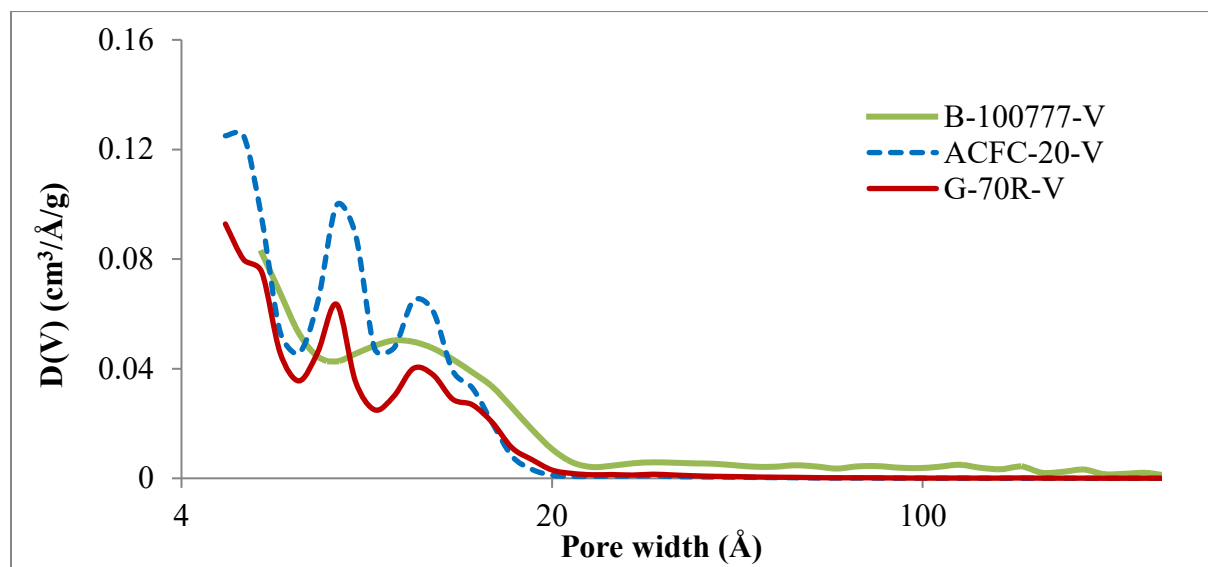


Figure 3-1. The pore size distribution of virgin activated carbons

Automotive paints contain aromatic compounds as the primary components accounting for more than 95% of the total emitted VOCs [21]. Hence, in this study, 1,2,4-trimethylbenzene (TMB, 98%, Sigma-Aldrich) was selected as a surrogate for VOCs from paint solvents. TMB has shown a high tendency to form heel in the presence of oxygen in previous studies [22]. During desorption, compressed N<sub>2</sub> (99.9984% pure, Praxair) and compressed dried air (99.999% pure, Praxair) were used as the purge gases.

### 3.3.2 Experimental Setup and Methodology

Description of the experimental setup is summarized here and the detailed description is provided elsewhere [15]. The experimental setup (Figure 3-2) consisted of an

adsorption/desorption tube, an adsorbate generation system, an organic gas measurement system, a heat application module, and a data acquisition and control system (DAC). For each experiment,  $1.0 \pm 0.05$  g of previously dried adsorbent was placed in a stainless-steel tube (10.2 mm inner diameter, 160.4 mm long). A syringe pump was used to inject a specified rate of liquid TMB in 10 standard liters per minute (SLPM) to generate an inlet concentration of 500 ppm<sub>v</sub> at 25 °C. The concentration of TMB was monitored using a flame ionization detector (FID; Series 9000, Baseline-Mocon Inc.) until stabilized at 500 ppm<sub>v</sub>, then the TMB stream was directed into the adsorption tube and adsorption started. The outlet concentration monitored using FID every 30 seconds to depict the breakthrough curve. After complete saturation, when the steady outlet concentration of 500 ppm<sub>v</sub> was observed (after 1 hour), the adsorption/desorption tube was weighed and wrapped with a heating tape and an insulation tape (Omega). The desorption step was performed by 1 SLPM purge gas. A power application module and a data acquisition and control (DAC) system controlled the applied power to maintain the bed temperature at 288 °C. Desorption was continued for 3 hours for complete desorption. The adsorption/desorption experiments were performed in 5 consecutive cycles to evaluate the cyclic performance of the adsorbents. All the experiments were duplicated, and the results were reported as arithmetic mean  $\pm$  standard deviation of two runs.

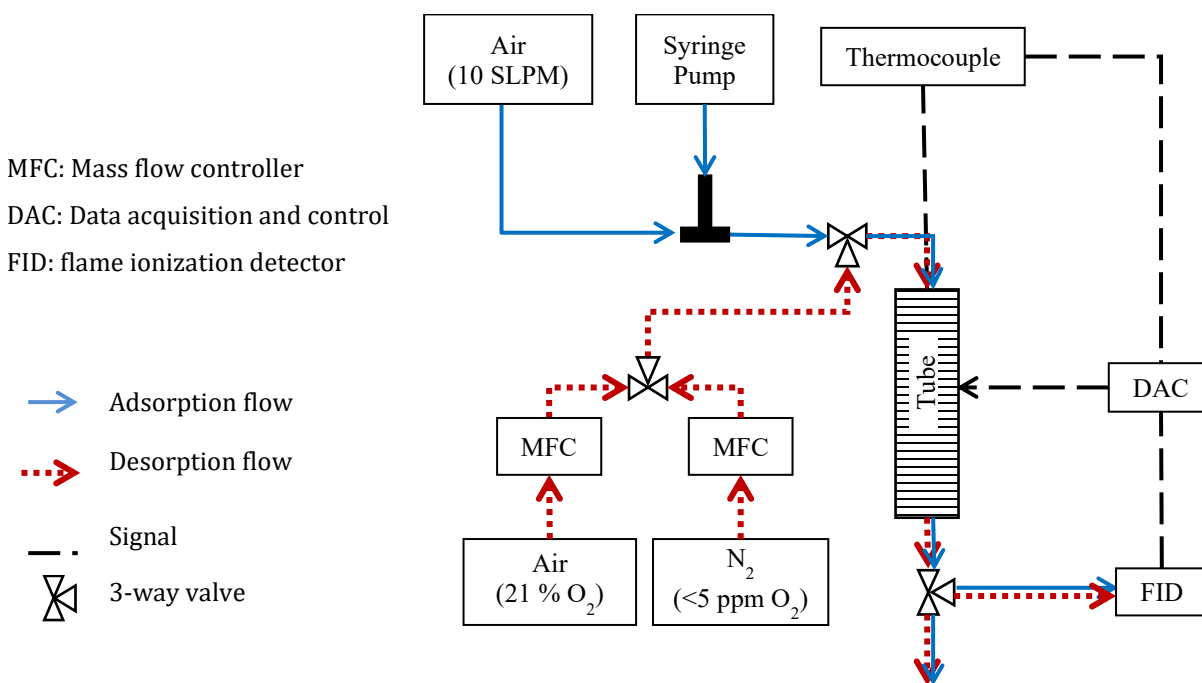


Figure 3-2. Schematic diagram of the adsorption-desorption setup

The weight of each adsorbent was measured before adsorption ( $W_{BA}$ ), after adsorption ( $W_{AA}$ ), and after desorption ( $W_{AD}$ ). The adsorption capacity ( $q$ ) was calculated as follows:

$$q_i (\%) = \frac{W_{AA_i} - W_{BA_i}}{W_I} \times 100$$

Where subscript “i” is the cycle number,  $W_I$  stands for the initial weight of dried virgin AC, and  $q_L$  is the total adsorption capacity loss after the 5<sup>th</sup> cycle.

The amount of non-desorbed species (also known as heel build-up) can be obtained by subtracting  $W_{AD}$  from  $W_{BA}$  after each adsorption/desorption cycle. Heel build-up ( $H_i$ ) is generally normalized

based on the initial weight of adsorbent to quantify the adsorption performance in cyclic use, and to characterize heel properties:

$$H_i (\%) = \frac{W_{ADi} - W_{BAi}}{W_i} \times 100$$

However, a comparison between different adsorbents should consider the adsorption capacity in addition to the weight of adsorbent. Adsorbents with higher capacity accommodate a higher amount of adsorbate in the pores and therefore in the case of any reaction involving the adsorbed phase, have a greater amount of reactants to form heel. Consider two samples with the same weight, one non-porous with zero adsorption capacity and another one highly porous with large adsorption capacity. Of course, in the earlier case no heel builds up as no adsorption occurs but heel may form in the second sample. Therefore, the adsorption capacity should be considered when comparing two different samples. AS a result, the heel build-up weight percent (Wt%) in this study was corrected by dividing ( $H_i$ ) by the adsorption capacity ( $q_i$ ) to calculate the corrected heel ( $H_{qi}$ ):

$$H_{qi}(\%) = \left( \frac{H_i}{q_i} \right) = \frac{W_{ADi} - W_{BAi}}{W_{AAi} - W_{BAi}} \times 100$$

The cumulative amount of heel ( $H_T$  or  $H_{qT}$ ) can be calculated by the summation of the produced heel from each cycle.

$$H_T(\%) = \sum_{i=1}^5 H_i (\%) \quad , \quad H_{qT}(\%) = \sum_{i=1}^5 H_{qi} (\%)$$

### 3.3.3 Characterization techniques

A volumetric gas sorption analyzer (Autosorb iQ2MP, Quantachrome) was used to evaluate the porous structure (surface area and pore size distribution) of the virgin and the 5-cycle tested adsorbents using nitrogen as a probe molecule. Adsorption was completed at nitrogen boiling point (-195.8 °C) and relative pressure ranging from  $10^{-7}$  to 1. Prior to analysis, 40 to 50 mg of each sample was degassed at 150 °C for 6 hours to remove adsorbed impurities. According to Brunauer, Emmet, and Teller (BET) model, N<sub>2</sub> isotherm at the low relative pressure range of 0.01 to 0.1 were used to calculate the specific surface area [23, 24]. Due to the disordered slit shape of the micropores in the activated carbons, the quenched solid density functional theory (QSDFT) method was used to estimate samples' pore size distribution (PSD), and to obtain micropore volumes (pore width <20Å) [25]. Total pore volume was calculated from N<sub>2</sub> isotherm at P/P<sub>0</sub> = 0.995.

Thermogravimetric analysis of the virgin and the 5-cycle tested ACs was carried out to evaluate the thermal stability of the heel developed in the adsorbent pores. To do so, samples' weights were measured during heating from 25 to 850 °C using TGA/DSC 1 (Mettler Toledo). To obtain high-resolution peaks from differential thermogravimetric (DTG) analysis, a slow heating rate of 2 °C /min with 50 standard cm<sup>3</sup>/min of N<sub>2</sub> (99.999% pure, Praxair) was used.

Surface elemental compositions and oxygen functional groups of the samples were analyzed using X-ray photoelectron spectroscopy (XPS, Kratos AXIS Ultra). The low-resolution spectra (0-1200 eV) were used to determine the surface atomic percentage of C, O, N, and S.

The surface oxygen functional groups (SOFGs) on the activated carbons' surface were also quantified using the Boehm titration method [26]. 10 mL of 0.025-N solutions of NaOH, Na<sub>2</sub>CO<sub>3</sub>, and NaHCO<sub>3</sub> were each added to 100 mg of dried carbon samples and shaken for 24 hours on a wrist shaker (Burrell Scientific). Thereafter, 5 mL of each solution was separated and back-titrated using 0.025-N HCl. The consumption of the weakest base, NaHCO<sub>3</sub>, was used to calculate the amount of strongest SOFGs (carboxylic groups), while Na<sub>2</sub>CO<sub>3</sub> was assumed to react with both lactone and carboxylic groups. The strongest base, NaOH, neutralized the total number of acidic groups (phenol, lactone, and carboxylic). Blank samples of each basic solution were also titrated for parallel reference and all titrations were triplicated and the average values are reported.

### **3.4 Results & Discussion**

#### **3.4.1 Adsorption capacity and heel build-up**

Figure 3-3 shows the 5-cycle adsorption breakthrough curves of the tested ACs. Using N<sub>2</sub> as the purge gas, the breakthrough curves showed no evident shifts between the cycles (Figure 3-3- a,c,e). However, using air (21% O<sub>2</sub>) resulted in the relatively remarkable and sequential shifts of the adsorption breakthrough curves hence, notably shortening the breakthrough time (Figure 3-3- b,d,f). This indicates the negative effect of oxygen during thermal desorption at 288 °C on adsorption capacity, which previously reported as heel build-up due to the oxidation of TMB at elevated temperatures [15].

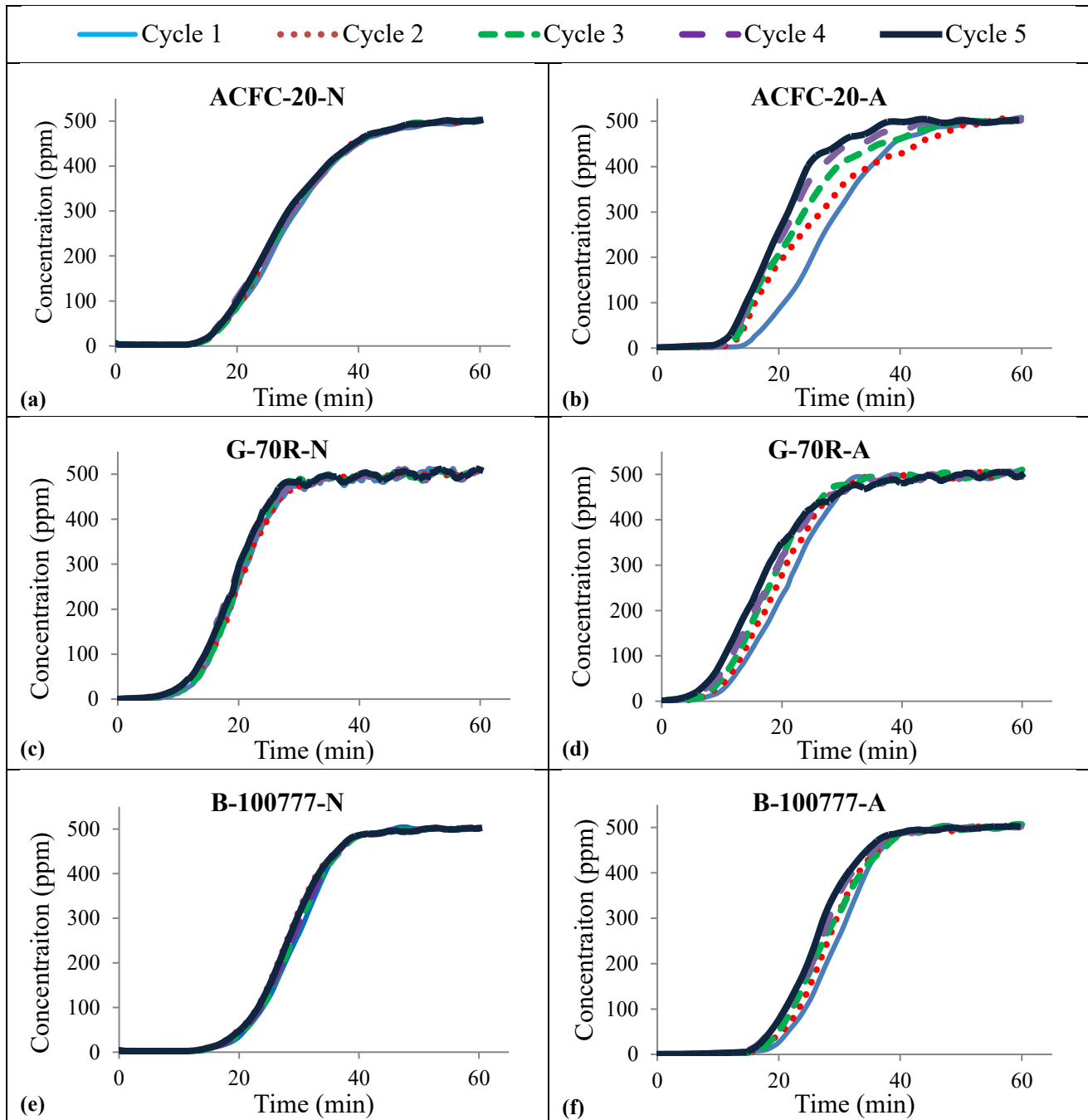


Figure 3-3. Breakthrough curves of TMB on ACFC-20, G-70R, and B-100777. N and A after the adsorbent name refers to ultra-pure nitrogen ( $\leq 5$  ppm<sub>v</sub> O<sub>2</sub>) and air ( $\sim 21\%$  O<sub>2</sub>) as desorption gas, respectively



Figure 3-3 shows the adsorption capacity and heel build-up of the first and last cycles. With both purge gases, gradual formation of heel for all the adsorbents with an almost constant adsorption capacity reduction per cycle was observed. Supporting the results from the breakthrough curves, negligible cumulative heel and total adsorption capacity losses ( $q_1 - q_5$ ) were observed in the case of N<sub>2</sub> desorption for all the adsorbents (<1.5 %). However, using air (21% O<sub>2</sub>), noticeably higher amounts of heel were observed, consequently higher adsorption capacity losses. Regarding the total heel ( $H_T$ ), B-100777-A and G-70R-A behaved similarly despite their dissimilar initial adsorption capacity, and ACFC-20-A resulted in nearly two times heel build-up compared to B-100777 although ACFC-20 showed less initial adsorption capacity. Taking the adsorption capacity into account, cumulative corrected-heel ( $H_{qT}$ ) was calculated to better correlate the physical properties of the three activated carbons with the heel build-up (Table 3-3). ACFC-20 with the highest microporosity (91.2%) exhibited  $H_{qT}$  of 30.5 % compared to 14.5 % for B-100777 with the microporosity of 37.1%; despite their similar specific surface area. The existence of larger pores (mesopores and macropores) in B-100777 can overcome the transport limitations of the micropores. In other words, having a hierarchy of pores eases the desorption and reduces heel build-up, particularly in the presence of oxygen. This can be concluded more clearly by comparing G-70R and B-100777; although G-70R has a lower surface area and total pore volume, it showed  $H_{qT}$  of 22.0% compared to 14.5% for B-100777 which again can be attributed to the relatively higher microporosity of G-70R (85.5 %).

Table 3-3. Adsorption capacity and heel build-up of activated carbons (Wt%)

Purge gas	Sample	1 <sup>st</sup> cycle adsorption capacity, $q_1$	5 <sup>th</sup> cycle adsorption capacity, $q_5$	Heel after the 1 <sup>st</sup> cycle, $H_1$	Cumulative heel, $H_T$	Corrected cumulative heel, $H_{qT}$
N <sub>2</sub> ( $\leq 5$ ppm <sub>v</sub> O <sub>2</sub> )	ACFC-20-N	61.2 $\pm$ 0.1	59.9 $\pm$ 0.2	0.2 $\pm$ 0.0	0.9 $\pm$ 0.1	1.5 $\pm$ 0.2
	G-70R-N	43.7 $\pm$ 0.1	43.4 $\pm$ 0.1	0.1 $\pm$ 0.0	0.5 $\pm$ 0.0	1.1 $\pm$ 0.0
	B-100777-N	66.2 $\pm$ 0.0	65.3 $\pm$ 0.1	0.1 $\pm$ 0.0	0.4 $\pm$ 0.1	0.6 $\pm$ 0.1
Air (21%O <sub>2</sub> )	ACFC-20-A	61.1 $\pm$ 0.1	49.3 $\pm$ 0.5	4.3 $\pm$ 0.2	18.6 $\pm$ 0.7	33.8 $\pm$ 1.3
	G-70R-A	43.8 $\pm$ 0.1	38.7 $\pm$ 0.3	1.7 $\pm$ 0.1	9.6 $\pm$ 0.4	23.4 $\pm$ 1.0
	B-100777-A	66.3 $\pm$ 0.1	62.3 $\pm$ 0.2	1.8 $\pm$ 0.1	9.6 $\pm$ 0.3	14.9 $\pm$ 0.5

The desorption profile of the activated carbons (Figure 3-4) shows the different desorption behavior of B-100777 compared to the other two microporous adsorbents. B-100777 desorption concentration peaked at noticeably lower temperatures than the other two adsorbents as a result of the co-presence of micropores and mesopores. In fact, higher diffusion resistance of microporous adsorbents (ACFC-20 and G-70R) would slow down the desorption process and expose the reactants (TMB and O<sub>2</sub>) to unwanted reactions at a higher temperature hence, promote heel build-up. Therefore, the hierarchical pore structure of adsorbents can be considered as an important parameter preventing heel build-up in adsorbents.

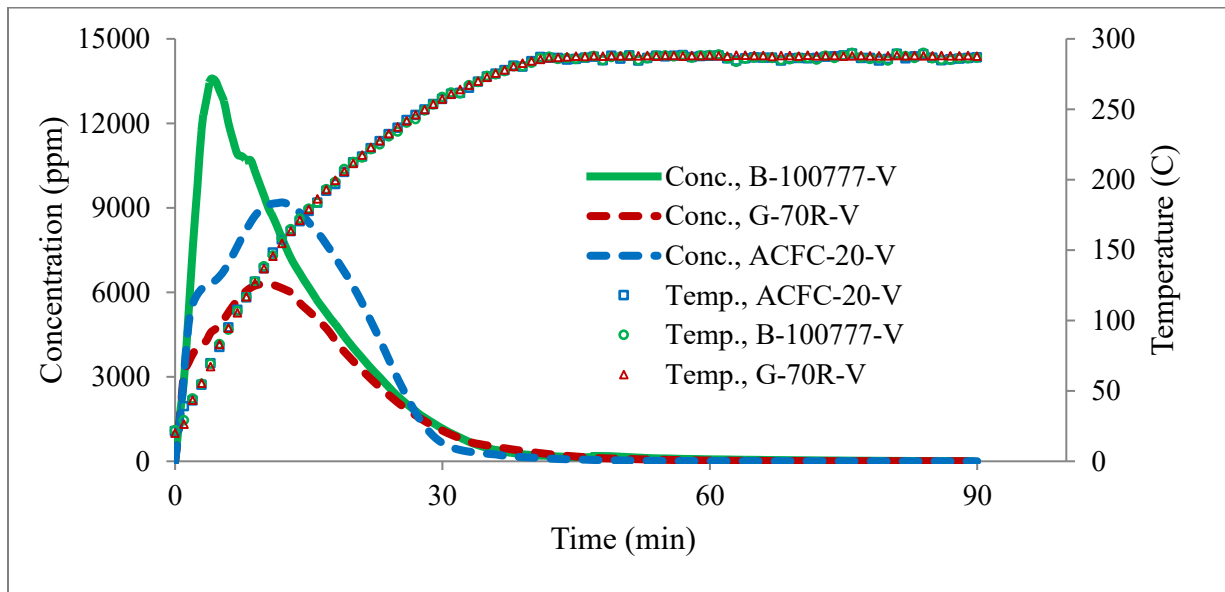


Figure 3-4. Temperature and desorption profile of TMB-loaded G-70R, B-100777, ACFC-20 for the 1<sup>st</sup> cycle using N<sub>2</sub>

### 3.4.2 Reversible and irreversible heel formation

Figure 3-5 shows the TGA results for all the adsorbents. The weight loss profile of samples desorbed in N<sub>2</sub> and the virgin samples overlapped, and no measurable differences were observed which agrees with the negligible heel formed in the case of using high purity N<sub>2</sub> as the purge gas. However, the samples desorbed using air (21% O<sub>2</sub>) showed noticeable weight losses beyond 288 °C up to 850 °C compared to the virgin ones.

The heel removed by heating to 850 °C ( $H_{R-850}$ ) can be calculated using the cumulative heel build-up percentage,  $H_T$  (%), and the DTG results normalized to the initial mass of virgin adsorbent:

$$H_{R-850} (\%) = \Delta WS_{850^\circ\text{C}} (\%) * \left( 1 + \frac{H_T(\%)}{100} \right) - \Delta WV_{850^\circ\text{C}} (\%)$$

$\Delta WS_{850^{\circ}\text{C}}$  and  $\Delta WV_{850^{\circ}\text{C}}$  are the weight losses (%) of the tested samples and virgin adsorbent, respectively, after TGA heating to 850°C.

Table 3-4. Removable heel percentage (%) by heating to 850 °C

	$H_{R-850}$	$(H_{R-850}/H_T) * 100$
ACFC-20-A	14.5	78
G-70R-A	7.7	80
B-100777-A	8.2	85

The percentages of the heel removed by heating to 850 °C relative to the cumulative heel build-up ( $H_{R-850}/H_T$ ) were calculated to be around 80% for all the samples desorbed in with (21% O<sub>2</sub>). About 20 % of the formed heel could not be removed by heating to 850 °C. This type of heel can be attributed to the carbonization of VOC that left charred residue in the adsorbents [15].

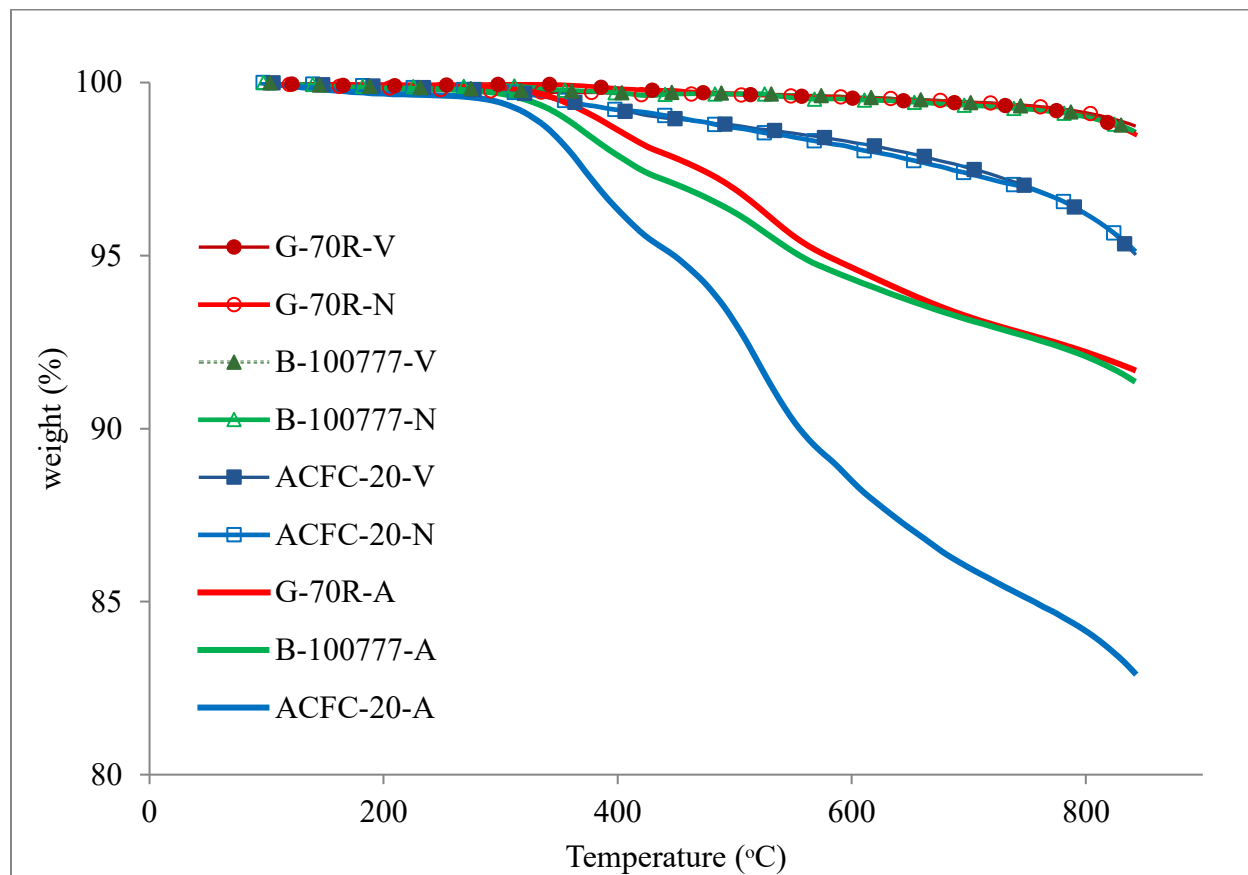


Figure 3-5. TGA of virgin and tested activated carbons

Figure 3-6 shows the DTG results indicating two major peaks for the samples desorbed with air (21% O<sub>2</sub>) at about 380 and 530 °C. These temperatures can represent either boiling points or decomposition temperatures of the products of reactions between TMB and oxygen. The chemical products of these reactions might be 1) high boiling point molecules strongly adsorbed to the carbon surface that need higher temperatures (350-400 °C) to leave the carbon, or 2) larger molecules formed and trapped into the pores with narrow openings which can only be removed by decomposition at very high temperatures (500-550 °C). ACFC-20-V with the highest microporosity exhibited the tallest DTG peaks, as expected since it developed the highest amount of heel. G-70R-A and B-100777-A displayed comparable peaks with higher weight loss at 350-

400 °C for B-100777-A, and at 500-550 °C for G-70R-A. this can be related to the existence of narrower slit-shaped pores in G-70R which trap the products of oxygen-induced reactions and result in heel formation inside the pores.

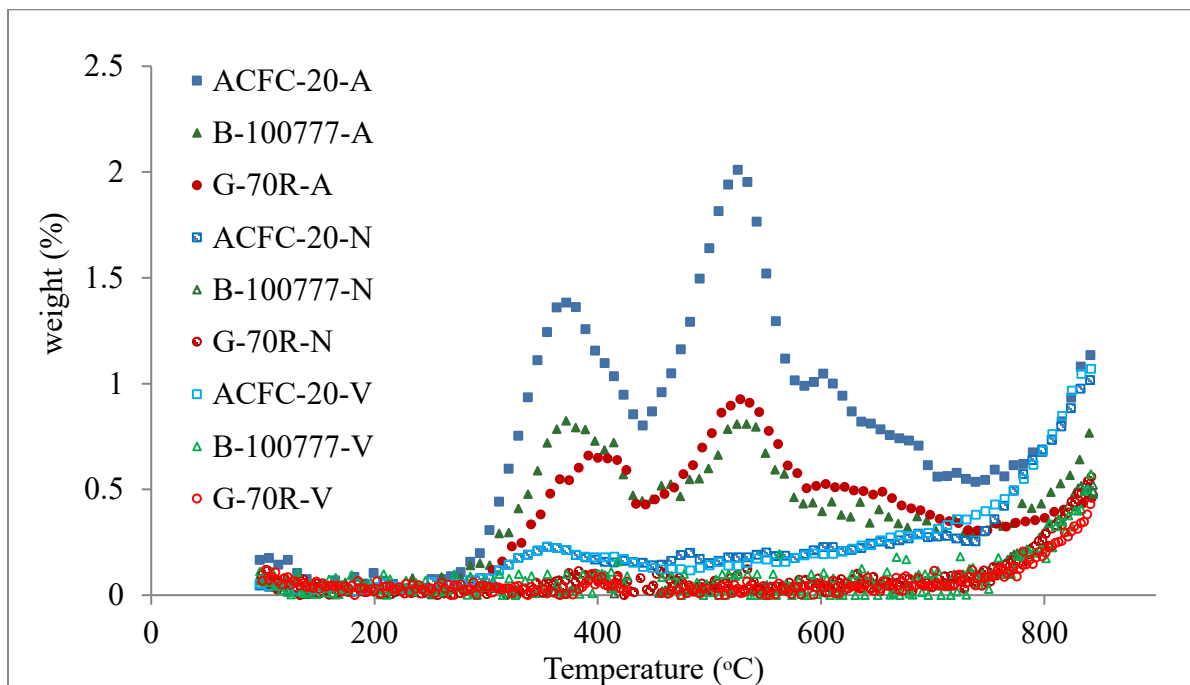


Figure 3-6. DTG of virgin and tested activated carbons

### 3.4.3 Surface area and pore size analysis

Figure 3-7 shows the pore size distributions (PSDs) for each adsorbent before and after the 5-cycle adsorption/desorption tests with N<sub>2</sub> and air (21% O<sub>2</sub>). For all adsorbents, PSD of the samples desorbed in N<sub>2</sub> was aligned with, but slightly below, that of the virgin samples, confirming the minimal heel build-up during high purity nitrogen desorption. However, the PSD of samples desorbed with air (21% O<sub>2</sub>) showed a noticeable reduction of the pore volume, mainly in the micropore region. For example, Figure 3-7c clearly shows how the micropore volume of B-100777

was reduced, while its pore volume distribution remained aligned with that of the virgin one throughout the mesopore region.

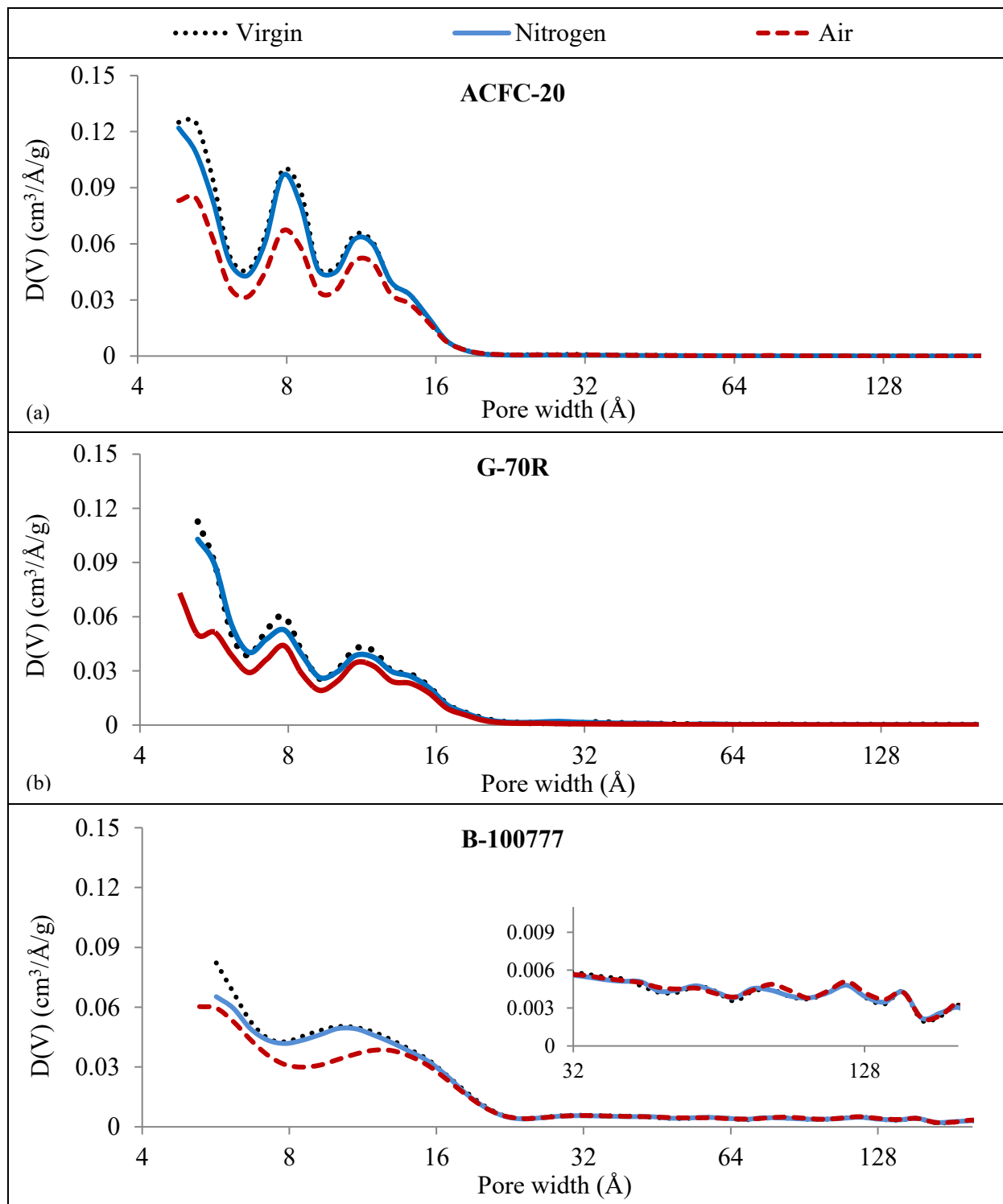


Figure 3-7. The pore size distribution of virgin and regenerated activated carbons



Table 3-5 summarizes the calculated data for the pore volume and specific surface area. For all the samples, micropore volume was reduced because of heel build-up which also decreased the available surface area. However, meso- and macropore volume remained nearly intact within each sample. For ACFC, micropore volume was reduced from 0.71 cm<sup>3</sup>/g for ACFC-V to 0.52 cm<sup>3</sup>/g for ACFC-A but the meso- macropore volume was not changed (0.2 cm<sup>3</sup>/g). Similarly, the meso- and macropore volumes of G-70R and B-10077 were not altered because of heel build-up. This confirms the contribution of the narrow micropores to heel build-up rather than the larger pores, perhaps due to the formation of larger molecules in the narrow pores as the most possible heel build-up mechanism in the presence of oxygen. These molecules are large enough to be strongly attached to the surrounding pore walls or even trapped inside the pores. Therefore, desorption would require temperatures higher than TMB boiling point to remove them in a single step or through two-steps of decomposition and removal process.

Table 3-5. BET surface area, micropore volume, meso-macropore volume, and the total pore volume of the tested activated carbons

Sample	BET surface area (m <sup>2</sup> /g)	Total pore volume (cm <sup>3</sup> /g)	Micropore volume (cm <sup>3</sup> /g)	Meso- and Macropore volume (cm <sup>3</sup> /g)
ACFC-20-V	1940±14	0.73±0.01	0.71±0.01	0.02±0.00
ACFC-20-N	1845±11	0.70±0.01	0.68±0.01	0.02±0.00
ACFC-20-A	1510±22	0.54±0.02	0.52±0.02	0.02±0.0
G-70R-V	1380±9	0.62±0.01	0.53±0.01	0.09±0.00
G-70R-N	1325±10	0.60±0.01	0.52±0.00	0.08±0.00
G-70R-A	1071±25	0.48±0.02	0.41±0.01	0.07±0.01
B-100777-V	1745±9	1.78±0.02	0.66±0.001	1.12±0.01
B-100777-N	1690±12	1.77±0.01	0.64±0.01	1.13±0.01
B-100777-A	1390±18	1.66±0.01	0.52±0.01	1.14±0.01

### 3.4.4 X-ray photoelectron spectroscopy (XPS)

While XPS analysis showed similar elemental compositions for the samples desorbed with N<sub>2</sub> as well as the virgin samples, a clear increase in surface oxygen was observed for all the samples desorbed by air (21% O<sub>2</sub>), Table 3-6. For samples desorbed in air, the surface content of Carbon, Nitrogen, and Sulfur remained nearly unchanged due to the inert role of nitrogen and the absence of sulfur in the purge gas; however, enriching these samples with oxygen resulted in relatively lower percentage values of Carbon, Nitrogen, and Sulfur on the surface. The increase of oxygen element in all the samples desorbed in the air suggests the oxidation as the main reaction.

Table 3-6. The surface atomic composition of virgin and regenerated activated carbons

Sample	Carbon (%)	Oxygen (%)	Nitrogen (%)	Sulfur (%)
ACFC-20-V	92.8	4.8	1.2	1.2
ACFC-20-N	93.1	4.3	1.5	1.1
ACFC-20-A	88.8	9.1	1.1	1.0
G-70R-V	90.8	6.1	1.4	1.7
G-70R-N	91.3	5.4	1.8	1.5
G-70R-A	81.9	15.5	1.2	1.4
B-100777-V	92.1	5.9	1.1	0.9
B-100777-N	91.7	6.2	1.3	0.8
B-100777-A	87.9	10.4	0.9	0.8

### 3.4.5 Boehm Titration

All samples were analyzed using Boehm titration to determine the concentration of different SOFGs. All virgin samples exhibited similar functional groups with about 0.1 mmol/g phenolic

group and a negligible amount of lactonic and carboxylic groups, confirming the similarity of the surface chemical properties of these three activated carbons. No noticeable differences were observed between the samples desorbed in N<sub>2</sub> and virgin samples. However, the amount of oxygen functional groups increased for all the samples desorbed by air (21% O<sub>2</sub>). The greatest increase in the SOFGs was observed for the phenolic groups followed by carboxylic groups.

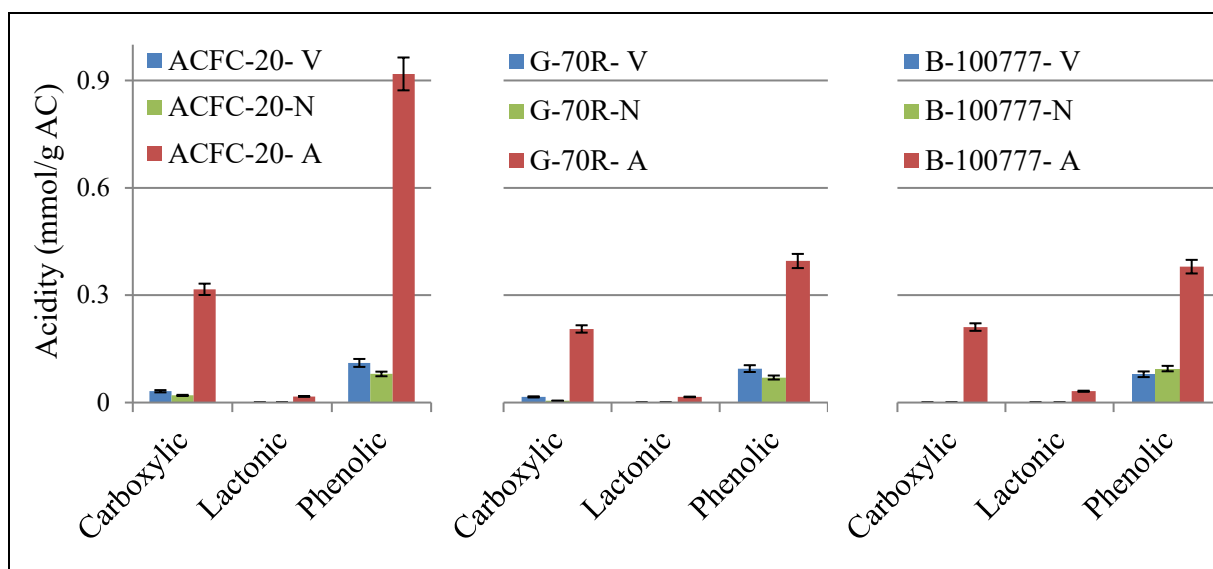


Figure 3-8. Boehm titration results for virgin and tested samples

It can be concluded that the increase of SOFGs was proportional to the heel formed on the samples. The total acidity of ACFC-20-A which has shown the highest cumulative heel was measured to be 1.25 mmol/g, higher than that of G-70R-A (0.62 mmol/g) and B-100777-A (0.62 mmol/g). To quantitatively compare the molar amount of detected functional groups (mmol/g) with the amount of heel (% g/g), the molecular weight of the formed molecules containing each SOFG is required. However, Various compounds with a wide range of molecular weight might be formed as products of the reaction between TMB and O<sub>2</sub>. A reasonable and simple estimate is to assume the lightest possible molecules representing these SOFGs. Therefore, Benzoic acid dimethyl was considered

as representative of the carboxylic group, methylphthalide for the lactonic group, and Dimethylphenol for the phenolic groups (Figure 3-9).

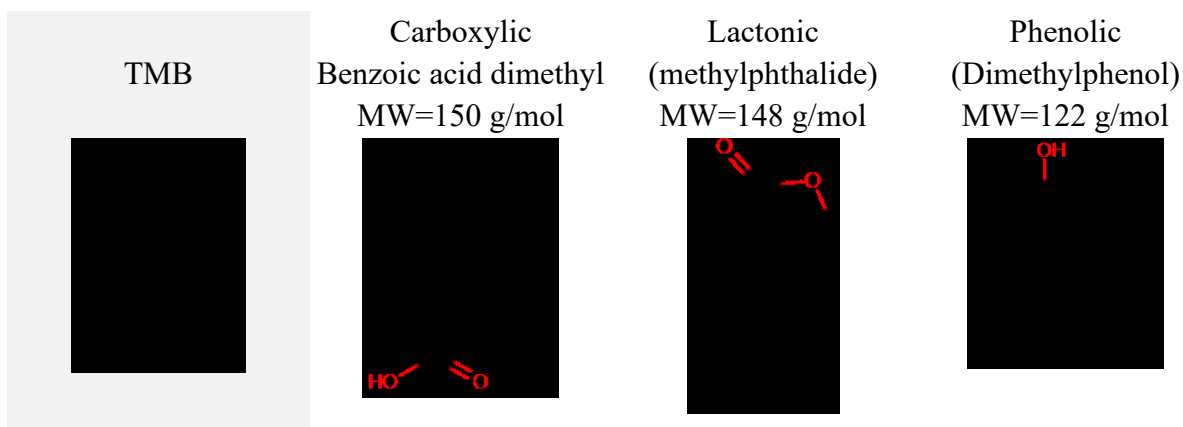


Figure 3-9. The lightest molecules representing SOFGs on the ACs' surface from TMB and O<sub>2</sub> reactions

With this assumption and using the molecular weight of each representative molecule, the acidity values were converted to weight percentage (Wt%) and reported in Table 3-7 using the following equation:

$$Wt\% = \frac{Acidity \left( \frac{mmol}{g} \right)}{MW \left( \frac{mol}{g} \right) * 1000} * 100$$

Table 3-7. Boehm titration analysis based on the molecular weight of the lightest possible molecules

	Weight percentage (Wt%) of oxygen-containing molecules		
	Carboxylic	Lactonic	Phenolic
ACFC-20-V	0.47±0.05	0.00±0.00	1.35±0.13
ACFC-20-N	0.30±0.02	0.00±0.00	0.98±0.08
ACFC-20-A	4.75±0.19	0.25±0.01	11.20±0.51

G-70R-V	0.24±0.02	0.00±0.00	1.16±0.12
G-70R-N	0.08±0.01	0.00±0.00	0.85±0.07
G-70R-A	3.09±0.15	0.23±0.01	4.83±0.24
B-100777-V	0.00±0.00	0.00±0.00	0.97±0.10
B-100777-N	0.00±0.00	0.00±0.00	1.16±0.09
B-100777-A	3.16±0.16	0.47±0.02	4.63±0.23

Finally, to compare the weight of assumed molecules containing the oxygen functional groups with the heel amount on the samples desorbed by air, the weight of SOFGs added to each adsorbent was calculated by subtracting the total SOFGs of the virgin samples from those of samples desorbed by air. Table 3-8 compares these Wt% values with the cumulative heel ( $H_T$ ) and the removable heel ( $H_{R-850}$ ) determined by TGA. The Wt% values for the SOFGs are slightly less than the  $H_T$  and  $H_{R-850}$  for each adsorbent, possibly because the lightest representative molecule for each functional group was assumed for the calculation. The ACFC-20-A that showed the highest cumulative heel of 18.6% resulted in the highest Wt% of the SOFG (14.4%). Similarly, the SOFG Wt% calculated for G-70R-A (6.8%) and B-100777-A (7.3%) agreed with the  $H_T$  values obtained from mass balance after the 5-cycle tests for G-70R-A (9.6%) and B-100777-A (9.6%) and correlated well with the removable heel ( $H_{R-850}$ ) obtained from TGA, which were 7.7% for G-70R-A and 8.2% for B-100777-A.

Table 3-8. Wt% of the total added SOFGs, cumulative heel ( $H_T$ ), and removable heel ( $H_{R-850}$ )

	Added SOFGs	$H_T$	$H_{R-850}$
ACFC-20-A	14.4	18.6	14.5
G-70R-A	6.8	9.6	7.7
B-100777-A	7.3	9.6	8.2

### 3.5 Conclusions

The effect of activated carbon's physical properties on heel build-up during desorption in low O<sub>2</sub> impurity ( $\leq 5$  ppm O<sub>2</sub>) and high O<sub>2</sub> content (air) was studied. 5-cycle adsorption/desorption tests of TMB on three commercial activated carbons with distinct physical properties were performed using high purity nitrogen and air as purge gases during desorption at 288 °C.

When N<sub>2</sub> ( $\leq 5$  ppm<sub>v</sub> O<sub>2</sub>) was used as the desorption purge gas, negligible impacts on heel build-up and breakthrough time were observed on the three activated carbons. On the other hand, using air as the desorption purge gas (21% O<sub>2</sub>) resulted in a large heel build-up and reduction in breakthrough time after each cycle. A higher amount of heel and consequently further adsorption capacity loss was observed for the adsorbents with higher microporosity. Monitoring the effluent TMB concentration during the desorption process showed a delay in the desorption of TMB from the microporous ACs. This delay extended the reaction time between TMB and O<sub>2</sub> and increased heel build-up for the ACs with higher microporosity.

Pore size distribution analysis of the samples desorbed by air (21% O<sub>2</sub>) showed a loss of pore volume mostly in the micropore region for all the three samples. Therefore, heel build-up was attributed to the formation of heavier molecules blocking the micropores as a result of TMB oxidation. Also, the abundance of micropores along with the scarcity of meso- macropores increased heel formation due to mass diffusion resistance, while the existence of the hierarchical pore structure resulted in lower heel build-up.

For all the samples desorbed by air, TGA showed that around 80% of the heel was removable by heating to a temperature of 850 °C in an inert atmosphere. Using DTG analysis, two major weight

loss peaks at around 380 and 530 °C were observed. This can be attributed to the boiling points or decomposition temperatures of heavier molecules formed as a result of the reaction of TMB with oxygen.

The increase in the surface oxygen content of the AC samples desorbed by air was explained using XPS analysis. Besides, Boehm titration on these samples showed a notable increase of SOFGs on these samples, which confirms the formation of oxygen-containing molecules during the desorption of TMB. These results support the proposed mechanism of heel build-up through oxidation reactions. The comparable values for the Wt% of the detected SOFGs and those of the removable heel from TGA showed that the produced oxygen-containing molecules are removable if a sufficient amount of energy is provided by high-temperature regeneration to either overcome the adsorption energy or thermal decomposition of trapped molecules.

### 3.6 References

- [1] Rafson H. J., *Odor and VOC control handbook*, Published by McGraw-Hill, New York, 1998.
- [2] Vega E., Mugica V., Carmona R. O., and Valencia E., "Hydrocarbon source apportionment in Mexico City using the chemical mass balance receptor model," *Atmospheric Environment*, vol. 34, no. 24, pp. 4121-4129, 2000.
- [3] Wypych G., "21 - Solvent Recycling, Removal, and Degradation" in *Handbook of Solvents (Third Edition)*, Chemical Technology Publishing, vol. 2, pp. 1635-1727, 2019.
- [4] Sircar S., "Pressure swing adsorption," *Industrial & Engineering Chemistry Research*, Editorial Material vol. 41, no. 6, pp. 1389-1392, 2002.
- [5] Levan M. D., "Thermal Swing Adsorption: Regeneration, Cyclic Behavior, and Optimization," in *Adsorption: Science and Technology*, A. E. Rodrigues, M. D. LeVan, and D. Tondeur, Eds. Dordrecht: Springer Netherlands, pp. 339-355, 1989.
- [6] Thomas W. J. and Crittenden B., "7 - Selected adsorption processes," in *Adsorption Technology & Design*, W. J. Thomas and B. Crittenden, Eds. Oxford: Butterworth-Heinemann, pp. 187-239, 1998.
- [7] De Jonge R. J., Breure A. M., and Van Andel J. G., "Reversibility of adsorption of aromatic compounds onto powdered activated carbon (PAC)," *Water Research*, vol. 30, no. 4, pp. 883-892, 1996.
- [8] Liu P. K. T., Feltch S. M., and Wagner N. J., "Thermal desorption behavior of aliphatic and aromatic hydrocarbons loaded on activated carbon," *Industrial & Engineering Chemistry Research*, vol. 26, no. 8, pp. 1540-1545, 1987.
- [9] Suzuki M., Misic D. M., Koyama O., and Kawazoe K., "Study of thermal regeneration of spent activated carbons: Thermogravimetric measurement of various single component



- organics loaded on activated carbons," *Chemical Engineering Science*, vol. 33, no. 3, pp. 271-279, 1978.
- [10] Urano K., Yamamoto E., and Takeda H., "Regeneration rates of granular activated carbons containing adsorbed organic matter," *Industrial & Engineering Chemistry Process Design and Development*, vol. 21, no. 1, pp. 180-185, 1982.
- [11] Vidic R. D., Suidan M. T., and Brenner R. C., "Impact of oxygen mediated oxidative coupling on adsorption kinetics," *Water Research*, vol. 28, no. 2, pp. 263-268, 1994.
- [12] Vidic R. D., Tessmer C. H., and Uranowski L. J., "Impact of surface properties of activated carbons on oxidative coupling of phenolic compounds," *Carbon*, vol. 35, no. 9, pp. 1349-1359, 1997.
- [13] Hashemi S. M., Lashaki M. J., Hashisho Z., Phillips J. H., Anderson J. E., and Nichols M., "Oxygen impurity in nitrogen desorption purge gas can increase heel buildup on activated carbon," *Separation and Purification Technology*, vol. 210, pp. 497-503, 2019.
- [14] Lashaki M. J., D. Atkinson J., Hashisho Z., H. Phillips J., Anderson J., Nichols M., and Misovski T., "Effect of desorption purge gas oxygen impurity on irreversible adsorption of organic vapors," *Carbon*, vol. 99, pp. 310-317, 2016.
- [15] Feizbakhshan M., Hashisho Z., Phillips J. H., Anderson J. E., Nichols M., "Effect of Oxygen impurity and desorption temperature on heel buildup on activated carbon," presented at the 68th Canadian Chemical Engineering Conference, Toronto, 2018.
- [16] Lashaki M. J., Atkinson J. D., Hashisho Z., Phillips J. H., Anderson J. E., and Nichols M., "The role of beaded activated carbon's pore size distribution on heel formation during cyclic adsorption/desorption of organic vapors," *Journal of Hazardous Materials*, vol. 315, pp. 42-51, 2016.

- [17] Lashaki M. J., Atkinson J. D., Hashisho Z., Phillips J. H., Anderson J. E., and Nichols M., "The role of beaded activated carbon's surface oxygen groups on irreversible adsorption of organic vapors," *Journal of Hazardous Materials*, vol. 317, pp. 284-294, 2016.
- [18] Hashisho Z., Rood M. J., Barot S., and Bernhard J., "Role of functional groups on the microwave attenuation and electric resistivity of activated carbon fiber cloth," *Carbon*, vol. 47, no. 7, pp. 1814-1823, 2009.
- [19] BAC Product Specifications [Online]. Available: <http://www.kurehacarbonproducts.com/bac.html>
- [20] "High-performance adsorbents based on activated carbon having high meso- and macroporosity," United States Patent US 2018/0125886, 2018.
- [21] Yuan B., Shao M., Lu S., and Wang B., "Source profiles of volatile organic compounds associated with solvent use in Beijing, China," *Atmospheric Environment*, vol. 44, no. 15, pp. 1919-1926, 2010.
- [22] Hashemi S. M., "Effect of desorption purge gas oxygen impurity on heel formation during regeneration of beaded activated carbon saturated with organic vapors," Master's Thesis, Civil and Environmental Eng., University of Alberta, 2017.
- [23] Brunauer S., Emmett P. H., and Teller E., "Adsorption of Gases in Multimolecular Layers," *Journal of the American Chemical Society*, vol. 60, no. 2, pp. 309-319, 1938.
- [24] Do D. D., *Adsorption Analysis: Equilibria and Kinetics* (Series on Chemical Engineering, no. Volume 2). Published by Imperial College Press and distributed by World Scientific Publishing Co., p. 916, 1998.
- [25] Neimark A. V., Lin Y., Ravikovitch P. I., and Thommes M., "Quenched solid density functional theory and pore size analysis of micro-mesoporous carbons," *Carbon*, vol. 47, no. 7, pp. 1617-1628, 2009.

- [26] Schönherr J., Buchheim R. J., Scholz P., and Adelhelm P., "Boehm Titration Revisited (Part I): Practical Aspects for Achieving a High Precision in Quantifying Oxygen-Containing Surface Groups on Carbon Materials," *Carbon*, vol. 4, no. 2, 2018.

# **CHAPTER 4: EFFECTS OF ADSORBENTS MATERIAL ON OXYGEN INDUCED HEEL BUILD-UP; COMPARISON OF ACTIVATED CARBON, ZEOLITE, AND POLYMER ADSORBENTS**

## **4.1 Chapter Overview**

The purpose of this chapter is to understand how to select a suitable adsorbent with the proper operating conditions when the cyclic TSA process is used in presence of oxygen. Three adsorbent materials (activated carbon, zeolite, and polymer) were studied via the temperature swing adsorption (TSA) process. The effect of two desorption temperatures (200 °C and 288°C) and three desorption purge gas oxygen concentrations ( $\leq 5$  ppm, 10,000 ppm, and 21%) on heel build-up and adsorption capacity of each adsorbent was investigated. Changes to the physical properties (surface area and pore volume) of each adsorbent were examined using N<sub>2</sub> adsorption. Further, the thermal stability of the formed heel on each adsorbent was analyzed using thermogravimetric analysis (TGA).

## **4.2 Introduction**

Volatile organic compounds (VOCs) are among the most common air pollutants [1]. VOCs are emitted from a wide range of industrial activities including oil and gas industries [2], paints and solvents [3], and transportation [4] as the major sectors. In the wake of environmental regulations [5, 6], various VOC abatement technologies have been developed under the two categories of destruction and recovery methods. In some industrial applications, involving costly VOCs such as

paint and coating, recovery methods including condensation, absorption, adsorption are advantageous over destruction methods [7]. Among these technologies, adsorption as the most economical and efficient control strategy has become increasingly popular [7-9].

Adsorption occurs as a result of interaction between the field of forces of the solid surface and fluid phase. The reverse phenomenon, desorption, is required to restore the adsorption capacity of adsorbent due to the accumulation of adsorbed substances on the solid surface. Various methods including thermal treatment [10], pressure variation [11], chemical extraction [12], and bio-regeneration [13] can be used for desorption. Choosing the proper desorption method relies upon different factors including properties of adsorbent and adsorbate. However, thermal desorption is the most economical method, particularly when adsorbents are thermally stable and the VOCs have very low vapor pressures [14, 15].

Activated carbon, zeolite, and polymer adsorbents have a high internal surface area and are widely used for VOCs emissions control. Activated carbon has been the first choice for the adsorption of VOCs on industrial scale owing to the low cost and high removal efficiency [9, 10, 16]. More recently, the use of zeolites and polymers has also emerged to control the emission of VOCs [17, 18]. Although Temperature Swing Adsorption (TSA) is the most common process for the regeneration of activated carbon and zeolite adsorbents [19], due to the low thermal stability of polymers, Pressure Swing Adsorption (PSA) is the most often method. Nevertheless, due to the simplicity and high removal efficiency, TSA may still be of interest in the case of polymer adsorbents but it must be ensured that the desorption temperature does not lead to bed fires [20].

The desorption operational conditions (i.e. temperature, purge gas composition and flowrate, and heating rate) can be optimized to save energy and reduce cost in the cyclic TSA process. At atmospheric pressure, generally, a temperature higher than the boiling point of the heaviest adsorbate is required to overcome the activation energy of adsorption. It is expected that increasing the desorption temperature shortens the process time and might improve the desorption efficiency by facilitating mass transfer and diffusion, specifically for the heavy adsorbates adsorbed in the narrow pores [21-23]. However, in the presence of any unwanted reactions, increasing the temperature can drive these reactions forward and result in heel formation on the adsorbents. To avoid any unfavorable reactions and bed fires during desorption, an inert purge gas such as N<sub>2</sub> is usually used [24]; however, impurities in the purge gas (mostly oxygen) can react with the adsorbate species or the adsorbent surface, which may result in heel build-up. Although using high purity nitrogen can diminish this type of heel, it increases the operational costs for nitrogen generation.

The objective of this study is to compare the performance of activated carbon, zeolite, and polymer adsorbent in the cyclic TSA process. For this purpose, 5-cycle adsorption/desorption experiments of TMB using the 3 adsorbent material were completed. During the desorption phase, the effect of temperature and purge gas oxygen impurities was also studied. The adsorbents were analyzed for the amount and stability of heel build-up, adsorption capacity loss, and changes to the specific surface area and pore volume.

## 4.3 Experimental

### 4.3.1 Adsorbent and Adsorbate

Activated carbon (BAC G-70R, Kureha Corporation), polymeric (DOWEX V503, DOW Chemical Company), and zeolite (HSZ-385, Y-type zeolite, Tosoh Corporation) were used in this study. They all are characterized by having a low content of ash and impurities, and high affinity to adsorb VOCs [35-37]. G-70R and V503 are beaded shape adsorbents with the particle size range of 0.3 to 1.0 mm; however, HSZ-385 was received as a powder hence it was pelletized, crushed, and sieved using the mesh standard numbers of 20 and 35 to select particles with a size range similar to the other two adsorbents. Prior to the 5-cycle adsorption tests, all the adsorbents were dried at 120 °C for 24 h and then stored in a desiccator until they reached room temperature.

To highlight the effect of oxygen presence on heel build-up, 1,2,4-trimethylbenzene (TMB, 98%, Sigma-Aldrich) was selected as a surrogate for VOCs emitted from the paint booth. TMB has shown earlier a high tendency to form heel [25, 38, 39].

### 4.3.2 Experimental setup and Methodology

Figure 4-1 shows the schematic of the adsorption/desorption setup used in this study and is described in detail elsewhere (Chapter 2). For each set of experiments, a stainless-steel adsorption tube (10.2 mm inner diameter, 160.4 mm long) was loaded with  $1.0 \pm 0.05$  g of dried adsorbent. In the adsorption step, a syringe pump was used to inject liquid TMB at a specified rate into a 10 standard liters per minute (SLPM) flow of air to generate an inlet concentration of 500 ppmv TMB at 25 °C. The concentration of TMB was monitored using a flame ionization detector (FID; Series

9000, Baseline-Mocon Inc.). After the TMB concentration was stabilized at 500 ppm<sub>v</sub>, adsorption was started by directing the TMB laden stream into the adsorption tube concurrent with starting the FID measurement of TMB concentration downstream of the adsorption tube to monitor adsorption breakthrough. Following saturation of the adsorbent, when the steady outlet concentration of 500 ppm<sub>v</sub> was observed (after 1 hour), adsorption was stopped, the weight of the adsorption tube was measured, and it was prepared for the desorption step by wrapping a heating tape and an insulation tape (Omega) around the tube.

In the desorption step, the required impurity of oxygen in the purge gas ( $\leq 5$  ppm, 10,000 ppm, and 21%) was achieved by mixing different flow ratios of compressed N<sub>2</sub> (99.9984% pure, Praxair) and compressed dried air (99.999% pure, Praxair). A power application module and a data acquisition and control (DAC) system controlled the applied power to maintain the bed temperature at the desired setpoint. Heating was continued for 3 hours to ensure complete desorption. The cyclic performance of the adsorbents was evaluated through 5 consecutive cycles of adsorption/desorption. Six sets of data were obtained for each of G-70R and HSZ-385 using two desorption temperatures of 200 °C and 288 °C and three different concentrations of oxygen in the purge gas ( $\leq 5$  ppm, 10,000 ppm, and 21%). For V503, desorption was performed with the three oxygen concentrations only at 200 °C due to the poor thermal stability of this polymeric adsorbent above this temperature. Each set of cyclic adsorption/desorption test was labeled by the temperature and the purge gas used during the thermal desorption. For example, 200\_5 and 200\_10 denote the desorption temperature of 200 °C with  $\leq 5$  ppm and 10,000 ppm oxygen impurity in the purge gas, respectively, and 288\_21 represents desorption at 288 °C with air (21% O<sub>2</sub>). All the experiments were duplicated, and the average values and standard deviation were reported herein.



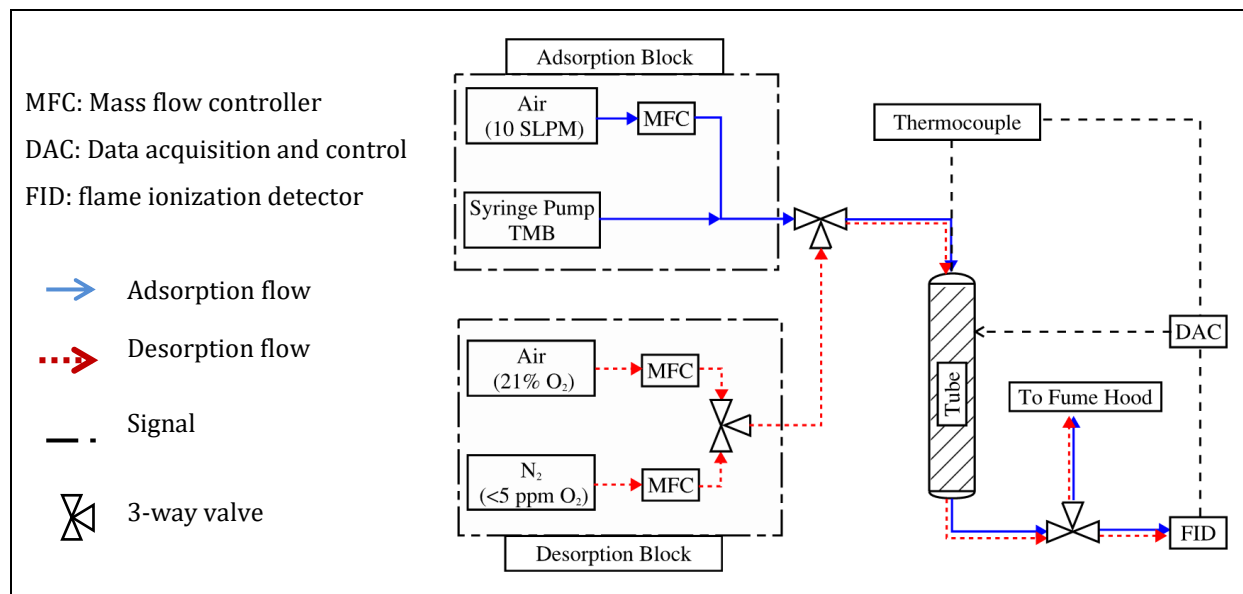


Figure 4-1, Schematic diagram of the adsorption-desorption setup

The weight of each adsorbent was measured before adsorption ( $W_{BA}$ ), after adsorption ( $W_{AA}$ ), and after desorption ( $W_{AD}$ ). The adsorption capacity ( $q$ ) was calculated as follows:

$$q_i (\%) = \frac{W_{AAi} - W_{BAi}}{W_i} \times 100$$

Where subscript “i” is the cycle number, and  $W_i$  stands for the initial weight of dried virgin AC.

The heel build-up percentage was calculated by subtracting  $W_{AD}$  from  $W_{BA}$  after each adsorption/desorption cycle and dividing the result to the initial weight of adsorbent:

$$H_i (\%) = \frac{W_{ADi} - W_{BAi}}{M_i} \times 100$$

Cumulative heel, which is the total added weight after 5 successive adsorption/desorption cycles, was calculated by adding up the heel of all 5 cycles.

### 4.3.3 Characterization techniques

A micropore surface area analyzer (Quantachrome, Autosorb iQ2MP) was used to evaluate the porous structure of the virgin and the 5-cycle tested adsorbents by using nitrogen as a probe molecule ( $10^{-6} < P/P_0 < 0.995$ ) at  $-196$  °C. Prior to analysis, 40 to 50 mg of each sample was degassed at  $150$  °C for 6 hours to remove impurities such as water vapor that might have been adsorbed later onto the samples. According to the Brunauer, Emmet, and Teller (BET) model, the slope and intercept of the  $N_2$  isotherm in the  $P/P_0$  range of 0.01 to 0.1 were used to calculate the specific surface area. The quenched solid density functional theory (QSDFT) method was used to obtain micropore volumes (pore width  $<20\text{Å}$ ) Total pore volume was also calculated from  $N_2$  adsorption at  $P/P_0 = 0.995$ .

Thermogravimetric analysis of the virgin and the 5-cycle tested adsorbents was carried out to evaluate the thermal stability of the heel developed into the adsorbent's pores. Samples' weights were measured during heating from  $25$  to  $850$  °C using a thermogravimetric analyzer (Mettler Toledo, TGA/DSC 1). To obtain high-resolution peaks from differential thermogravimetric (DTG) analysis, a slow heating rate ( $2$  °C /min) with  $50$  standard  $\text{cm}^3/\text{min}$  of  $N_2$  (99.999% pure, Praxair) was used.

## 4.4 Results & Discussion

### 4.4.1 Adsorption/Desorption at 200 °C

Figure 4-2, Figure 4-3, and Figure 4-4 show the 5-cycle breakthrough curves for the three adsorbents tested at the desorption temperature of 200 °C. The effect of purge gas oxygen content on the breakthrough time was noticeably different for each adsorbent.

G-70R demonstrated the longest breakthrough time (5% of influent concentration) among the adsorbents. The breakthrough time decreased during subsequent adsorption cycles on this adsorbent with the highest impact observed in the case of purge gas oxygen content of 21% (Figure 4-2). The 5-cycle tests on V-503 were found to be largely different for the three purge gas conditions (Figure 4-3). This adsorbent performed well when the oxygen content was the least ( $\leq 5$  ppm) and the breakthrough curves of different cycles overlapped on each other. The increase of oxygen content to 10,000 ppm resulted in small shifts in the breakthrough curves after each adsorption cycle with no visible changes in the curve shape. However, for the tests performed with 21% oxygen in the purge gas, the shape of the curve changed after the first cycle with almost immediate breakthrough times for the second cycle onward.

HSZ-385, a Y-Type zeolite with a high  $\text{SiO}_2/\text{Al}_2\text{O}_3$  ratio, has been shown to have high thermal stability [29]. The impacts of purge gas oxygen content on the HSZ-385 were not visible and the overlapped breakthrough curves for all three cases suggest a limited reduction in adsorption breakthrough times of these samples (Figure 4-4).

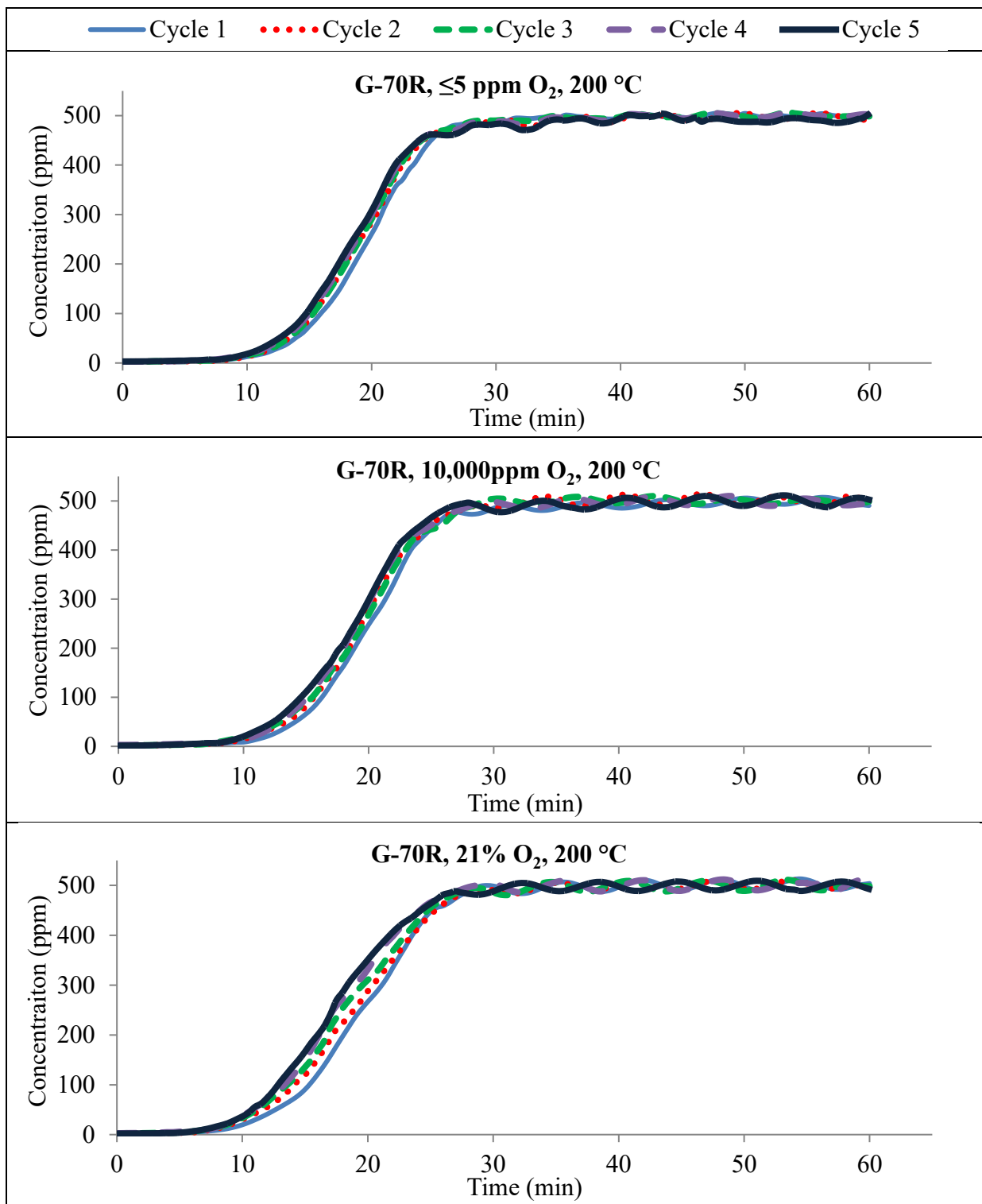


Figure 4-2. Adsorption breakthrough curves for TMB on G-70R samples desorbed at 200°C with different oxygen content in the purge gas

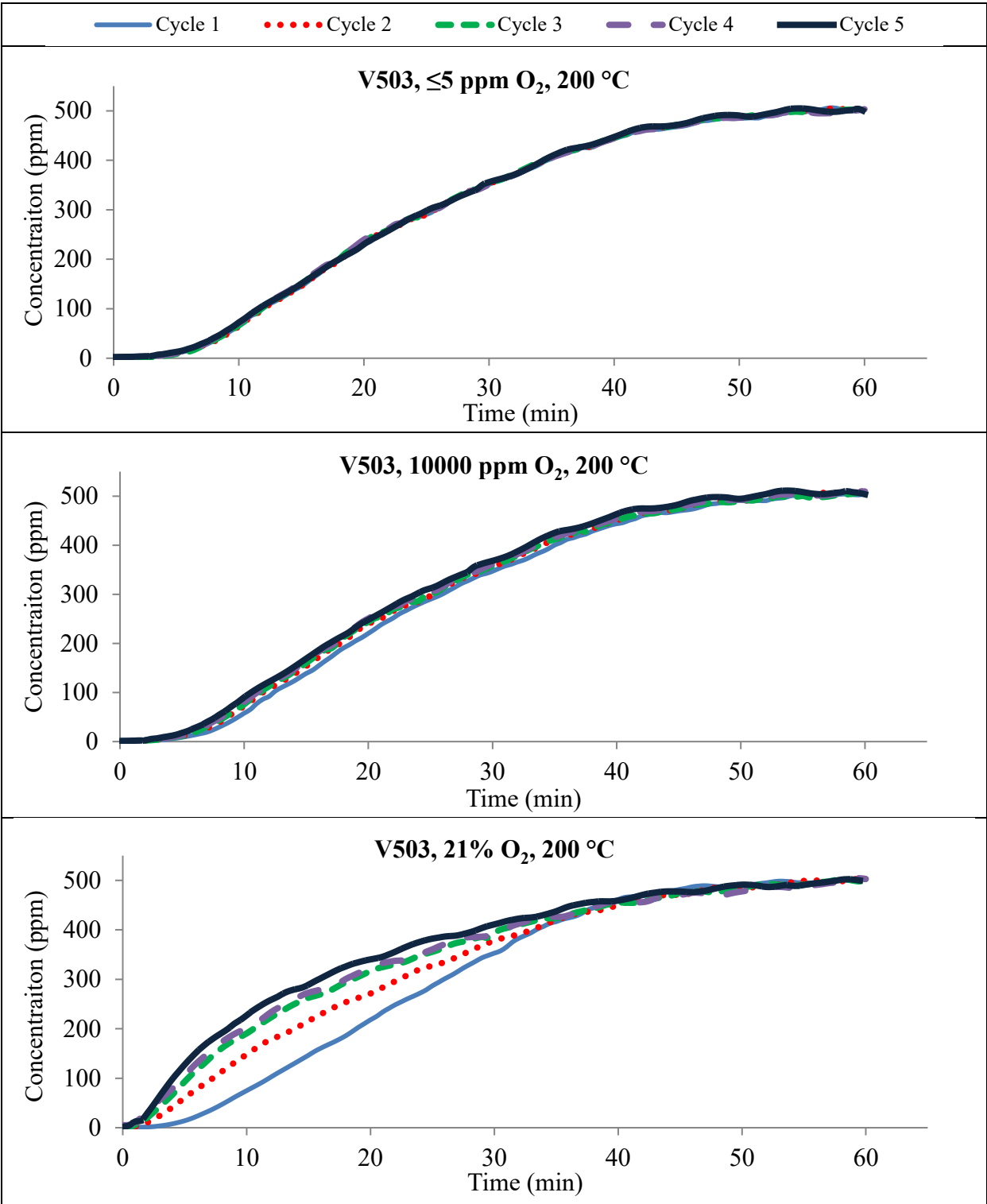


Figure 4-3. Adsorption breakthrough curves for TMB on V503 samples desorbed at 200°C with different oxygen content in the purge gas

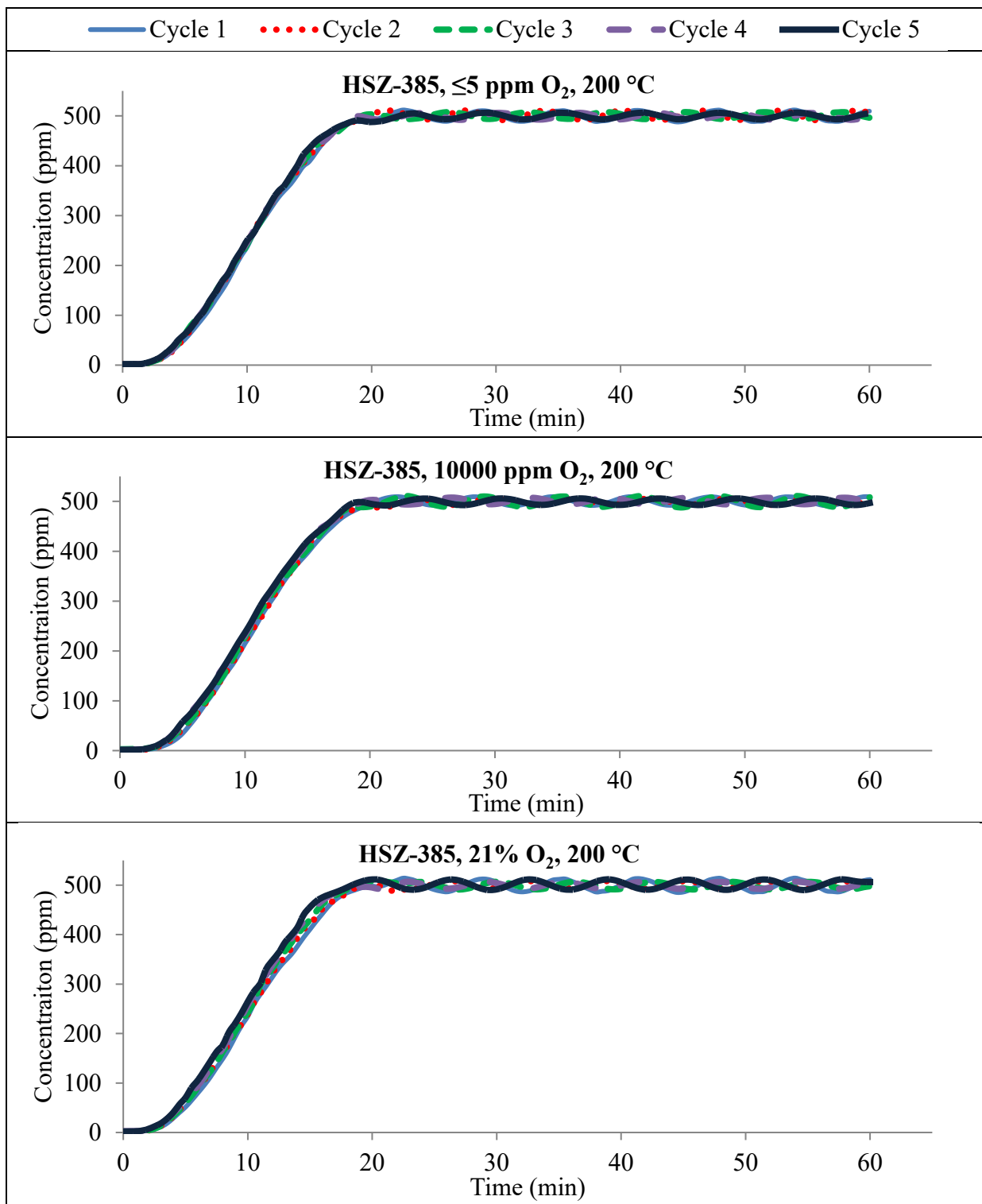


Figure 4-4. Adsorption breakthrough curves for TMB on HSZ-385 samples desorbed at 200°C with different oxygen content in the purge gas

In the case of G-70R desorbed with  $\leq 5$  ppm  $O_2$  in the purge gas, 1.50 % heel was observed after the 1<sup>st</sup> cycle with nearly no change for the next 4 cycles resulting in 1.60 % cumulative heel (Figure 4-5). The heel for the 1<sup>st</sup> cycle can be attributed to the strong physical adsorbate-adsorbent interaction in activated carbon's narrow micropores which made the temperature of 200 °C insufficient to desorb TMB (boiling point of 169.4 °C) [26]. However, for the subsequent cycles, negligible heel addition was observed since those narrow micropores have already been filled in the first cycle. This implies that using high purity  $N_2$  as the purge gas could keep the adsorption capacity of activated carbon nearly constant over cyclic use. Increasing the purge gas oxygen concentration to 10,000 ppm increased the cumulative heel to 2.1 %, which shows the negative effect of oxygen impurity in the thermal desorption of activated carbon. However, due to the increased energy consumption and production cost of high purity nitrogen, this small change in heel buildup suggests an optimization opportunity for a cost analysis study. Finally, using air with 21 % of oxygen as the desorption purge gas showed a substantial and steady formation of heel in each cycle on the G-70R resulting in 6.5 % of the cumulative heel (Figure 4-5). This can be explained by the exposure of TMB to a relatively large number of oxygen molecules, which provides enough collisions between oxygen and TMB molecules and stimulates the reactions between  $O_2$  and TMB. The result of these reactions is heel build-up in the narrow pores of activated carbon [25].

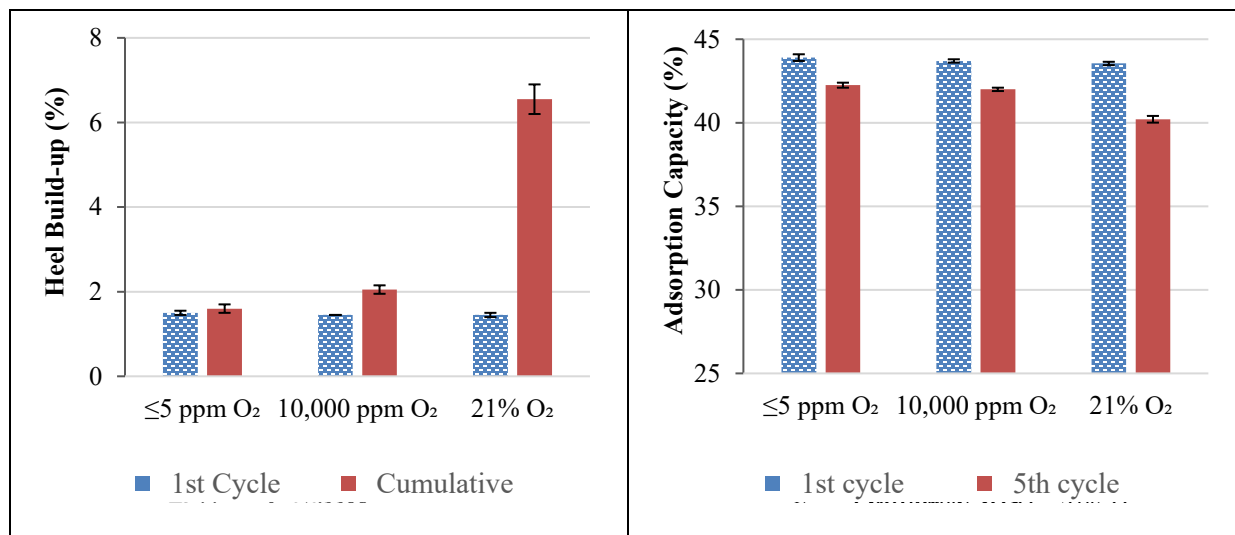


Figure 4-5. Adsorption capacity and heel build-up for activated carbon G-70R desorbed at 200 °C. Error bars indicate the standard deviation of the arithmetic mean of two sets of data

Using Dowex V503, complete desorption of TMB was observed using  $\leq 5$  ppm O<sub>2</sub> in the purge gas, with a negligible cumulative heel of 0.2 % and only 0.1 % adsorption capacity loss after 5 adsorption/desorption cycles. This shows that Dowex V503 can withstand a desorption temperature of 200°C when the oxygen content is  $\leq 5$  ppm.

Using 10,000 ppm O<sub>2</sub> in the purge gas, the 5-cycle cumulative heel slightly increased to 0.35 % on Dowex V503; however, it resulted in a relatively higher adsorption capacity loss of 1.3 %. Further increase of the oxygen content in the purge gas to 21%, i.e. using air as a desorption purge gas, the cumulative heel on Dowex V503 was observed to be 2.1%, however, the adsorption capacity was largely reduced from the 1<sup>st</sup> cycle through the 5<sup>th</sup> cycle by 14.7%, which is disproportionate to the heel amount. Comparing the breakthrough curves of this case with the two other cases of oxygen contents, a different breakthrough profile can be seen with notable changes in the slope of breakthrough curves over the 5 cycles (Figure 4-3). This can be attributed to damages to the pore structure of Dowex V503 because of pore network distortion or material



decomposition rather than pore blockage. Key building blocks of Dowex V503 are built from styrene and it has been previously reported that the benzene ring of styrene can be aggressively attacked by the oxygen molecules at elevated temperatures [27, 28]. Therefore, the entire surface of this styrene-based adsorbent can be negatively affected during desorption in presence of high oxygen content. Consequently, since Dowex V503 cannot tolerate oxygen presence at 200 °C, it is not suitable for thermal desorption at or above 200 °C.

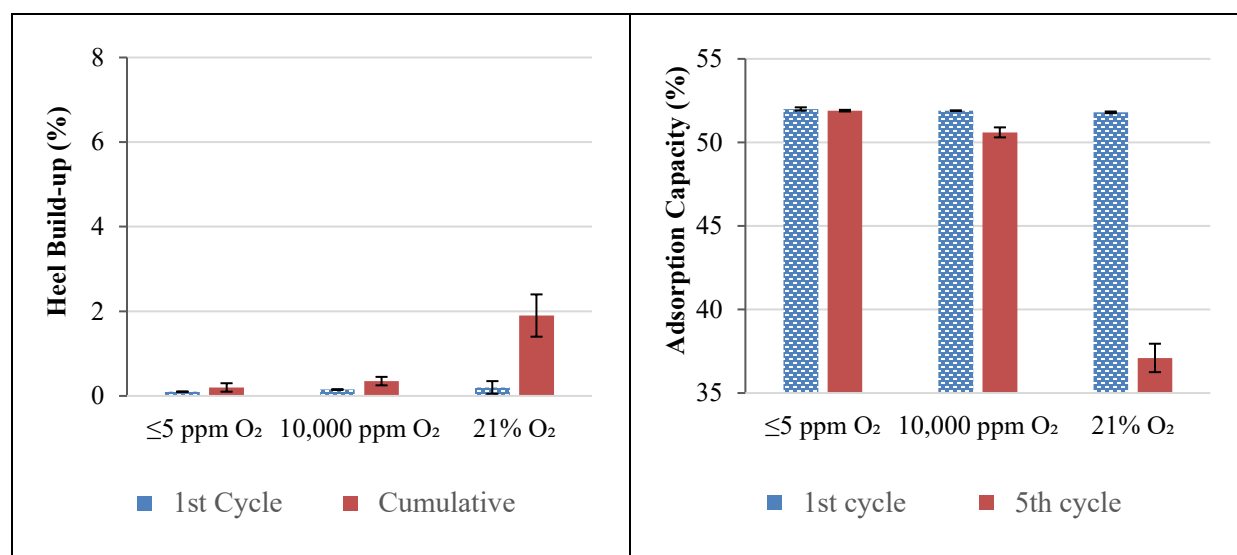


Figure 4-6. Adsorption capacity and heel build-up for polymer adsorbent Dowex V503 desorbed at 200 °C. Error bars indicate the standard deviation of the arithmetic mean of two sets of data

The 5-cycle cumulative heel build-ups on zeolite HSZ-385 were observed as little as 0.25%, 0.35%, 0.85% for the desorption with ≤5 ppm O<sub>2</sub>, 10,000 ppm O<sub>2</sub>, and 21% O<sub>2</sub>, respectively. Accordingly, the adsorption capacity loss for HSZ-385 from the 1<sup>st</sup> cycle to the 5<sup>th</sup> cycle was less than 0.40 % for all the three O<sub>2</sub> concentrations (Figure 4-7) which indicates the negligible effect of oxygen at this temperature on heel build-up and consequently adsorption capacity loss on HSZ-

385. These experiments showed the durability of HSZ-385 for the cyclic adsorption of VOCs and desorption in presence of oxygen.

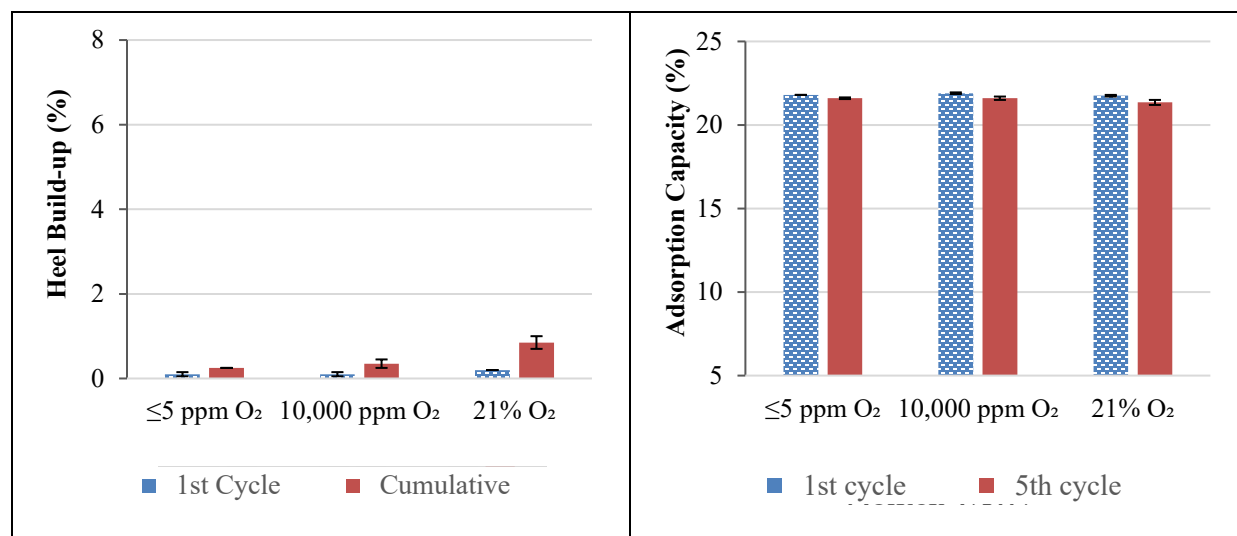


Figure 4-7. Adsorption capacity and heel build-up for zeolite HSZ-385 samples desorbed at 200 °C. Error bars indicate the standard deviation of the arithmetic mean of two sets of data

#### 4.4.2 Adsorption/Desorption at 288 °C

The 5-cycle adsorption tests with the desorption temperature of 288 °C were performed only on G-70R and HSZ-385. Dowex V503 was excluded due to its inability to withstand 288 °C at high oxygen concentrations. Figure 4-8 and Figure 4-9 show the 5-cycle breakthrough curves for G-70R and HSZ-385 adsorbents tested at the desorption temperature of 288 °C.

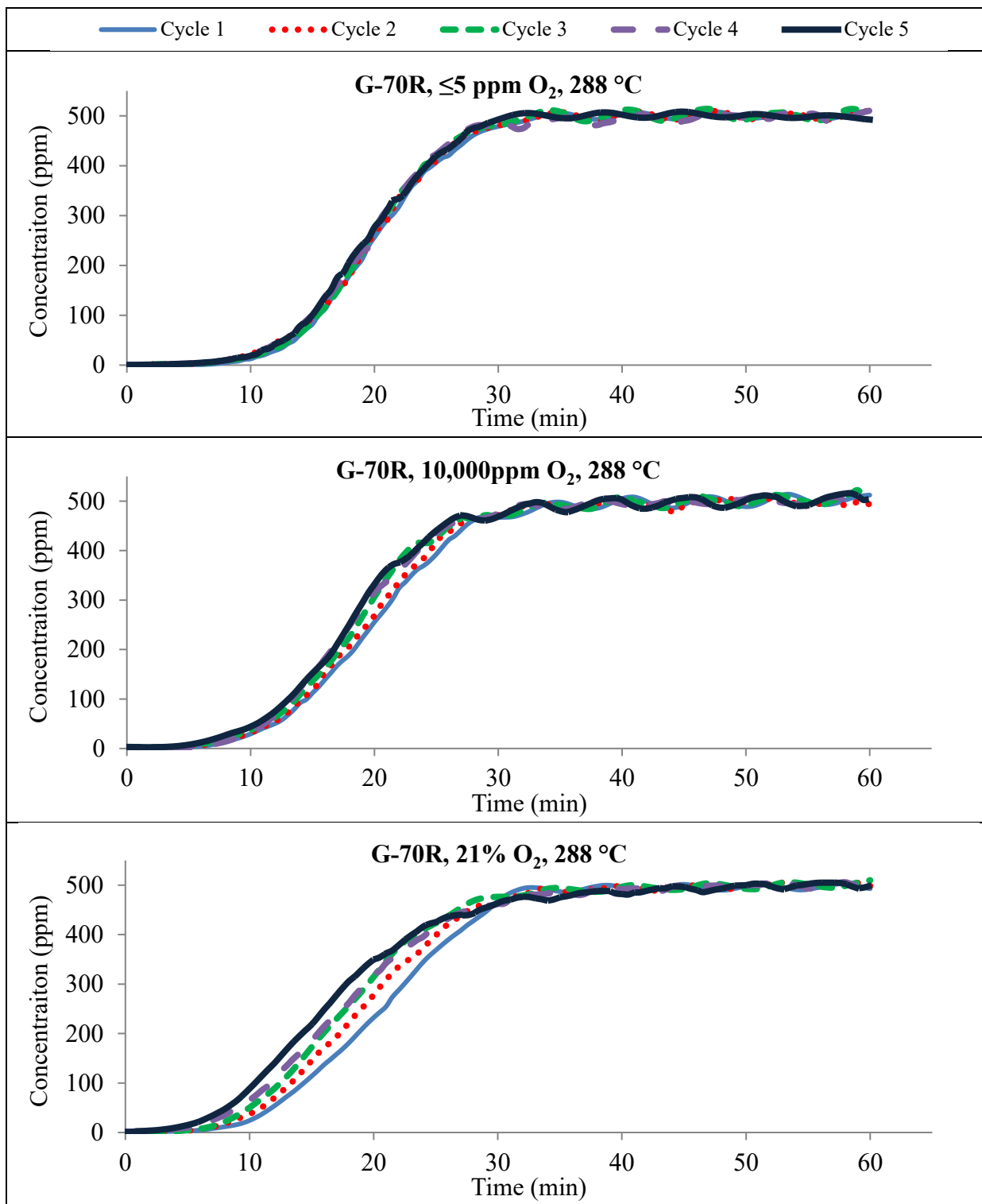


Figure 4-8. Adsorption breakthrough curves for TMB on G-70R samples desorbed at 288°C with different oxygen impurities

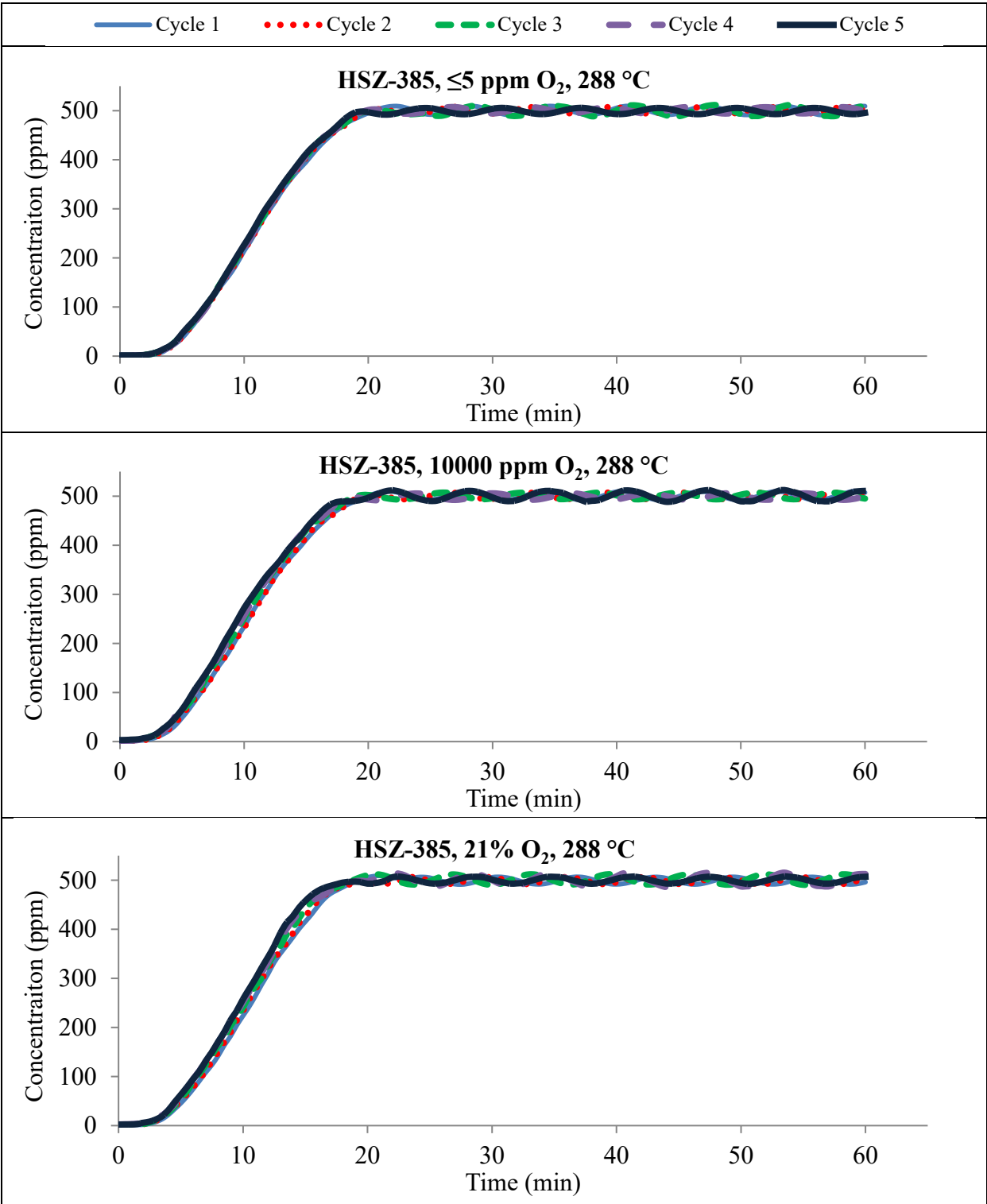


Figure 4-9. Adsorption breakthrough curves for TMB on HSZ-385 samples desorbed at 288°C with different oxygen impurities

Desorption of G-70R at 288 °C with  $\leq 5$  ppm O<sub>2</sub> in the purge gas resulted in lower heel build-up compared to 200 °C (Figure 4-5 and Figure 4-10). However, in the presence of 10,000 ppm or 21% O<sub>2</sub>, desorption at 288 °C increased the cumulative heel build-up compared to 200 °C. Consequently, the adsorption capacity of tested activated carbon decreased by 6.55% and 9.60% when 10,000 ppm and 21% O<sub>2</sub> were used as purge gases, respectively. This indicates two opposite effects of temperature on heel build-up. Increasing of the desorption temperature enhances heat and mass transfer. At a low oxygen level, an elevation in temperature will provide the required activation energy to desorb those adsorbates strongly attached to the narrow micropores. However, in the presence of high oxygen concentrations, a temperature increase can reinforce oxygen-induced reactions and magnify heel build-up.

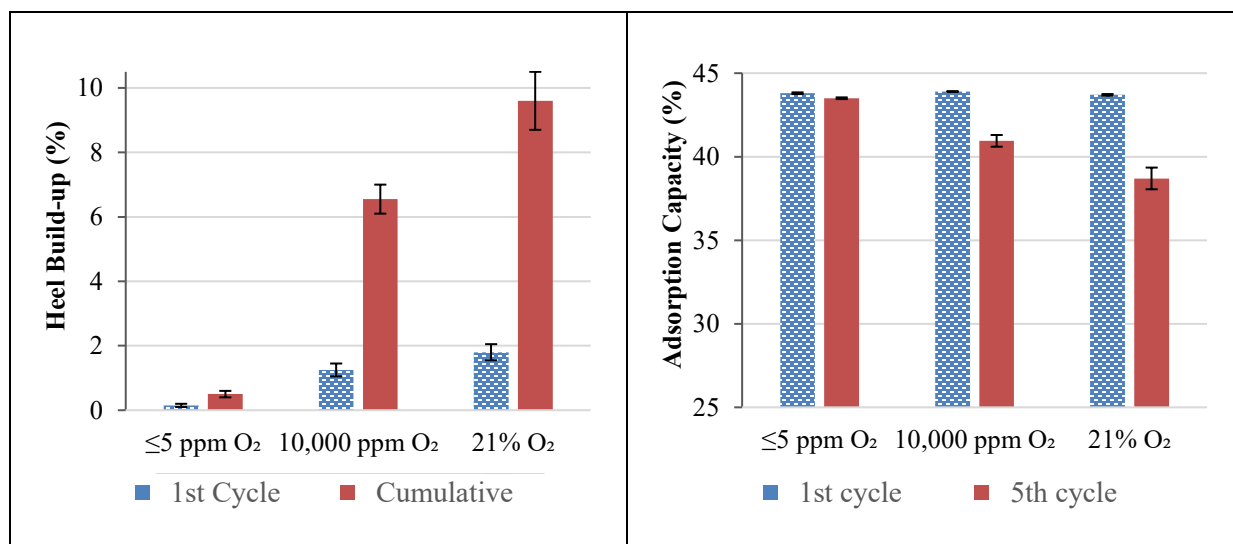


Figure 4-10. Adsorption capacity and heel build-up for G-70R desorbed at 200 °C (error bars obtained from duplicated results)

HSZ-385 was also tested at 288 °C using the three desorption purge gases (Figure 4-11). Similar to the tests at 200 °C, HSZ-385 performed well over the cyclic adsorption of TMB at 288 °C with or without the presence of oxygen (Figure 4-11). In contrast to the observations in the case of G-

70R, increasing the desorption temperature of HSZ-385 neither increased heel build-up nor reduced the adsorption capacity. Although increasing the purge gas oxygen content and temperature promote oxidation reactions, these reactions do not leave a noticeable amount of heel during desorption of HSZ-385 which can be attributed to the different material and pore structure of zeolite adsorbent compared to activated carbon. HSZ-385 has a sharp pore size distribution of around 9 Å that limits the co-presence of TMB and oxygen and prevents further oxygen-induced reactions.

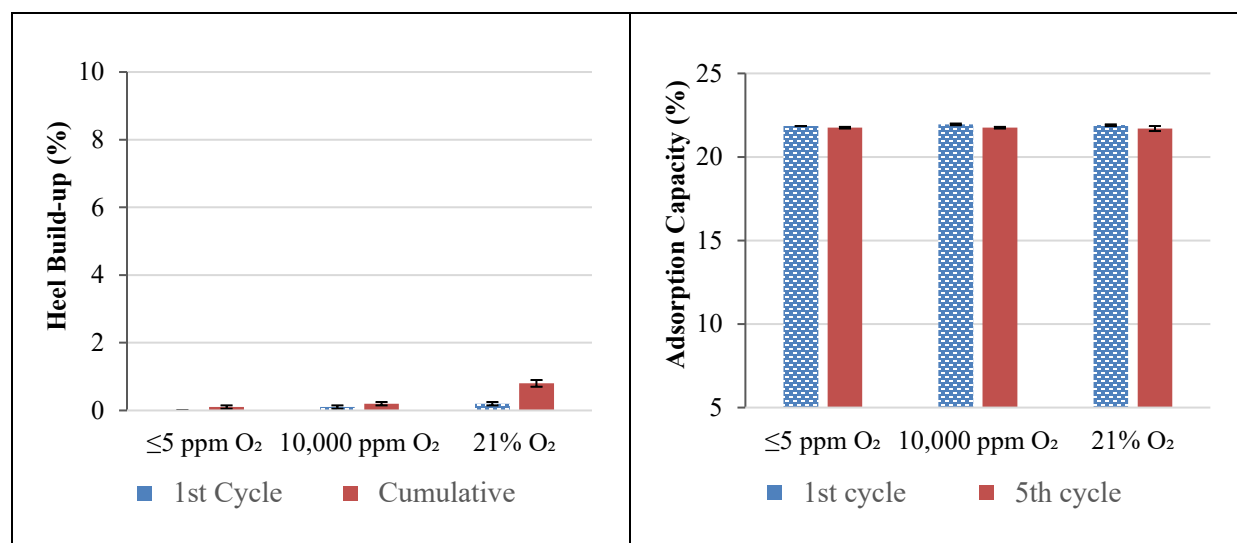


Figure 4-11. Adsorption capacity and heel build-up of 5-cycle on HSZ-385 samples desorbed at 288 °C (error bars obtained from duplicated results)

#### 4.4.3 Surface analysis results

Figure 4-12. shows the N<sub>2</sub> adsorption isotherm, BET surface area, and the total pore volume of virgin and regenerated G-70R samples (after 5 adsorption/desorption cycles). The results are in agreement with the amount of heel build-up and TMB adsorption capacity obtained from the mass balance measurements. Using high purity nitrogen (≤5 ppm O<sub>2</sub>) as the purge gas, the 5-cycle

adsorption experiment with the desorption temperature of 288 °C (288\_5) resulted in the least changes to the pore structure of G-70R by only 3.1% reduction in the total pore volume and 4.0% loss of surface area. However, in both cases of using 10,000 ppm and 21% O<sub>2</sub> in the purge gas, desorption at the lower temperature of 200 °C resulted in less pore blockage and reduction of available adsorption sites. The total pore volume of 200\_10 and 288\_10 samples respectively decreased by 7.4% and 14.0% compared to that of virgin G-70R. Similarly, the calculated BET surface area and pore volume of 200\_21 were higher than the 288\_21.

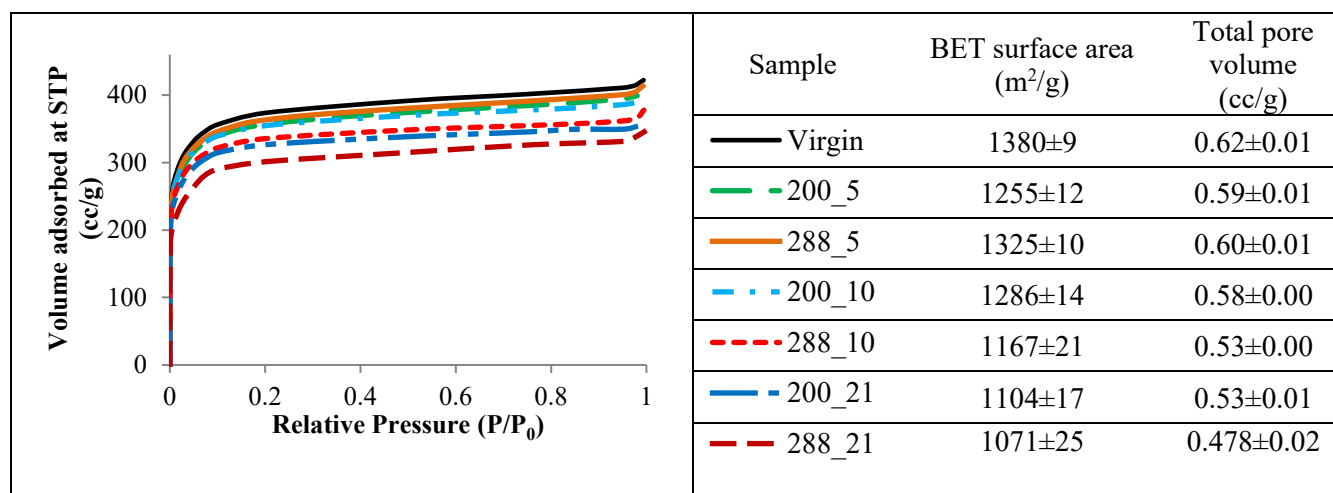


Figure 4-12. N<sub>2</sub> adsorption isotherm on virgin and regenerated G-70R

It can be observed from the N<sub>2</sub> isotherms in Figure 4-12 that those heel build-ups on the tested G\_70R reduced the performance of this adsorbent mostly at the low relative vapor pressures. Since narrow micropores are mostly involved in the low concentration adsorption [30], it can be concluded that the formation of heel has mainly blocked the narrow micropores in this carbon adsorbent.

The N<sub>2</sub> isotherms of Dowex V503 were found to be consistent with the mass balance results (Figure 4-13). Negligible differences in total pore volume and BET surface area were observed

between the virgin sample and 200\_5. Increasing the oxygen content in the desorption purge gas to 10,000 ppm showed a moderate impact on the surface characteristics of Dowex V503 with 10 to 12 % loss of the BET surface area and total pore volume. Finally, using air as the desorption purge gas (21% O<sub>2</sub>) resulted in a large change in the BET surface area of virgin Dowex V503 (from 1120 m<sup>2</sup>/g to 220 m<sup>2</sup>/g) which explains the immediate breakthrough in the 5th cycle for 200\_21 (Figure 4-3). In order to understand the oxidizing effect of oxygen molecule itself on Dowex V503, a virgin Dowex V503 sample was heated to 200 °C using air as the purge gas for 15 hours equivalent to the 5 cycles desorption time (5 x 3 hours) and labeled as “Control”. Figure 4-13 shows the destructive effect of oxygen’s presence on Dowex V503 which resulted in a notable decrease in the available pore volume and surface area of this polymeric adsorbent [31].

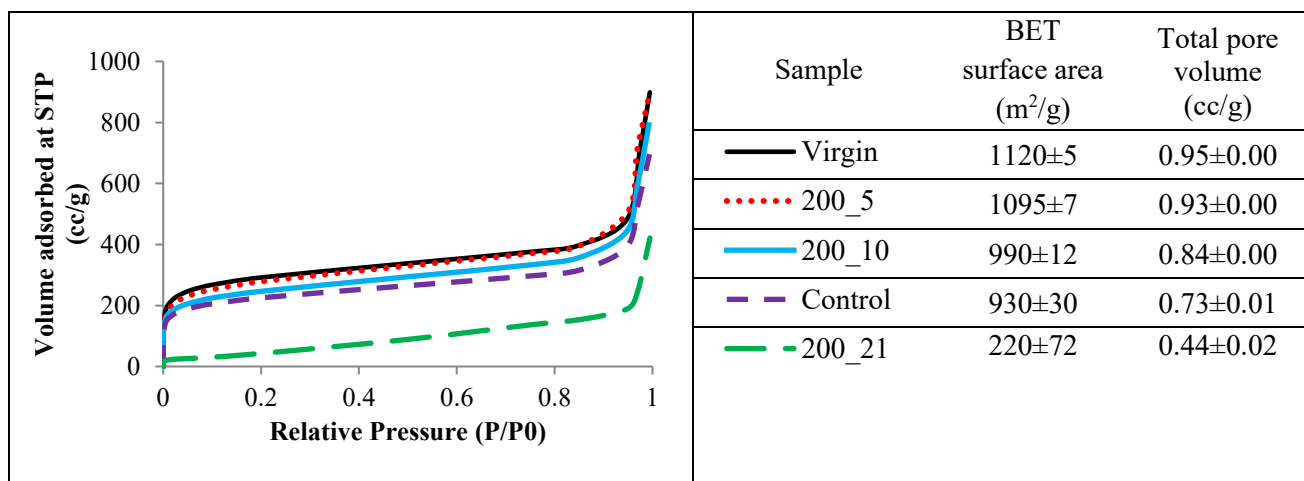


Figure 4-13. N<sub>2</sub> adsorption isotherm on virgin, regenerated, and control samples of Dowex V503

Figure 4-14 shows that all the N<sub>2</sub> isotherms curves of HSZ-285 were overlaid on each other indicating a negligible change to the surface characteristics of the samples. Although increasing the oxygen content in the purge gas to 21% resulted in a small decrease in the pore volume (3.9%)



and surface area (3.8%) in the worst case for this adsorbent, HSZ-385 performance at varying concentrations of oxygen and desorption temperatures was stable.

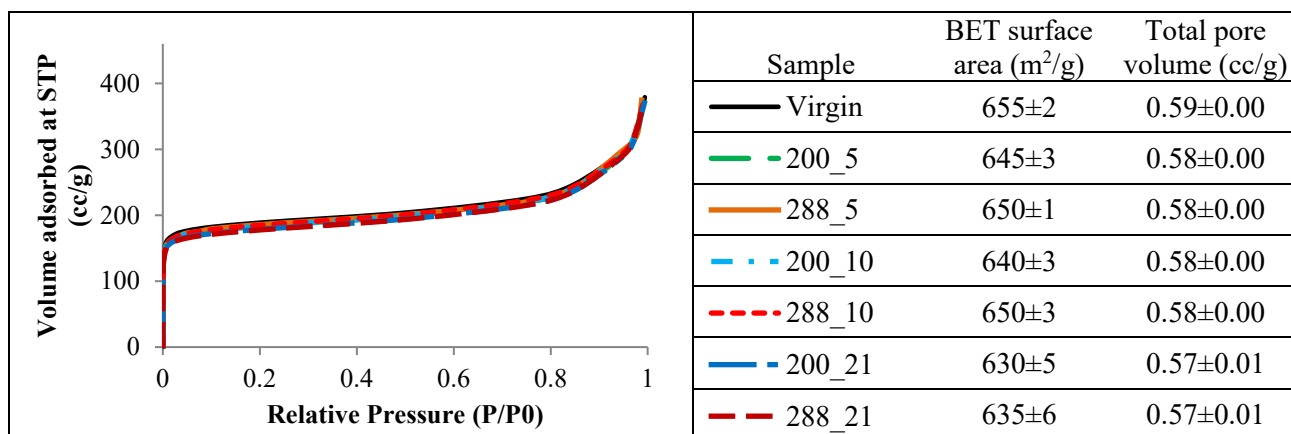


Figure 4-14. N<sub>2</sub> adsorption isotherm on virgin and regenerated HSZ-385

#### 4.4.4 Thermogravimetric analysis results

The evaluation of heel build-up on Dowex-V503 using TGA failed to provide reliable results due to the relatively low degradation temperature of this adsorbent starting from ~250 °C [32, 33]. However, the high thermal stability of G-70R and HSZ-385 allowed precise examination of the formed heel in these two adsorbents. Figure 4-15 shows the DTG results of the virgin samples and the samples desorbed by air (21% oxygen in the purge gas) at 200 °C and 288 °C, labeled as 200\_21 and 288\_21, respectively.

In the case of G-70R, the DTG profile of the 200\_21 sample depicted a peak at around 380 °C followed by a broad peak ranging from 450 °C to 650 °C. However, the 288\_21 sample displayed two distinguishable sharp peaks at approximately 380 °C and 530 °C which indicates two different types of heel in terms of thermal stability [34].

In the case of HSZ-385, no sharp peak appeared in the DTG profile due to the limited heel build-up, yet similar to the G-70R, different DTG profiles can be observed for the 200\_21 and 288\_21 samples (Figure 4-15-b) indicating differences in the thermal stability of the formed heel at these two temperatures. That is to say, regardless of adsorbent material, oxidation reactions during TMB desorption resulted in different products depending on the temperature. However, the physical properties of the adsorbents (e.g. pore size distribution) determine the amount of heel.

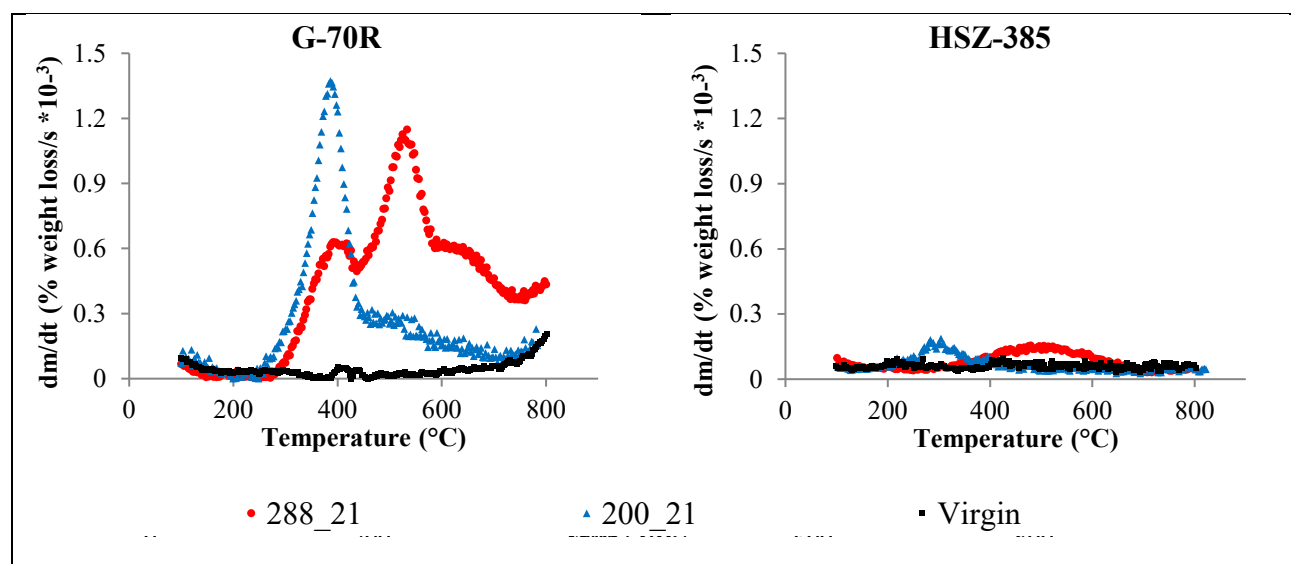


Figure 4-15. DTG analysis of samples desorbed by air at 200 °C and 288 °C compared to virgin ones: a) activated carbon G-70R, b) zeolite HSZ-385

#### 4.5 Conclusions

Activated carbon (G-70R), polymer (Dowex V503), and zeolite (HSZ-385) were examined in the cyclic adsorption of TMB followed by thermal desorption with different operational conditions; varying concentrations of oxygen in the purge gas at two temperatures of 200 °C and 288 °C.

Desorption of the activated carbon G-70R with high purity nitrogen resulted in lower heel build-up at a desorption temperature of 288 °C compared to at 200 °C. However, by increasing the oxygen content in the purge gas and consequently introducing oxidation reactions, increasing the desorption temperature increased the heel build-up rate. Therefore, using 10,000 ppm O<sub>2</sub> or air (21% O<sub>2</sub>) as the purge gas, higher heel build-up was observed at a desorption temperature of 288 °C compared to 200 °C. It was concluded that the combined effect of temperature and O<sub>2</sub> impurity in the purge gas should be considered to minimize heel build-up on activated carbon. Therefore, using lower purity purge N<sub>2</sub> and lower desorption temperature can extend the service life of activated carbon and results in potential energy saving.

Dowex V503 performed well only in the absence of oxygen (high purity N<sub>2</sub>) and at a desorption temperature of 200 °C. Increasing either the purge gas oxygen content or the desorption temperature destroyed the pore structure of Dowex V503 due to the oxidative or thermal degradation of the polymer which indicates the failure of this adsorbent in cyclic thermal swing adsorption.

Varying temperatures and O<sub>2</sub> concentrations of the purge gas had little impacts on the cyclic adsorption performance of zeolite HSZ-385 and this adsorbent performed the best in terms of adsorption capacity loss and cumulative heel build-up among the three adsorbents in all the test conditions. Increasing the purge gas oxygen content slightly increased the heel formation over the 5-cycle use of this adsorbent but overall the effect of desorption temperature on the amount of heel build-up was negligible. However, DTG results showed that the heel formed at the higher desorption temperature is more thermally stable and would need more energy to be removed.

#### 4.6 References

- [1] Kampa M., and Castanas E., "Human health effects of air pollution," *Environmental Pollution*, vol. 151, no. 2, pp. 362-367, 2008.
- [2] Gilman J. B., Lerner B. M., Kuster W. C., and de Gouw J. A., "Source Signature of Volatile Organic Compounds from Oil and Natural Gas Operations in Northeastern Colorado," *Environmental Science & Technology*, vol. 47, no. 3, pp. 1297-1305, 2013.
- [3] Freitag W., and Stoye D., *Paints, Coatings, and Solvents: Wiley*, 2008.
- [4] Barletta B., Meinardi S., Sherwood Rowland F., Chan C.-Y., Wang X., Zou S., Yin Chan L., and Blake D. R., "Volatile organic compounds in 43 Chinese cities," *Atmospheric Environment*, vol. 39, no. 32, pp. 5979-5990, 2005.
- [5] OSHA. "Volatile Organic Compounds in Air," <https://www.osha.gov/dts/sltc/methods/partial/pv2120/pv2120.html>.
- [6] U.S. EPA. "Volatile Organic Compound Rules," <https://www.epa.gov/sips-in/article-8-volatile-organic-compound-rules>.
- [7] Berenjian A., Chan N., and Malmiri H. J., "Volatile Organic Compounds removal methods: a review," *American Journal of Biochemistry and Biotechnology*, vol. 8, no. 4, pp. 220-229, 2012.
- [8] Khan F. I., and Kr. Ghoshal A., "Removal of Volatile Organic Compounds from polluted air," *Journal of Loss Prevention in the Process Industries*, vol. 13, no. 6, pp. 527-545, 2000.
- [9] Ruhl M. J., "Recover VOCs via adsorption on activated carbon," *Chemical Engineering Progress*, 89(7), 1993.
- [10] Hemphill L., and Robert S. Kerr Environmental Research Laboratory A., Okla, *Thermal Regeneration of Activated Carbon: National Technical Information Service*, 1978.

- [11] Ruthven D. M., Farooq S., and Knaebel K. S., Pressure Swing Adsorption: Wiley, 1993.
- [12] Rydberg J., Solvent Extraction Principles and Practice, Revised and Expanded: Taylor & Francis, 2004.
- [13] Cecen F., and Aktas Ö., Activated Carbon for Water and Wastewater Treatment: Integration of Adsorption and Biological Treatment: Wiley, 2011.
- [14] Bandosz T. J., "Gas Adsorption Equilibria: Experimental Methods and Adsorptive Isotherms," Journal of the American Chemical Society, vol. 127, no. 20, pp. 7655-7656, 2005.
- [15] Thomas W. J., and Crittenden B., "5 - Processes and cycles," Adsorption Technology & Design, W. J. Thomas and B. Crittenden, eds., pp. 96-134, Oxford: Butterworth-Heinemann, 1998.
- [16] Ludlow D. K., "Activated Carbon Adsorption By Roop Chand Bansal and Meenakshi," Journal of the American Chemical Society, vol. 128, no. 32, pp. 10630-10630, 2006.
- [17] Cruciani G., "Zeolites upon heating: Factors governing their thermal stability and structural changes," Journal of Physics and Chemistry of Solids, vol. 67, no. 9, pp. 1973-1994, 2006.
- [18] Ghafari M., and Atkinson J. D., "Impact of styrenic polymer one-step hyper-cross-linking on volatile organic compound adsorption and desorption performance," Journal of Hazardous Materials, vol. 351, pp. 117-123, 2018.
- [19] Schnelle K. B., Dunn R. F., and Ternes M. E., Air Pollution Control Technology Handbook: CRC Press, 2015.
- [20] "Choosing an Adsorption System for VOC: Carbon, Zeolite, Or Polymers" The Clean Air Technology Center, EPA Technical Bulletin, 1999.

- [21] Ferro-García M. A., Joly J. P., Rivera-Utrilla J., and Moreno-Castilla C., “Thermal desorption of chlorophenols from activated carbons with different porosity,” *Langmuir*, vol. 11, no. 7, pp. 2648-2651, 1995.
- [22] Kim K. J., Kang C. S., You Y. J., Chung M. C., Woo M. W., Jeong W. J., Park N. C., and Ahn H.-G., “Adsorption–desorption characteristics of VOCs over impregnated activated carbons,” *Catalysis Today*, vol. 111, no. 3, pp. 223-228, 2006.
- [23] Lashaki M. J., Fayaz M., Wang H., Hashisho Z., Philips J. H., Anderson J. E., and Nichols M., “Effect of Adsorption and Regeneration Temperature on Irreversible Adsorption of Organic Vapors on Beaded Activated Carbon,” *Environmental Science & Technology*, vol. 46, no. 7, pp. 4083-4090, 2012.
- [24] Hofelich T. C., LaBarge M. S., and Drott D. A., “Prevention of thermal runaways in carbon beds,” *Journal of Loss Prevention in the Process Industries*, vol. 12, no. 6, pp. 517-523, 1999.
- [25] Feizbakhshan M., Hashisho Z., Philips J. H., Anderson J. E., and Nichols M., “Effect of Oxygen impurity and desorption temperature on heel buildup on activated carbon,” in 68th Canadian Chemical Engineering Conference, Toronto, 2018.
- [26] Chareonpanich M., Zhang Z.-G., and Tomita A., “Hydrocracking of Aromatic Hydrocarbons over USY-Zeolite,” *Energy & Fuels*, vol. 10, no. 4, pp. 927-931, 1996.
- [27] Yaws C. L., "Chapter 2 - Physical Properties – Inorganic Compounds," *The Yaws Handbook of Physical Properties for Hydrocarbons and Chemicals (Second Edition)*, C. L. Yaws, ed., pp. 684-810, Boston: Gulf Professional Publishing, 2015.
- [28] Stahlbush J. R., and Strom R. M., “A decomposition mechanism for cation exchange resins,” *Reactive Polymers*, vol. 13, no. 3, pp. 233-240, 1990.
- [29] Niessner N., and Wagner D., “Practical guide to structures, properties and applications of styrenic polymers,” 2013.

- [30] D D. D., Adsorption Analysis: Equilibria And Kinetics (With Cd Containing Computer Matlab Programs): World Scientific Publishing Company, 1998.
- [31] Rabek J. F., "Chapter 4 Oxidative Degradation of Polymers," Comprehensive Chemical Kinetics, C. H. Bamford and C. F. H. Tipper, eds., pp. 425-538: Elsevier, 1975.
- [32] Chauhan R. S., Gopinath S., Razdan P., Delattre C., Nirmala G. S., and Natarajan R., "Thermal decomposition of expanded polystyrene in a pebble bed reactor to get higher liquid fraction yield at low temperatures," Waste Management, vol. 28, no. 11, pp. 2140-2145, 2008.
- [33] Pfäffli P., Zitting A., and Vainio H., "Thermal degradation products of homopolymer polystyrene in air," Scandinavian Journal of Work, Environment & Health, no. 2, pp. 22-27, 1978.
- [34] Bansal R. C., and Goyal M., "Activated carbon adsorption," 2005.
- [35] BAC Product Specifications [Online] Available: <http://www.kurehacarbonproducts.com/bac.html>
- [36] Dow Chemical Product Catalog [Online]. Available: <https://www.dow.com/en-us/product-catalog.html>
- [37] TOSOH Zeolite [Online]. Available: <https://www.tosoh.com/our-products/advanced-materials/zeolites-for-catalysts>.
- [38] Niknaddaf S., Atkinson J. D., Shariaty P., Lashaki M. J., Hashisho Z., Philips J. H., Anderson J. E., and Nichols M. "Heel formation during volatile organic compound desorption from activated carbon fiber cloth," *Carbon*, vol. 96, pp. 131-138, 2016.
- [39] Hashemi S. M., Lashaki M. J., Hashisho Z., Phillips J. H., Anderson J. E., and Nichols M., "Oxygen impurity in nitrogen desorption purge gas can increase heel buildup on activated carbon," *Separation and Purification Technology*, vol. 210, pp. 497-503, 2019.

## **CHAPTER 5: MECHANISM OF VOC'S HEEL BUILD-UP THROUGH OXYGEN INDUCED REACTIONS**

### **5.1 Chapter Overview**

Oxygen induced reactions during desorption of VOCs was shown in the previous chapters to negatively impact the cyclic process of adsorption. The purpose of this chapter is to establish a severe condition of high oxygen concentration to analyze and characterize the products of such reactions. For this purpose, three activated carbons (ACs) and one zeolite adsorbent were exposed to 2000 ppm<sub>v</sub> of 1,2,4-trimethylbenzene (TMB) in air (21% oxygen) at 3 different temperatures (150, 200, and 250 °C). Thermogravimetric analysis (TGA), was used to assess the thermal stability of the heel formed on the samples. Also, the porous structure of the samples was studied using nitrogen adsorption and surface area analysis. Besides, gas chromatography-mass spectrometry (GC-MS) analysis of the effluent gases was performed to understand the mechanism of heel build-up.

### **5.2 Introduction**

Adsorption process has been one of the common techniques for controlling the emission of volatile organic compounds (VOCs) [1]. With respect to the reusability advantage of some costly VOCs and adsorbents, the cyclic process of adsorption has been of interest in many industrial applications including painting and coating [2-5]. In such industries, thermal desorption is a preferred method as it has shown success in the desorption of moderate to low volatile VOCs commonly found in solvents [6, 7].



Desorption temperatures higher than the boiling point of adsorbed species are required to completely desorb VOCs. Increasing the desorption temperature enhances adsorbates removal and transfer to the mobile phase. However, an elevated temperature promotes undesirable reactions in the presence of oxygen which could lead to heel build-up on the adsorbents, reduce their life-span, and increase the frequency of adsorbate replacements [8-10]. In the liquid phase and during adsorption, several studies have reported oxygen-induced reactions of VOCs in the presence of dissolved oxygen [11-14]. Grant and King [15] observed that substantial availability of oxygen in the adsorption of phenolic compounds promotes oxidative coupling on activated carbon. Bamford and Tipper [16] reported that an elevated temperature (180-210 °C) can provide the required activation energy for the formation of phenolate radicals and according to Vidic et al. [17, 18] these radicals lead to the oxidative coupling of phenolic compounds on activated carbons. Lu et al [31] studied the impact of adsorbent pore size distribution (PSD) on the multicomponent solute adsorption on activated carbon and reported that the narrow PSD could be effective in hampering the oligomerization of phenolic compounds in the presence of oxygen. They concluded that adsorbents with narrow PSD are more capable of hampering oligomerization than those with wide PSD.

In the gaseous phase, likewise, the oxygen impurity of desorption purge gas has been reported to reduce the life-span of activated carbon due to the heel formation [8, 10, 19]. Desorption temperature was found to substantially contribute to this heel build-up by promoting the oxygen-induced reactions on activated carbon. The various peaks in the thermal gravimetric analysis (TGA) curves were used as evidence to conclude the occurrence of reactions influenced by oxygen.

However, there is little information available about the product of such reactions and how the selection of adsorbents can affect the associated heel build-up.

In the present study, a variety of adsorbents (activated carbon and zeolite) were tested at different temperatures (150, 200, and 250 °C) to improve the understanding of heel build-up in presence of oxygen. Dry air with 21% oxygen content was used as the mobile phase for an extended duration to stimulate a harsh desorption condition. The effluent gas was condensed and analyzed with GC-MS to identify the products of oxygen-induced reactions. In addition, several characterization techniques were used to understand the mechanism of heel build-up.

### **5.3 Materials and Methods**

#### **5.3.1 Adsorbate and Adsorbents**

1,2,4-trimethylbenzene (TMB, 98%, Sigma-Aldrich) was selected as a surrogate for VOCs emitted from the automotive paint booth. Previous studies have shown that TMB has a high tendency to form heel [9, 10].

Three activated carbons (B-100777 supplied by Blucher GmbH, G-70R supplied by Kureha Corporation, and ACFC-20 supplied by Nippon Kynol Company) and one zeolite (HSZ-385 provided by Tosoh Ltd.) were used as the adsorbents in this study. All the selected ACs possess a high affinity towards TMB adsorption with similar surface chemical compositions. Also, they all have negligible ash contents (< 0.1%) [20-22] that reduces the involvement of catalytic reactions in heel build-up. However, they possess different physical properties with a wide range of specific surface area (1380 to 1940 m<sup>2</sup>/g), micropore volume (0.53 to 0.73 cc/g), and total pore volume

(0.62 to 1.78 cc/g). The selected zeolite (HSZ-385) is a high-silica Y-type zeolite with hydrophobic surface properties, making it highly adsorbing for VOCs. Further, it has a wide pore size of  $\sim 9 \text{ \AA}$  [23] with a relatively high affinity for TMB adsorption [24]. Table 5-1 shows some physical and chemical characteristics of these adsorbents.

Table 5-1. Physical and chemical properties of the selected adsorbents

Sample	Physical properties*			Chemical composition**			
	Specific surface area (m <sup>2</sup> /g)	Micropore volume (cc/g)	Total pore volume (cc/g)	C%	O%	N%	S%
G-70R	1380	0.53	0.62	90.8	6.1	1.4	1.7
B-100777	1745	0.66	1.78	92.1	5.9	1.1	0.9
ACFC-20	1940	0.73	0.80	92.8	4.8	1.2	1.2
HSZ-385	650	0.26	0.58	SiO <sub>2</sub> /Al <sub>2</sub> O <sub>3</sub> [23]			

\*Obtained by N<sub>2</sub> adsorption at -195.8 °C for AC and by Ar adsorption at -185.8 °C for zeolite

\*\*Obtained from XPS analysis

B-100777 and G-70R were received in the beaded shape with the particle size of less than 1.0 mm so they were used with no further modifications. ACFC-20 was cut into 1×1 mm pieces while HSZ-385 was received as a powder, hence, it was pelletized, crushed, and sieved using the mesh standard numbers of 20 and 35 to select particles with a size range similar to. Prior to the 5-cycle adsorption tests, all the adsorbents were dried in an oven in air at 150 °C for 24 h and then stored in a desiccator until they reached room temperature.

### 5.3.2 Experimental setup and Methods

The experimental setup consisted of five essential modules: an adsorption/reaction tube, a temperature control system, an organic concentration measurement system, an organic vapor generation system, and a condensation setup (Figure 2-1). For each experiment,  $4.0 \pm 0.05$  g of previously dried adsorbent was placed inside a stainless steel adsorption tube (1.57 cm inner diameter and  $20 \pm 0.5$  cm length). Quartz wool was used to support the adsorbent inside the tube, and a thermocouple (Omega) was inserted into the center and middle of the adsorbent bed. A Heating tape (Omega) was wrapped around the tube and fittings and connected to a variac transformer (Staco Energy). Previous studies revealed that oxygen-induced reactions at high oxygen concentrations (21%) occur at temperatures as low as 200 °C. Therefore, a range of temperature around 200 °C was selected (150 °C, 200 °C, or 250 °C), and a data acquisition and control (DAC) interface was used to maintain the bed temperature during the experiments. A flame ionization detector (FID; Series 9000, Baseline-Mocon Inc.) was calibrated and used to monitor the TMB inlet concentration to ensure stability, and to measure TMB outlet concentrations at constant time intervals (every 30 sec) to detect breakthrough curves. A mass flow controller (Alicat Scientific) maintained the inlet flow rate of 5 standard liter per minute (SLPM) of air (99.999% pure, Praxair), and a syringe pump (kd Scientific, KDS-220) injected liquid TMB into the air stream to generate a constant inlet concentration of (2000 ppm<sub>v</sub>). During the experiments, a Friedrichs condenser (Pyrex) coupled with a chilling circulating bath (Cole-Parmer Polystat) was used to condense the evolved gas at 5°C. The condensate of each experiment was collected, in 8mL sample vials (Fisher brand), and capped for further GC-MS analysis. Each experiment lasted for 90 min. upon finishing the experiment, the reaction bed was cooled down to lab temperature

and the adsorbents were weighed and stored for further analysis. The weight gain percentage ( $\Delta W\%$ ) of each sample was calculated as follows:

$$\Delta W (\%) = \frac{W_A - W_B}{W_B} \times 100$$

Where  $W_B$  and  $W_A$  (g) are the weights of samples before and after the experiments, respectively.

The breakthrough time was calculated as the time effluent concentration reaches 5% of the inlet concentration, in this study 100 ppm<sub>v</sub>.

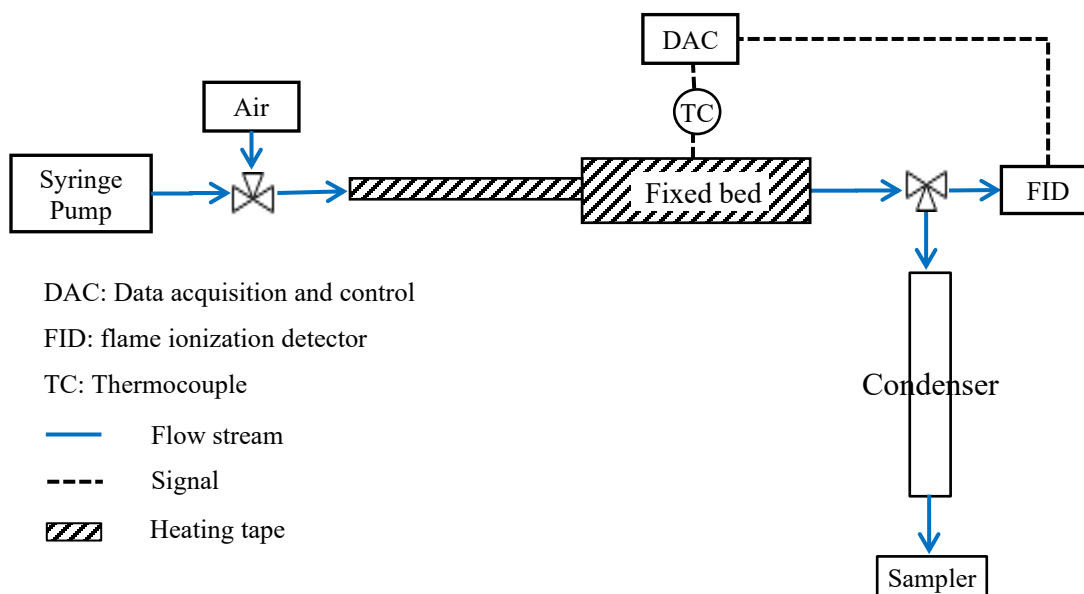


Figure 5-1. Schematic of the experimental setup

### 5.3.3 Characterization Methods

A micropore surface area analyzer (Quantachrome, Autosorb iQ2MP) was used to examine the pore size distribution of the adsorbent samples. Prior to any analysis, 40-50 mg of each sample was degassed at 150 °C under vacuum for an extended time of 12 hours to remove contaminants

such as moisture. N<sub>2</sub> isotherms at -195.8 °C (boiling point of liquid nitrogen) for AC samples and Ar isotherms at -185.8 °C (boiling point of liquid argon) for zeolite samples were obtained at relative pressures (P/P<sub>0</sub>) ranging from 10<sup>-7</sup> to 1. The specific surface area was calculated from the slope and intercept of the isotherms' curve based on the Brunauer, Emmet, and Teller (BET) model in the low range of P/P<sub>0</sub> (0.01-0.1) [25, 26]. The total pore volumes were also recorded from the N<sub>2</sub> isotherm at P/P<sub>0</sub> = 0.995. The Quenched Solid Density Functional Theory (QSDFT) method was used to determine pore size distributions and micropore volumes (pore width <20Å) [27].

A thermogravimetric analyzer (TGA, Mettler Toledo, TGA/DSC 1) was used to evaluate the thermal stability of virgin and tested samples. The temperature of each sample was increased from room temperature to 850 °C. N<sub>2</sub> (99.999% pure) at a constant flow rate of 50 standard cc/min was used to purge the system and a relatively slow heating rate of 2 °C/min was selected to obtain high-resolution peaks in differential thermogravimetric (DTG) graphs.

A GC-MS system composed of a gas chromatograph (Agilent Technologies model 7890A) interfaced with an inert MSD with Triple-Axis Detector (Agilent Technologies, 5975C) was used for the analysis of adsorption tube effluent's condensate. The GC was equipped with a DB-EUPAH capillary column that is 60 m long with a 0.25 mm diameter and 0.25 µm film thickness (Agilent J&W). The injected sample was carried through the column using helium at a flow rate of 1.6 mL/min at a linear velocity of 34 cm/s. The injection volume was 1 µL, and the injection port temperature of 280 °C. The split ratio was 100:1. The initial GC oven temperature was set to 150 °C and maintained for 5 min, afterward, the temperature was increased to 310 °C at a rate of 10 °C/min and held at that temperature for up to 10 min. The NIST/EPA/NIH libraries were used for compound identifications.

#### 5.4 Results & Discussion

Figure 5-2. Adsorption breakthrough curves at 150, 200, and 250°C shows the effluent concentrations measured by the FID during TMB adsorption at 150, 200, and 250 °C. Comparing the performance of adsorbents at the same temperature, the longest breakthrough time was observed for ACFC-20 followed by B-100777, G-70R, and HSZ-385. This trend is in agreement with the trends in the micropore volume and surface area of the selected adsorbents (Table 5-1).

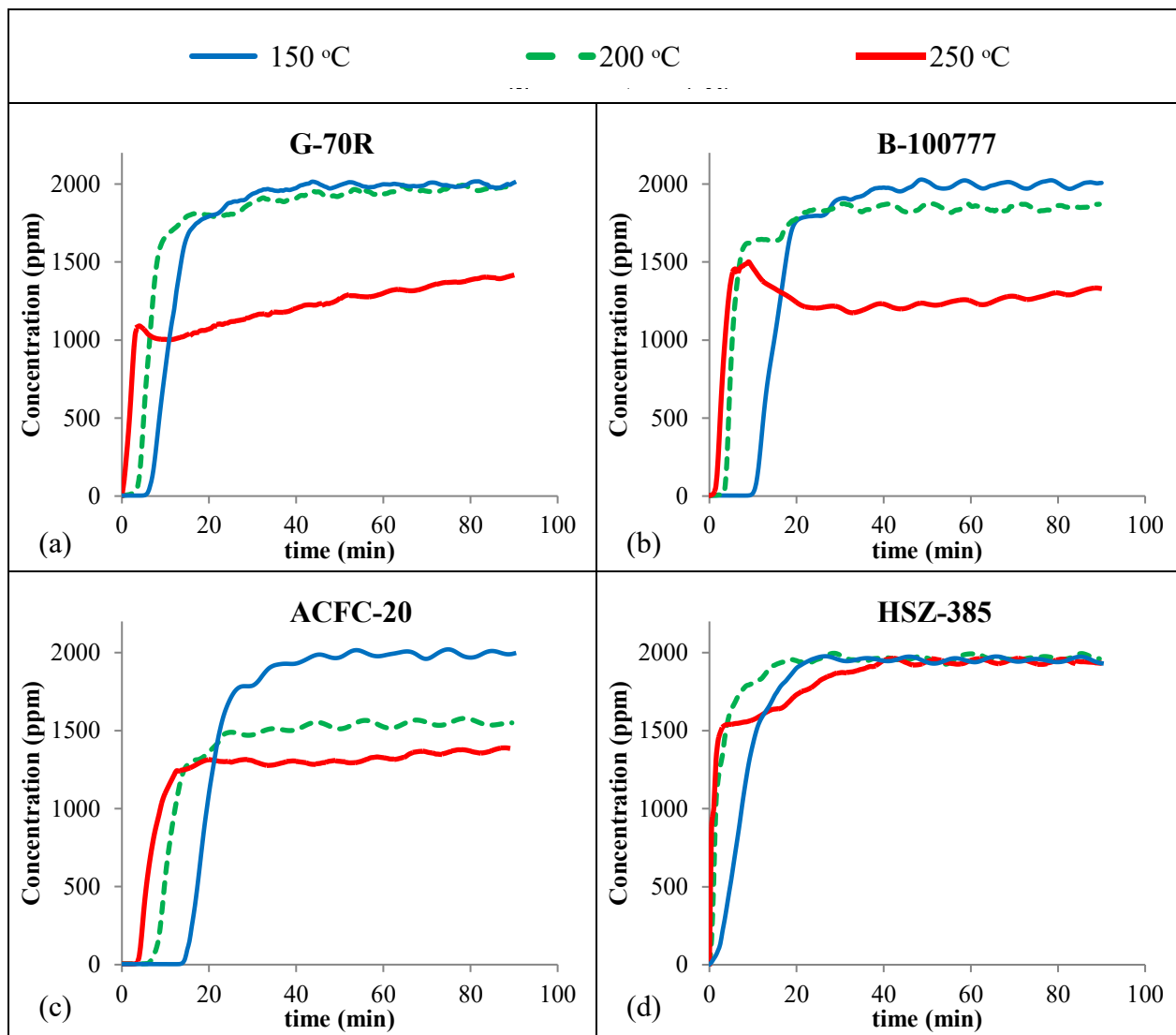


Figure 5-2. Adsorption breakthrough curves at 150, 200, and 250 °C, based on FID measurements

For each adsorbent, increasing the adsorption temperature shortened the breakthrough time. For instance, for ACFC-20, increasing the adsorption temperature from 150 to 200 and 250 °C (Figure 5-2-c) reduced the breakthrough time from 15 to 8 and 4.5 min, respectively. Also, increasing the temperature affected the effluent concentration plateau (known as saturation concentration), particularly for the AC samples. At 200 °C, the breakthrough curves plateaued at ~1500 ppm for ACFC-20, at ~1850 ppm for B-100777, and at ~1950 ppm for G-70R, while HSZ-385 saturation



concentration reached 2000 ppm (the inlet concentration) similar to that of 150 °C. Similarly, at 250 °C, the breakthrough curve of HSZ plateaued at 2000 ppm, however, it reached saturation later than those of 150 and 200 °C and with an irregular profile (Figure 5-2-d). At this temperature (250 °C), the breakthrough curves on the three ACs leveled off at even lower concentrations, ranging between 1300 to 1450 ppm. This can be explained by the formation of new compounds at elevated temperatures due to some reactions between TMB and oxygen. In such reactions, TMB is consumed and consequently, its concentration in the effluent stream decreases. The reaction products may be partially adsorbed, form heel, or be carried away from the adsorption bed right after their formation. In either case, due to the limited pore volume of adsorbents, it is expected to observe a saturation concentration of 2000 ppm<sub>v</sub> even though with delay. However, the products of oxygen-induced reactions might be heavier than TMB with higher boiling points which could lead to their condensation and deposition in the tubing connecting the adsorption tube outlet and FID inlet. Furthermore, FID was initially calibrated for TMB detection and since the response factor of FID can be reduced to much lower levels in response to oxygen-substituted hydrocarbons [28], it may underestimate the concentration of the products of oxygen-induced reactions.

Figure 5-3-b shows the weight gain percentage ( $\Delta W\%$ ) of each sample following the adsorption experiments. For each adsorbent, a lower  $\Delta W\%$  was observed by increasing the test temperature from 150 °C to 200 °C, which follows the same trend as the breakthrough time. This can be explained by the reduction of adsorption affinity of adsorbents when the temperature increases. However, increasing the adsorption temperature to 250 °C resulted in a higher  $\Delta W\%$  compared to that at 200 °C despite a shorter breakthrough time at 250 °C. This can be attributed to the accumulation or deposition of the product of oxygen-induced reactions on the adsorbent surface or in the pores, which is also known as heel formation [8-10].

Among the adsorbents, HSZ-385 showed the least  $\Delta W\%$  at all three temperatures. Specifically, HSZ-385 resulted in a notably lower  $\Delta W\%$  at 250 °C (1.3%), while all the AC samples showed a substantially high  $\Delta W\%$ , 18.8 to 22.3 %, at the same temperature of 250 °C.

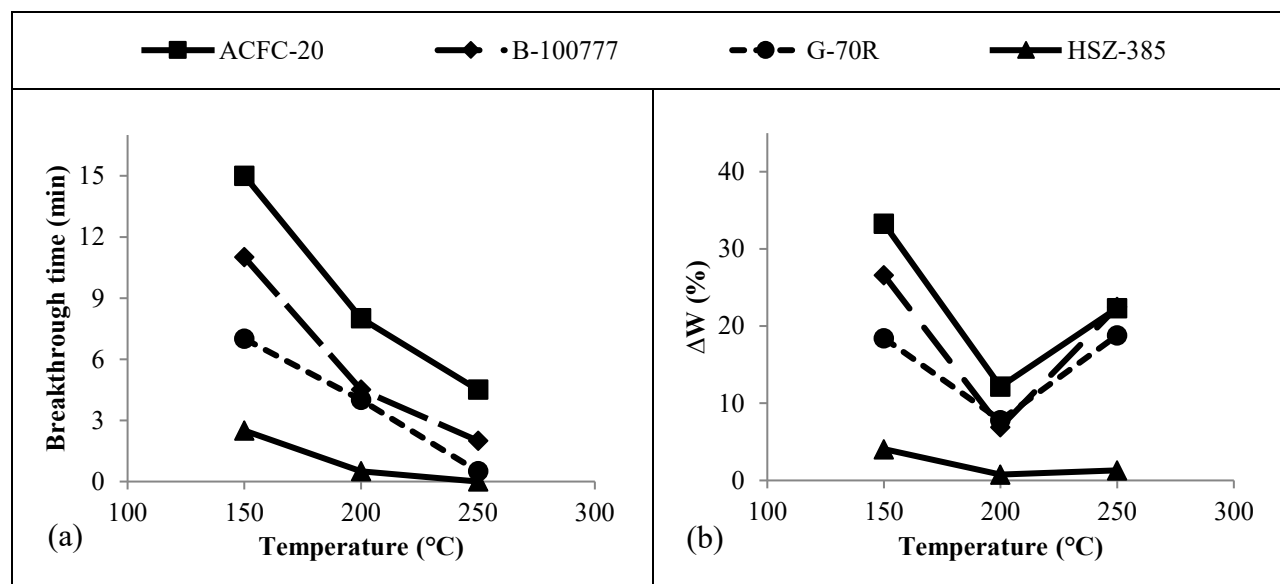


Figure 5-3. Breakthrough time (min) and the weight gain percentage ( $\Delta W\%$ ) of adsorbents in different test temperatures

Figure 5-4 shows the pore size distribution of the degassed adsorbents. All the ACs demonstrated a reduction in the pore volume, mainly in the micropore region ( $<20 \text{ \AA}$ ), with the increase of the test temperature. The greatest reduction in the AC pore volume was observed for  $250 \text{ }^\circ\text{C}$ , consistent with the highest  $\Delta W\%$  at this temperature. HSZ-385, however, showed no tangible pore volume changes, corresponding to the minimal weight gain percentage on this adsorbent.

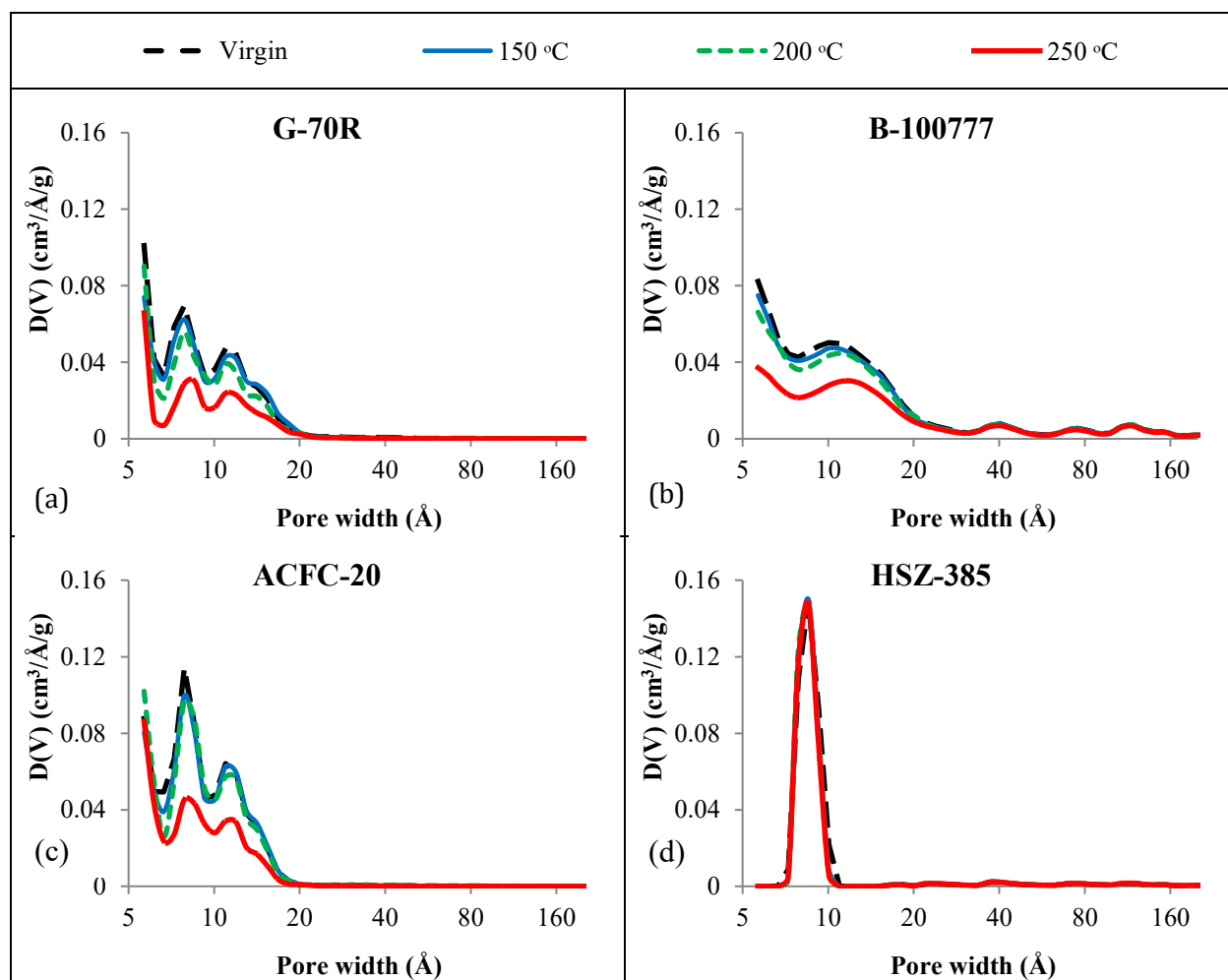


Figure 5-4. Pore size distribution (PSD) of the of adsorbents tested at the adsorption temperatures of  $150$ ,  $200$ , and  $250 \text{ }^\circ\text{C}$

Table 5-2 shows how the BET surface area and pore volume of the samples changed compared to the virgin adsorbents. For all the samples BET surface area decreased by increasing the test temperature. The meso-macropore volume of AC samples tested at 150 °C and 200 °C was measured to be similar to that of virgin and mostly micropore volume was decreased for these samples. However, the pore volume of AC samples tested at 250°C was affected in all the size ranges and meso-macropore volume of these samples also decreased due to the accumulation of heel on the surface and in the larger pores than >20 Å. Repeatedly, it can be seen that increasing the test temperature had minor effects on the HSZ-385.

Table 5-2 BET surface area, micropore volume, meso-macropore volume, and the total pore volume of the tested adsorbent

Sample*	BET surface area (m <sup>2</sup> /g)	Total pore volume (cm <sup>3</sup> /g)	Micropore volume (cm <sup>3</sup> /g)	Meso- and Macropore volume (cm <sup>3</sup> /g)
ACFC-20-V	1940±14	0.73±0.01	0.71±0.01	0.02±0.00
ACFC-20-150	1852±	0.70±0.00	0.67±0.01	0.03±0.01
ACFC-20-200	1779±	0.66±0.01	0.64±0.01	0.02±0.00
ACFC-20-250	898±	0.30±0.02	0.30±0.01	0.01±0.01
G-70R-V	1380±9	0.62±0.01	0.53±0.01	0.09±0.00
G-70R-150	1314±	0.59±0.01	0.51±0.00	0.08±0.00
G-70R-200	1121±	0.51±0.00	0.43±0.01	0.08±0.01
G-70R-250	754±	0.31±0.02	0.28±0.01	0.03±0.02
B-100777-V	1745±9	1.78±0.02	0.66±0.01	1.12±0.01
B-100777-150	1684±	1.75±0.01	0.62±0.00	1.13±0.01
B-100777-150	1496±	1.67±0.01	0.55±0.02	1.12±0.01
B-100777-250	995±	1.31±0.04	0.37±0.03	0.94±0.05
HSZ-385-V	653±2	0.45±0.00	0.26±0.00	0.19±0.00

HSZ-385-150	631±4	0.45±0.00	0.25±0.00	0.20±0.00
HSZ-385-200	614±4	0.43±0.00	0.24±0.00	0.19±0.00
HSZ-385-250	602±4	0.43±0.01	0.24±0.00	0.19±0.01

\*Note: “V” denotes the virgin adsorbents and the tested samples were labeled by the tested temperature (i.e. HSZ-385-250 refers to the HSZ-385 sample tested at 250 °C)

After completing the TGA at 850 °C, the weight loss percentage of each sample was calculated and plotted for the tested temperature (Figure 5-5). For each sample, consistent with the previously calculated  $\Delta W\%$  (Figure 5-3-b), the weight losses were greater for the 150 and 250°C tests compared to those of 200°C.

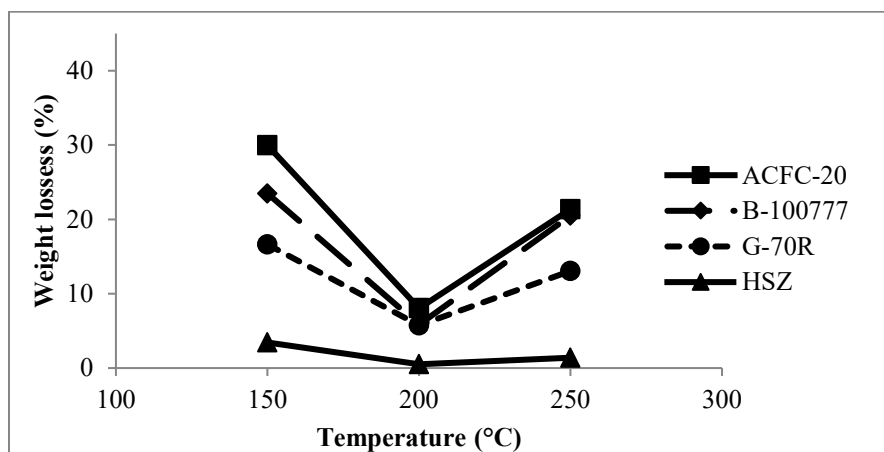


Figure 5-5. Weight losses calculated from TGA results

Figure 5-6 shows the weight loss peaks obtained from the DTG analysis. For the test temperature of 150 °C, a single bell curve was observed for all the samples, with a similar peak around the boiling point of TMB that is 169 °C (Figure 5-6-d). Therefore, this peak can mainly be attributed to desorption of physically adsorbed TMB.

In the case of samples tested at 200°C, the AC adsorbents displayed single low-temperature DTG peaks starting at ~200 °C and falling at ~400 °C. The peaks were about the same location for the three ACs but shifted towards higher temperatures compared to the 150 °C tests. Still, they can be attributed to some physisorbed adsorbates that require higher temperatures (up to 400 °C) to be desorbed. However, these adsorbates, which could be formed during the test, should be heavier than TMB that. Unlike the AC samples, the HSZ-385 tested at 200 °C did not show any clear DTG peak which corresponds well to the instant breakthrough curve of the test and its negligible  $\Delta W\%$ .

Unlike the DTG curve for the AC samples tested at 150 °C and 200 °C that showed a single peak, the ACs tested at 250 °C demonstrated several overlapping peaks ranging from 250 °C to 850 °C. Considering higher reaction rates between the oxygen molecules and TMB at 250 °C, it is expected that more compounds with higher boiling points or thermal stability were formed on these samples. Since adsorption energy and thermal stability of a compound determine whether if it is desorbed in its original form or not, these peaks can be due to the desorption of physisorbed compound with higher boiling points than TMB or thermal cracking and desorption of decomposition products. Again, no distinct DTG peak was detected for HSZ-385 tested at 250 °C.

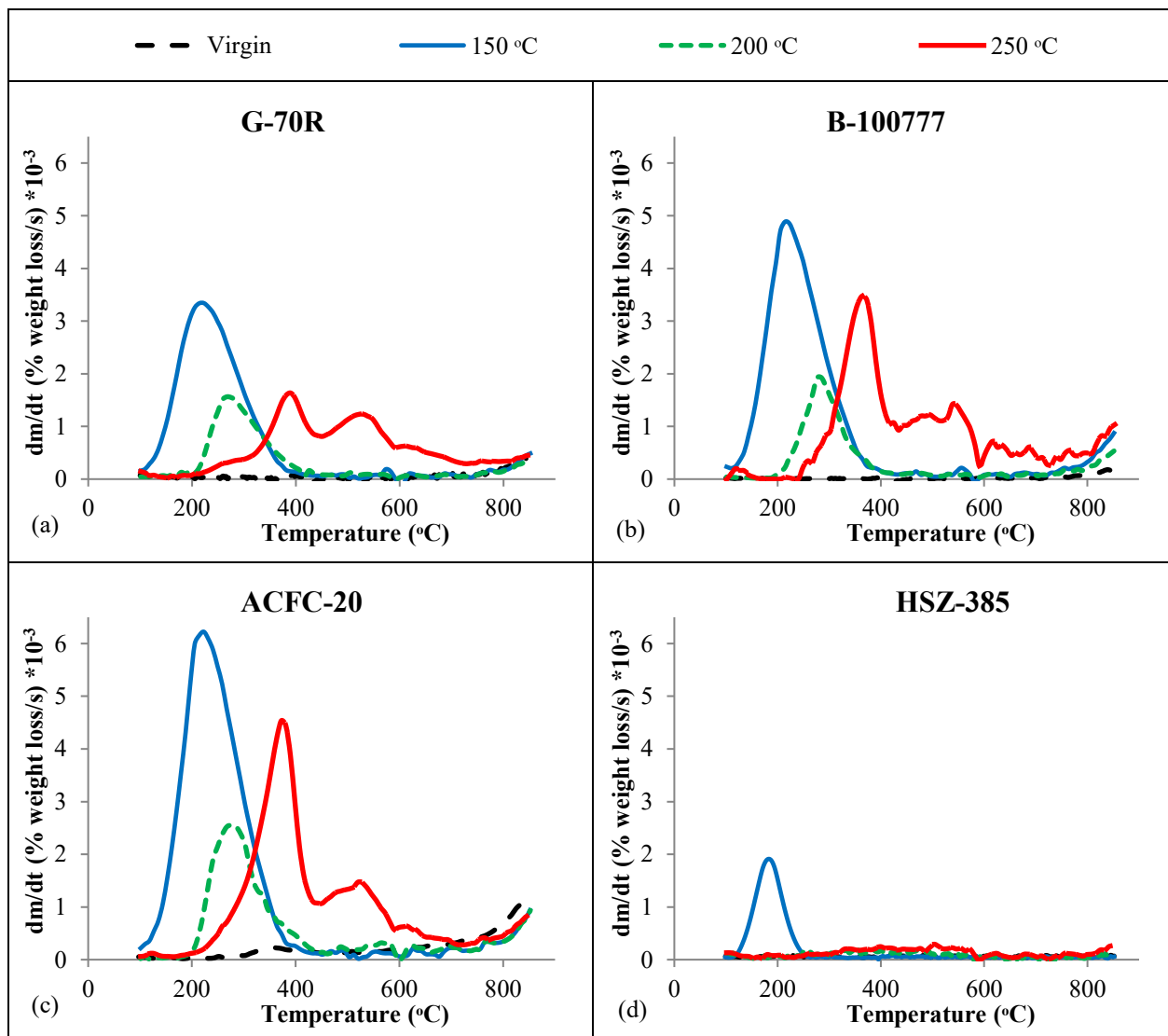


Figure 5-6. DTG results of adsorbents tested

Figure 5-7 shows the GC-MS chromatograms for the condensates of the effluent gases. For each peak in these chromatograms, the detected mass spectrum was matched with the NIST/EPA/NIH library spectra and the associated compounds were listed in Table 5-3. In some cases, a few compounds emerged from the column in relatively close retention time, in such cases only one of the compounds was reported due to their similar structure and functional groups. TMB chromatograph can be found in Figure A-2 in Appendix A.

For the condensate of the effluent gases collected from the tests performed at 150 °C, GC-MS analysis revealed only a major high-intensity peak of TMB at the retention time (RT) of 4 min. This suggests that for all the tested adsorbents, no other compounds are present in the effluent at this temperature, which is consistent with the DTG results.

In the case of ACs tested at 200 °C, at least two additional major peaks at around 6 and 7 minutes RT were observed. For these two peaks, the detected molecules are 2,5-Dimethylbenzaldehyde and 2,4-Dimethylphenol that can be formed by substituting a methyl branch (-CH<sub>3</sub>) in TMB with an aldehyde (-CHO) and a hydroxyl (-OH) group, respectively. The higher boiling points of these compounds (201 °C to 281 °C) compared to TMB is the reason for the additional DTG peaks for these samples (Figure 5-6). For the HSZ-385 sample tested at 200 °C, only one major peak appeared in addition to that of TMB. This peak was attributed to Durene (1,2,4,5-Tetramethylbenzene). Durene, with an additional methyl group compared to TMB, has a boiling point of 200 °C (Table 5-3) which is close to the test temperature. This explains why no DTG peak was observed for this sample since the temperature of 200 °C was able to remove all the TMB and Durene.

Finally, analysis of the condensate of the effluent gases collected from the tests performed at 250 °C showed a wide range of aromatic compounds with different branched and substituted structures. In the case of ACs, several compounds were detected in approximately similar retention times. The MS results revealed compounds with very high melting points (up to ~200 °C) and boiling points (up to ~550 °C). The wide range of boiling points agrees with the broad and overlapping DTG peaks of these samples. Further, the presence of high melting point compounds confirms our hypothesis about the condensation of heavy compounds in the experimental setup and FID



inlet tubing and explains the low concentration plateau in the FID breakthrough curves (Figure 5-2). Another possible reason for the bias in FID measurement is the substitution or/and addition of oxygen that reduces the FID response factor as most of the detected compounds have at least an oxygen functional group. In the case of HSZ-385, although there was negligible weight gain percentage ( $\Delta W\%$ , Figure 5-3-b) and limited changes in the adsorbent PSD (Figure 5-4-d) as well as no major DTG peaks (Figure 5-6-d), GC-MS analysis of the effluent gas revealed several sharp peaks that can be attributed to the formation of high molecular weight compounds with the boiling points of up to  $\sim 420$  °C and the melting point of up to  $\sim 160$  °C. However, the kinetic diameters of these molecules are probably larger than the pore size of HSZ-385 ( $\sim 9$  Å) [23], which suggests that they were formed outside the adsorbent microporous network and appeared in the hot effluent gas. This observation agrees with what previous studies had reported in the liquid phase that the adsorbents with narrow PSD are more effective in hampering the oligomerization of phenolic compounds under oxic conditions [31]. In contrast, the existence of a wide pore size distribution in the AC samples made it possible for oxygen molecules and TMB to collide and successfully form different compounds, therefore, accumulation and formation of heel that reduces volume and surface area of the ACs over a wide range of pore sizes (Figure 5-4).

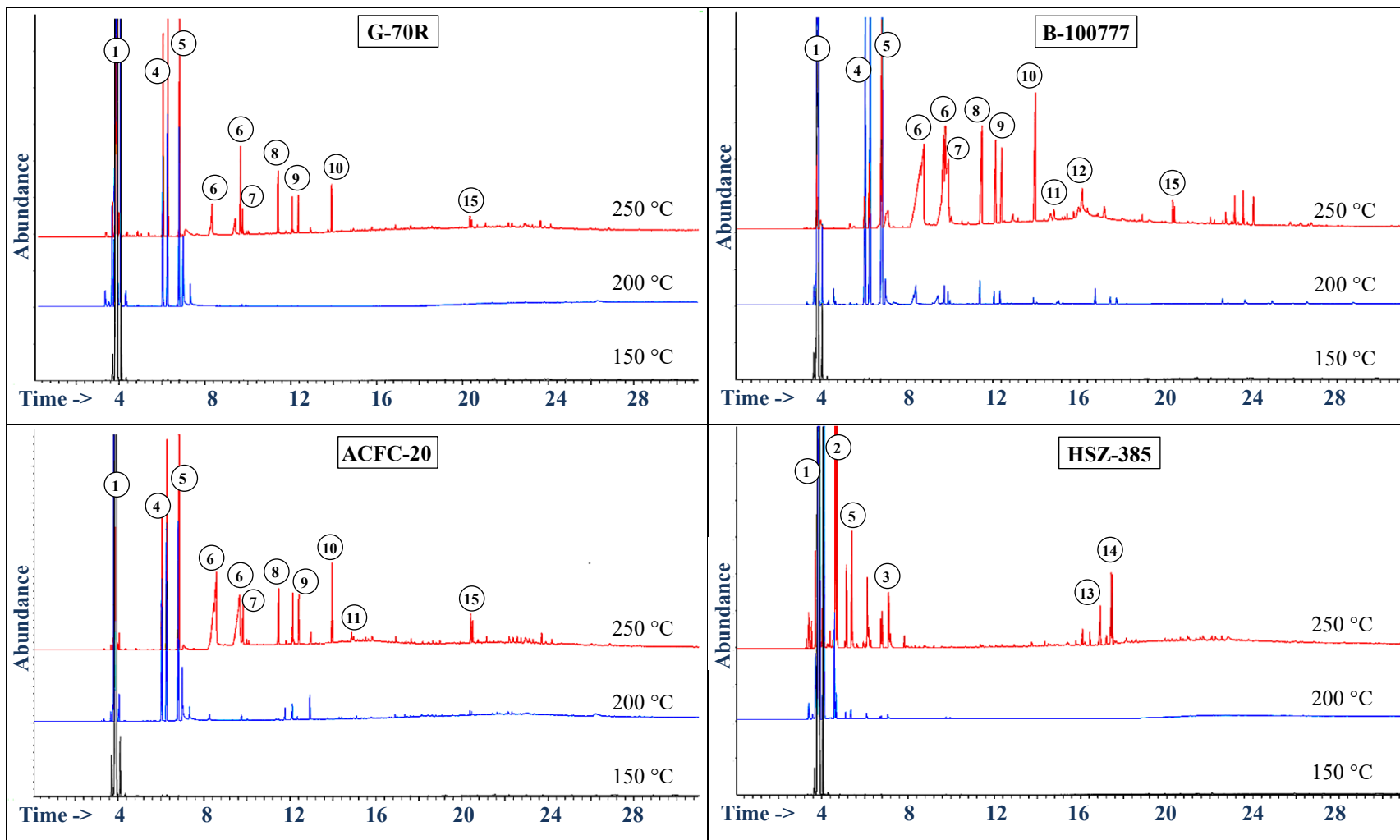
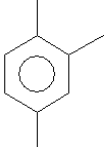
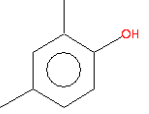
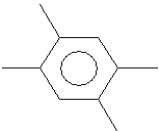
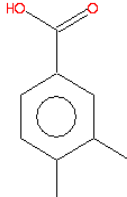
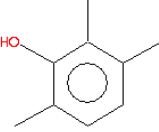
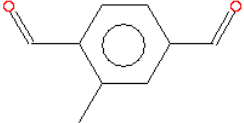
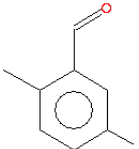
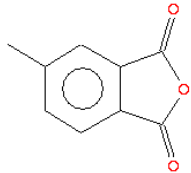
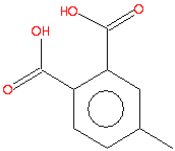
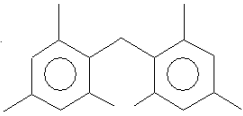
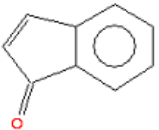
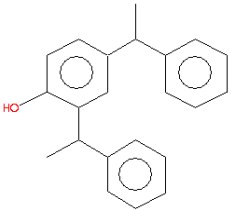
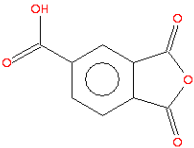
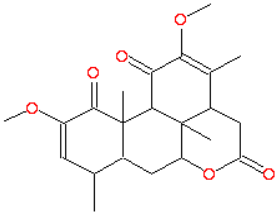
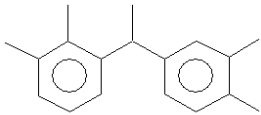


Figure 5-7. Chromatogram of the effluent condensate for the samples tested at 150, 200, and 250 °C

Table 5-3. Properties of organic compounds identified using GC-MS analysis

No.	Name and structure	MW	PB (°C)	MP(°C)	No.	Name and structure	MW	BP(°C)	MP(°C)
1	1,2,4-Trimethylbenzene 	120.2	169.5	-43.7	5	2,4-Dimethylphenol 	122.2	211.0	24.7
2	1,2,4,5-Tetramethylbenzene 	134.2	197.0	79.4	6	3,4-Dimethylbenzoic acid 	150.2	271.7	166.2
3	2,3,6-Trimethylphenol 	136.2	223.8	62.2	7	2-Methylterephthalaldehyde 	148.2	*266.0	*47.6
4	2,5-Dimethylbenzaldehyde 	134.2	220.2	N/A	8	4-Methylphthalic anhydride 	162.1	295.2	90.2

No.	Name and structure	MW	PB (°C)	MP(°C)	No.	Name and structure	MW	BP(°C)	MP(°C)
9	4-Methylphthalic acid 	180.2	233.1	147.7	13	Dimesitylmethane 	252.4	*351.8	*114.1
10	1-Indanone 	132.2	244.2	42.2	14	2,4-Bis(1-phenylethyl)phenol 	302.4	*422.1	*159.1
11	Trimellitic anhydride 	192.1	288.2	165.2	15	Quassin 	388.5	*507.0	*215.9
12	1,1-Bis(3,4-dimethylphenyl)ethane 	238.4	316.1	*94.0					

Molecular weight (MW), Boiling point (BP), and melting point (MP) were taken from *The Yaws Handbook* [29]

\* Predicted using the US Environmental Protection Agency's EPISuite™ [30]

## 5.5 Conclusions

In this study, three activated carbons (G-70R, B-100777, and AFC-20) and one zeolite adsorbent (HSZ-385) were exposed to 2000 ppm<sub>v</sub> of TMB in air (21% oxygen) at 150, 200, and 250 °C for 1.5 hours. For each test, the adsorption breakthrough curve was obtained using an FID and the weight of adsorbent was measured before and after the test to calculate the weight gain percentage ( $\Delta W\%$ ). The thermal stability of the tested samples against the elevated temperatures (up to 850 °C) was evaluated using thermogravimetric analysis (TGA). The porous structure of tested and virgin samples was studied using nitrogen adsorption analysis, BET method, and QSDFT model. Finally, for each test, GC-MS analysis of the effluent gases was performed to understand the mechanism of heel build-up and products of oxygen-induced reactions.

For the individual adsorbents, the adsorption breakthrough time decreased when the test temperature increased. Consequently, lower weight gains ( $\Delta W\%$ ) were observed at 200 °C compared to 150 °C. In contrast, increasing the adsorption temperature to 250 °C resulted in a higher  $\Delta W\%$  compared to that at 200 °C, albeit not notable for the zeolite adsorbent. This was attributed to the accumulation or deposition of the product of oxygen-induced reactions on the adsorbent surface or in the pores, which is similar to what happens during thermal desorption and is known as heel formation.

TGA analysis of the AC samples tested at 150 °C and 200 °C showed only a single low-temperature peak (<400 °C) that was attributed to desorption of physisorbed compounds. However, the desorption of heel formed at the test temperature of 250 °C resulted in a few overlapped peaks

ranging from 250 °C to 850 °C. The presence of a broad range of organic compounds in terms of molecular weight, boiling and melting point, chemical structure, and functional group in the effluent gases of 250 °C tests was confirmed by GC-MS analysis. It was concluded that the wide pore size distribution of ACs allowed the formation and accumulation of these compounds in the pores which resulted in heel build-up.

In the case of zeolite samples, limited or no reduction in the pore volume was observed which is consistent with the minor weight gains on this adsorbent. DTG analysis also indicated no major peak other than a low-temperature peak around the boiling point of TMB. However, GC-MS analysis of the effluent gases of this adsorbent at 250 °C indicated the presence of oxygenated aromatic compounds heavier than TMB. It was concluded that although increasing temperature promotes the oxygen-induced reactions, the sharp pore size distribution of zeolite hinders the formation of molecules bigger than the pore size. Therefore, molecular sieve adsorbents could be advantageous in the cyclic process of VOC adsorption when high oxygen impurity exists.

## 5.6 References

- [1] Berenjian A., Chan N., and Malmiri H. J., "Volatile Organic Compounds removal methods: a review," *American Journal of Biochemistry and Biotechnology*, vol. 8, no. 4, pp. 220-229, 2012.
- [2] Roelant G. J., Kemppainen A. J., and Shonnard D. R., "Assessment of the Automobile Assembly Paint Process for Energy, Environmental, and Economic Improvement," *Journal of Industrial Ecology*, vol. 8, no. 1-2, pp. 173-191, 2004.

- [3] Papasavva S., Kia S., Claya J., and Gunther R., "Characterization of automotive paints: an environmental impact analysis," *Progress in Organic Coatings*, vol. 43, no. 1, pp. 193-206, 2001.
- [4] "Air Pollutant Emission Inventory (APEI) Report," <http://www.ec.gc.ca/pollution/default.asp?lang=En&n=A17452DA-1&offset=8&toc=show>.
- [5] Kim B. R., "VOC Emissions from Automotive Painting and Their Control: A Review," *Environmental Engineering Research*, vol. 16, no. 1, pp. 1-9, 2011.
- [6] Khan F. I., and Kr. Ghoshal A., "Removal of Volatile Organic Compounds from polluted air," *Journal of Loss Prevention in the Process Industries*, vol. 13, no. 6, pp. 527-545, 2000.
- [7] Kolta T., "Selecting Equipment to Control Air Pollution from Automotive Painting Operations," 1992.
- [8] Feizbakhshan M, Hashisho Z., Phillips J. H., Anderson J. E., and Nichols M., "Effect of Oxygen impurity and desorption temperature on heel buildup on activated carbon," in 68th Canadian Chemical Engineering Conference, Toronto, 2018.
- [9] Niknaddaf S., Atkinson J. D., Shariaty P., Lashaki M. J., Hashisho Z., Phillips J. H., Anderson J. E., and Nichols M., "Heel formation during volatile organic compound desorption from activated carbon fiber cloth," *Carbon*, vol. 96, pp. 131-138, 2016.
- [10] Hashemi M. S., Lashaki M. J., Hashisho Z., Phillips J. H., Anderson J. E., and Nichols M., "Oxygen impurity in nitrogen desorption purge gas can increase heel buildup on activated carbon," *Separation and Purification Technology*, vol. 210, pp. 497-503, 2019.
- [11] Vidic R. D., Tessmer C. H., and Uranowski L. J., "Impact of surface properties of activated carbons on oxidative coupling of phenolic compounds," *Carbon*, vol. 35, no. 9, pp. 1349-1359, 1997.

- [12] Vidic R. D., Suidan M. T., Traegner U. K., and Nakhla G. F., "Adsorption isotherms: illusive capacity and role of oxygen," *Water Research*, vol. 24, no. 10, pp. 1187-1195, 1990.
- [13] Vidic R. D., Suidan M. T., and Brenner R. C., "Impact of oxygen mediated oxidative coupling on adsorption kinetics," *Water Research*, vol. 28, no. 2, pp. 263-268, 1994.
- [14] Suidan M., "Role of dissolved oxygen on the adsorptive capacity of activated carbon for synthetic and natural organic matter," 1991.
- [15] Grant T. M., and King C. J., "Mechanism of irreversible adsorption of phenolic compounds by activated carbons," *Industrial & Engineering Chemistry Research*, vol. 29, no. 2, pp. 264-271, 1990.
- [16] Giese B., "C. H. Bamford, C. F. H. Tipper (Eds.): *Comprehensive Chemical Kinetics*, Vol. 16, *Liquid-Phase Oxidation*, Elsevier, Amsterdam 1980.
- [17] Vidic R. D., and Suidan M. T., "Role of dissolved oxygen on the adsorptive capacity of activated carbon for synthetic and natural organic matter," *Environmental Science & Technology*, vol. 25, no. 9, pp. 1612-1618, 1991.
- [18] Vidic R. D., Suidan M. T., Sorial G. A., and Brenner R. C., "Effect of molecular oxygen on adsorptive capacity and extraction efficiency of granulated activated carbon for three ortho-substituted phenols," *Journal of Hazardous Materials*, vol. 38, no. 3, pp. 373-388, 1994.
- [19] Lashaki M. J., Fayaz M., Wang H., Hashisho Z., Philips J. H., Anderson J. E., and Nichols M., "Effect of Adsorption and Regeneration Temperature on Irreversible Adsorption of Organic Vapors on Beaded Activated Carbon," *Environmental Science & Technology*, vol. 46, no. 7, pp. 4083-4090, 2012.



- [20] Hashisho Z., Rood M. J., Barot S., and Bernhard J., "Role of functional groups on the microwave attenuation and electric resistivity of activated carbon fiber cloth," *Carbon*, vol. 47, no. 7, pp. 1814-1823, 2009.
- [21] "BAC Product Specifications," Kureha Corporation.
- [22] High-performance adsorbents based on activated carbon having high meso- and macroporosity, United States US 2018/0125886, Blücher GmbH, 2018.
- [23] "TOSOH Zeolite," 2019; <https://www.tosoh.com/our-products/advanced-materials/zeolites-for-catalysts>.
- [24] Amdebrhan B. T., "Evaluating the Performance of Activated Carbon, Polymeric, and Zeolite Adsorbents for Volatile Organic Compounds Control," University of Alberta, 2018.
- [25] Do D. D., *Adsorption Analysis: Equilibria and Kinetics*: Published by Imperial College Press and distributed by World Scientific Publishing Co., 1998.
- [26] Standardization I. O. f., "ISO 9277:2010, Determination of the specific surface area of solids by gas adsorption - BET method," 2010.
- [27] Neimark A. V., Lin Y., Ravikovitch P. I., and Thommes M., "Quenched solid density functional theory and pore size analysis of micro-mesoporous carbons," *Carbon*, vol. 47, no. 7, pp. 1617-1628, 2009.
- [28] "ASTM D7675-2015: Standard Test Method for Determination of Total Hydrocarbons in Hydrogen by FID-Based Total Hydrocarbon (THC) Analyzer."
- [29] Yaws C. L., *The Yaws Handbook of Physical Properties for Hydrocarbons and Chemicals: Physical Properties for More Than 54,000 Organic and Inorganic Chemical Compounds, Coverage for C1 to C100 Organics and Ac to Zr Inorganics*: Elsevier Science, 2015.

- [30] EPA U., "Estimation Programs Interface Suite™ for Microsoft® Windows, v 4.11," United States Environmental Protection Agency, Washington, DC, USA, 2020.
- [31] Qiuli Lu, George A. Sorial, The role of adsorbent pore size distribution in multicomponent adsorption on activated carbon, Carbon 42 3133–3142 2004

## **CHAPTER 6: CONCLUSIONS AND RECOMMENDATIONS**

### **6.1 Dissertation Overview**

One of the major challenges in the cyclic adsorption/desorption of VOCs is the occurrence of oxygen-induced reaction and thus heel build-up in the porous structure of adsorbents. Heel build-up decreases adsorption capacity and service time of adsorbents and increases operation and maintenance costs associated with more frequent adsorbent replacement. Therefore, this research aimed at understanding factors affecting heel formation in the presence of oxygen, during thermal desorption of VOCs. Using the results from cyclic adsorption/desorption experiments and characterization tests, the mechanism of oxygen-induced reactions and the nature of associated heel were explained and suggestions made on the selection of operating conditions and adsorbent material and properties.

### **6.2 Conclusions**

In Chapter 2, the effect of desorption temperature and purge gas oxygen impurity on the cyclic adsorption/desorption of TMB on a beaded activated carbon (G-70R) was studied. It was observed that increasing the desorption temperature accelerates desorption as it increases heat and mass transfer, however, it does not necessarily improve the removal efficiency. Depending on the oxygen impurity level in the desorption purge gas, increasing the desorption temperature could increase or decrease heel build-up since higher temperatures may promote oxygen-induced reactions. If oxygen is sufficiently present in the purge gas, it can react with TMB and form heel in the adsorbent. Hence, desorption efficiency is a function of the combined effect of purge gas O<sub>2</sub> impurity and desorption temperature. The results suggested several optimization opportunities to

enhance the desorption efficiency, to reduce the operational costs, and to increase the service life of activated carbon in cyclic adsorption processes.

Chapter 3 studied the effect of activated carbon's physical properties on the formation of heel in the adsorbent. The performance of three commercial activated carbons (B100777, ACFC-20, G-70R) with distinct physical properties was examined in 5-cycle adsorption/desorption tests of TMB. It was observed that oxygen-induced reactions are more prone to occur in the AC with a higher microporosity. The absence of a hierarchical pore structure in the AC increases the diffusion resistance and hampers desorption, consequently, extends the reaction time between TMB and oxygen and increases heel build-up. The affected samples by the oxygen-induced heel were analyzed using Boehm titration and three main surface functional oxygen groups (Carboxylic, Lactonic, and Phenolic), were detected. TGA analysis of the tested ACs showed that the heel is removable if enough energy is provided through a high-temperature regeneration (up to 850 °C) to either overcome the adsorption energy or thermally decompose the chemically formed heel.

In Chapter 4, the effect of the adsorbent material on the cyclic adsorption of TMB was studied at different thermal desorption conditions using three different adsorbents: activated carbon (G-70R), zeolite (HSZ-385), and polymer (Dowex V503). G-70R performed well when high purity nitrogen was used as the purge gas with a better performance at the higher desorption temperature but increasing the purge gas oxygen content increased the heel formation on this adsorbent. However, most of the heel (~80% W/W) was shown to be removable. Dowex V503 performed well only with high purity N<sub>2</sub> and the desorption temperature of 200 °C. Increasing either the purge gas oxygen content or the desorption temperature destroyed the pore structure of Dowex V503 due to

the oxidative or thermal degradation of polymers. This indicates the limited application of this adsorbent in cyclic thermal swing adsorption as it must be assured that oxygen level and temperature are maintained below a certain limit. Finally, HSZ-385 performed the best among the three adsorbents and the desorption temperature and O<sub>2</sub> concentrations of the purge gas had little impacts on the cyclic adsorption/desorption of this adsorbent. The 5-cycle tests on HSZ-385 were completed with little heel build-up but still, it could be seen that the increase of the purge gas oxygen content may slowly increase the heel formation through the long-term use of zeolite adsorbent.

Chapter 5 aimed at improving the understanding of heel build-up in the presence of oxygen. An extreme condition of high oxygen concentration was established to analyze and characterize the products of oxygen-induced reactions and to better understand the mechanism of heel build-up. Three activated carbons (G-70R, B-100777, and AFC-20) and one zeolite adsorbent (HSZ-385) were exposed to 2000 ppm<sub>v</sub> of TMB in air (21% oxygen) at 150, 200, and 250 °C for 1.5 hours. Increasing the temperature of adsorption bed from 150 to 200 and 250 °C decreased the adsorption breakthrough time of individual adsorbents. Correspondingly, lower weight gains ( $\Delta W\%$ ) were observed at 200 °C compared to 150 °C. However, when the test temperature increased from 200 to 250 °C, the AC adsorbents showed substantially higher weight gains ( $\Delta W\%$ ). In the case of HSZ-385 tested at 250 °C, a limited weight gain was observed and its pore volume slightly decreased compared to the virgin sample. Despite this minor impact on HSZ-385 compared to the ACs (1:20), GC-MS analysis of the effluent gases revealed the formation of new compounds heavier than TMB at 250 °C for HSZ-385. In the case of AC samples tested at 250 °C, the presence of a broad range of organic compounds in terms of molecular weight, chemical structure, and the

functional group was confirmed by GC-MS analysis. It was concluded that increasing temperature in the presence of a high level of oxygen enhances the oxygen-induced reactions in both zeolite and AC adsorbents, however, the confined pore opening of zeolite hinders the formation of molecules bigger than its pore size and limits heel formation. Therefore, in this context, molecular sieve adsorbents could be advantageous in the cyclic process of VOC adsorption when high oxygen impurity exists.

### **6.3 Recommendations**

This research investigated the combined effect of desorption purge gas oxygen impurity and temperature on heel formation of TMB on various adsorbent material with different properties. As a result, the following recommendations can be made for future research:

- This study showed that desorption efficiency is a multivariable function. Both purge gas O<sub>2</sub> impurity level and temperature should be considered when optimizing desorption conditions to enhance the desorption efficiency and to increase the adsorbent's life-span. Further, since producing high purity nitrogen is costly, the cost of nitrogen purification can be considered as another effective parameter for operation cost minimization.
- It was indicated that the formed heel is mostly removable using high-temperature regeneration. Future work should investigate physical or chemical regeneration methods to recover the spent adsorbents. Also, understanding the chemical reactions of oxygen and VOCs with different functionalities could be useful to predict the regeneration behavior.
- Using different thermal desorption techniques such as microwave heating may be another topic of interest to study the effect of oxygen on heel build-up. Microwave heating directly

heats the adsorbate inside the pores of the adsorbent which may result in different desorption behaviors from conventional heating. Also, different desorption heating rates may introduce time constraints for the diffusion of the adsorbate out of the pores and provide more time for the adsorbate to react with oxygen inside the pores. Therefore, the effect of heating rate on heel build-up can also be investigated to minimize the desorption efficiency and to increase the adsorbent life-span.

- The presence of oxidizing gas such as carbon dioxide or the presence of water at high temperatures might oxidize the carbon species formed during regeneration. Hence, investigation of the effect of regeneration gas and humidity on organic vapor decomposition during regeneration of activated carbon adsorbent is recommended.
- In this study, all the successive adsorption/desorption experiments were completed for 5 cycles and an excessive concentration of oxygen was used in some cases to amplify the results. However, in real industrial applications, oxygen impurities are lower and therefore, heel formation and adsorption capacity reduction may occur over more cycles and a long time. For this purpose, an automated adsorption/desorption setup could be built to test the effect of various parameters for more cycles and to evaluate the long-term changes in the physical and chemical properties of the adsorbent.

## BIBLIOGRAPHY

Air Pollutant Emission Inventory (APEI) Report,"

<http://www.ec.gc.ca/pollution/default.asp?lang=En&n=A17452DA-1&offset=8&toc=show>.

Aktaş Ö. and Çeçen F., "Effect of type of carbon activation on adsorption and its reversibility," *Journal of Chemical Technology & Biotechnology*, vol. 81, no. 1, pp. 94-101, 2006.

Amdebrhan B. T., "Evaluating the Performance of Activated Carbon, Polymeric, and Zeolite Adsorbents for Volatile Organic Compounds Control," University of Alberta, 2018.

ASTM D7675-2015: Standard Test Method for Determination of Total Hydrocarbons in Hydrogen by FID-Based Total Hydrocarbon (THC) Analyzer."

BAC Product Specifications [Online] Available: <http://www.kurehacarbonproducts.com/bac.html>

Bandosz T. J., "Gas Adsorption Equilibria: Experimental Methods and Adsorptive Isotherms," *Journal of the American Chemical Society*, vol. 127, no. 20, pp. 7655-7656, 2005.

Bansal R. C., Goyal M., *Activated Carbon Adsorption*: Published by CRC Press, 2005.

Barletta B., Meinardi S., Sherwood Rowland F., Chan C.-Y., Wang X., Zou S., Yin Chan L., and Blake D. R., "Volatile organic compounds in 43 Chinese cities," *Atmospheric Environment*, vol. 39, no. 32, pp. 5979-5990, 2005.

Berenjian A., Chan N., and Malmiri H. J., "Volatile Organic Compounds removal methods: a review," *American Journal of Biochemistry and Biotechnology*, vol. 8, no. 4, pp. 220-229, 2012.

Breck W. D., *Zeolite Molecular Sieves: Structure, Chemistry, and Use*: Wiley, 1974.

Brunauer S., Emmett P. H., and Teller E., "Adsorption of Gases in Multimolecular Layers," *Journal of the American Chemical Society*, vol. 60, no. 2, pp. 309-319, 1938.



## Bibliography

- Cecen F., and Aktas Ö., *Activated Carbon for Water and Wastewater Treatment: Integration of Adsorption and Biological Treatment*: Wiley, 2011.
- Chareonpanich M., Zhang Z.-G., and Tomita A., "Hydrocracking of Aromatic Hydrocarbons over USY-Zeolite," *Energy & Fuels*, vol. 10, no. 4, pp. 927-931, 1996.
- Chauhan R. S., Gopinath S., Razdan P., Delattre C., Nirmala G. S., and Natarajan R., "Thermal decomposition of expanded polystyrene in a pebble bed reactor to get higher liquid fraction yield at low temperatures," *Waste Management*, vol. 28, no. 11, pp. 2140-2145, 2008.
- Chen W., Wang X., Hashisho Z., Feizbakhshan M., Shariaty P., Niknaddaf S., and Zhou X., "Template-free and fast one-step synthesis from enzymatic hydrolysis lignin to hierarchical porous carbon for CO<sub>2</sub> capture," *Microporous and Mesoporous Materials*, vol. 280, pp. 57-65, 2019.
- Choosing an Adsorption System for VOC: Carbon, Zeolite, Or Polymers, The Clean Air Technology Center, EPA Technical Bulletin, 1999.
- Cruciani G., "Zeolites upon heating: Factors governing their thermal stability and structural changes," *Journal of Physics and Chemistry of Solids*, vol. 67, no. 9, pp. 1973-1994, 2006.
- Dąbrowski A., Podkościelny P., Hubicki Z., and Barczak M., "Adsorption of phenolic compounds by activated carbon—a critical review," *Chemosphere*, vol. 58, no. 8, pp. 1049-1070, 2005.
- De Jonge R. J., Breure A. M., and Van Andel J. G., "Reversibility of adsorption of aromatic compounds onto powdered activated carbon (PAC)," *Water Research*, vol. 30, no. 4, pp. 883-892, 1996.
- Do D. D., *Adsorption Analysis: Equilibria and Kinetics* (Series on Chemical Engineering, no. Volume 2). Published by Imperial College Press and distributed by World Scientific Publishing Co., p. 916, 1998.
- Dow Chemical Product Catalog [Online]. Available: <https://www.dow.com/en-us/product-catalog.html>

## Bibliography

- Effects of an ozone-generating air purifier on indoor secondary particles in three residential dwellings," *Indoor Air*, vol. 15, no. 6, pp. 432-444, 2005.
- EPA U., "Estimation Programs Interface Suite™ for Microsoft® Windows, v 4.11," United States Environmental Protection Agency, Washington, DC, USA, 2020.
- Feizbakhshan M., Hashisho Z., Phillips J. H., Anderson J. E., Nichols M., "Effect of Oxygen impurity and desorption temperature on heel buildup on activated carbon," presented at the 68th Canadian Chemical Engineering Conference, Toronto, 2018.
- Ferro-García M. A., Joly J. P., Rivera-Utrilla J., and Moreno-Castilla C., "Thermal desorption of chlorophenols from activated carbons with different porosity," *Langmuir*, Article vol. 11, no. 7, pp. 2648-2651, 1995.
- Flowe M. The Energy Costs Associated with Nitrogen Specifications [Online]. Available: <https://www.airbestpractices.com/system-assessments/air-treatmentn2/energy-costs-associated-nitrogen-specifications>
- Freitag W., and Stoye D., *Paints, Coatings, and Solvents*: Wiley, 2008.
- Ghafari M., and Atkinson J. D., "Impact of styrenic polymer one-step hyper-cross-linking on volatile organic compound adsorption and desorption performance," *Journal of Hazardous Materials*, vol. 351, pp. 117-123, 2018.
- Giese B., "C. H. Bamford, C. F. H. Tipper (Eds.): *Comprehensive Chemical Kinetics*, Vol. 16, *Liquid-Phase Oxidation*, Elsevier, Amsterdam 1980.
- Gilman J. B., Lerner B. M., Kuster W. C., and de Gouw J. A., "Source Signature of Volatile Organic Compounds from Oil and Natural Gas Operations in Northeastern Colorado," *Environmental Science & Technology*, vol. 47, no. 3, pp. 1297-1305, 2013.
- Godish T., Davis W. T., and Fu J. S., *Air Quality*. CRC Press, 2014.

## Bibliography

- Grant T. M. and King C. J., "Mechanism of Irreversible Adsorption of Phenolic Compounds by Activated Carbons," *Industrial and Engineering Chemistry Research*, Article vol. 29, no. 2, pp. 264-271, 1990.
- Hashemi S. M., "Effect of desorption purge gas oxygen impurity on heel formation during regeneration of beaded activated carbon saturated with organic vapors," Master's Thesis, Civil and Environmental Eng., University of Alberta, 2017.
- Hashemi S. M., Lashaki M. J., Hashisho Z., Phillips J. H., Anderson J. E., and Nichols M., "Oxygen impurity in nitrogen desorption purge gas can increase heel buildup on activated carbon," *Separation and Purification Technology*, vol. 210, pp. 497-503, 2019.
- Hashisho Z., Rood M. J., Barot S., and Bernhard J., "Role of functional groups on the microwave attenuation and electric resistivity of activated carbon fiber cloth," *Carbon*, vol. 47, no. 7, pp. 1814-1823, 2009.
- Hemphill L., and Robert S. Kerr Environmental Research Laboratory A., Okla, Thermal Regeneration of Activated Carbon: National Technical Information Service, 1978.
- High-performance adsorbents based on activated carbon having high meso- and macroporosity, United States US 2018/0125886, Blücher GmbH, 2018.
- Hofelich T. C., Labarge M. S., and Drott D. A., "Prevention of thermal runaways in carbon beds," *Journal of Loss Prevention in the Process Industries*, vol. 12, no. 6, pp. 517-523, 1999.
- Huang B., Lei C., Wei C., and Zeng G., "Chlorinated volatile organic compounds (Cl-VOCs) in environment — sources, potential human health impacts, and current remediation technologies," *Environment International*, vol. 71, pp. 118-138, 2014.
- Indoor air quality: organic pollutants: report on a WHO meeting, Berlin, West, 23-27 August 1987, Copenhagen: World Health Organization, Regional Office for Europe, 1989.
- ISO 9277:2010, Determination of the specific surface area of solids by gas adsorption - BET method, 2010.

## Bibliography

- Kampa M., and Castanas E., "Human health effects of air pollution," *Environmental Pollution*, vol. 151, no. 2, pp. 362-367, 2008.
- Khan F. I. and Kr. Ghoshal A., "Removal of Volatile Organic Compounds from polluted air," *Journal of Loss Prevention in the Process Industries*, vol. 13, no. 6, pp. 527-545, 2000.
- Kim B. R., "VOC Emissions from Automotive Painting and Their Control: A Review," *Environmental Engineering Research*, vol. 16, no. 1, pp. 1-9, 2011.
- Kim K. J., Kang C. S., You Y. J., Chung M. C., Woo M. W., Jeong W. J., Park N. C., and Ahn H. G., "Adsorption-desorption characteristics of VOCs over impregnated activated carbons," *Catalysis Today*, vol. 111, no. 3, pp. 223-228, 2006.
- Kolta T., "Selecting Equipment to Control Air Pollution from Automotive Painting Operations," 1992. Available: <http://dx.doi.org/10.4271/920189>.
- Kolta T., "Selecting Equipment to Control Air Pollution from Automotive Painting Operations," 1992.
- Lashaki M. J., Atkinson J. D., Hashisho Z., Phillips J. H., Anderson J. E., and Nichols M., "The role of beaded activated carbon's pore size distribution on heel formation during cyclic adsorption/desorption of organic vapors," *Journal of Hazardous Materials*, vol. 315, pp. 42-51, 2016.
- Lashaki M. J., Atkinson J. D., Hashisho Z., Phillips J. H., Anderson J. E., Nichols M., and Misovski T., "Effect of desorption purge gas oxygen impurity on irreversible adsorption of organic vapors," *Carbon*, vol. 99, pp. 310-317, 2016.
- Lashaki M. J., Fayaz M., Wang H., Hashisho Z., Philips J. H., Anderson J. E., and Nichols M., "Effect of Adsorption and Regeneration Temperature on Irreversible Adsorption of Organic Vapors on Beaded Activated Carbon," *Environmental Science & Technology*, vol. 46, no. 7, pp. 4083-4090, 2012.

## Bibliography

- Lashaki M. J., Understanding and improving gas phase capture of organic vapors by carbonaceous adsorbents, Ph.D. Thesis, University of Alberta, 2016.
- Leffler J. E. and Grunwald E., Rates and Equilibria of Organic Reactions: As Treated by Statistical, Thermodynamic and Extrathermodynamic Methods. Dover Publications, 2013.
- Leng C. C. and Pinto N. G., "Effects of surface properties of activated carbons on adsorption behavior of selected aromatics," Carbon, vol. 35, no. 9, pp. 1375-1385, 1997.
- Levan M. D., "Thermal Swing Adsorption: Regeneration, Cyclic Behavior, and Optimization," in Adsorption: Science and Technology, A. E. Rodrigues, M. D. LeVan, and D. Tondeur, Eds. Dordrecht: Springer Netherlands, pp. 339-355, 1989.
- Liu P. K. T., Felch S. M., and Wagner N. J., "Thermal desorption behavior of aliphatic and aromatic hydrocarbons loaded on activated carbon," Industrial & Engineering Chemistry Research, vol. 26, no. 8, pp. 1540-1545, 1987.
- Ludlow D. K., "Activated Carbon Adsorption By Roop Chand Bansal and Meenakshi," Journal of the American Chemical Society, vol. 128, no. 32, pp. 10630-10630, 2006.
- Luengas A., Barona A., Hort C., Gallastegui G., Platel V., and Elias A., "A review of indoor air treatment technologies," Reviews in Environmental Science and Bio/Technology, vol. 14, no. 3, pp. 499-522, 2015.
- Lukomskaya A. Y., Tarkovskaya I. A., and Strelko V. V., "Chemisorption of o-xylene on activated carbons," Theoretical and Experimental Chemistry, journal article vol. 22, no. 3, pp. 357-360, 1986.
- Musso H., "Phenol Oxidation Reactions," Angewandte Chemie International Edition, vol. 29, no. 12, pp. 723-735, 1963.
- Neimark A. V., Lin Y., Ravikovitch P. I., and Thommes M., "Quenched solid density functional theory and pore size analysis of micro-mesoporous carbons," Carbon, vol. 47, no. 7, pp. 1617-1628, 2009.

## Bibliography

- Niessner N., and Wagner D., "Practical guide to structures, properties and applications of styrenic polymers," 2013.
- Niknaddaf S., Atkinson J. D., Shariaty P., Lashaki M. J., Hashisho Z., Philips J. H., Anderson J. E., and Nichols M. "Heel formation during volatile organic compound desorption from activated carbon fiber cloth," *Carbon*, vol. 96, pp. 131-138, 2016.
- OSHA. "Volatile Organic Compounds in Air,"  
<https://www.osha.gov/dts/sltc/methods/partial/pv2120/pv2120.html>.
- Papasavva S., Kia S., Claya J., and Gunther R., "Characterization of automotive paints: an environmental impact analysis," *Progress in Organic Coatings*, vol. 43, no. 1, pp. 193-206, 2001.
- Pfäffli P., Zitting A., and Vainio H., "Thermal degradation products of homopolymer polystyrene in air," *Scandinavian Journal of Work, Environment & Health*, no. 2, pp. 22-27, 1978.
- Popescu M., Joly J. P., Carré J., and Danatoiu C., "Dynamical adsorption and temperature-programmed desorption of VOCs (toluene, butyl acetate and butanol) on activated carbons," *Carbon*, vol. 41, no. 4, pp. 739-748, 2003.
- Qiuli Lu, George A. Sorial, The role of adsorbent pore size distribution in multicomponent adsorption on activated carbon, *Carbon* 42 3133–3142 2004
- Rabek J. F., "Chapter 4 Oxidative Degradation of Polymers," *Comprehensive Chemical Kinetics*, C. H. Bamford and C. F. H. Tipper, eds., pp. 425-538: Elsevier, 1975.
- Rafson H. J., *Odor and VOC control handbook*, Published by McGraw-Hill, New York, 1998.
- Roelant G. J., Kemppainen A. J., and Shonnard D. R., "Assessment of the Automobile Assembly Paint Process for Energy, Environmental, and Economic Improvement," *Journal of Industrial Ecology*, vol. 8, no. 1-2, pp. 173-191, 2004.

## Bibliography

- Rouquerol J., Avnir D., Fairbridge C. W., Everett D. H., Haynes J. M., Pernicone N., Ramsay J. D. F., Sing K. S. W., and Unger K. K., "Recommendations for the characterization of porous solids (Technical Report)," *Pure and Applied Chemistry*, vol. 66, no. 8, pp. 1739-1758, 1994.
- Ruhl M. J., "Recover VOCs via adsorption on activated carbon," *Chemical Engineering Progress*, 89(7), 1993.
- Ruthven D. M., Farooq S., and Knaebel K. S., *Pressure Swing Adsorption*: Wiley, 1993.
- Ruthven D. M., *Principles of Adsorption and Adsorption Processes*: Wiley, 1984.
- Rydberg J., *Solvent Extraction Principles and Practice, Revised and Expanded*: Taylor & Francis, 2004.
- Sabio E., González-Martín M. L., Ramiro A., González J. F., Bruque J. M., Labajos-Broncano L., and Encinar J. M., "Influence of the Regeneration Temperature on the Phenols Adsorption on Activated Carbon," *Journal of Colloid and Interface Science*, vol. 242, no. 1, pp. 31-35, 2001.
- Schnelle K. B., Dunn R. F., and Ternes M. E., *Air Pollution Control Technology Handbook*: CRC Press, 2015.
- Schönherr J., Buchheim R. J., Scholz P., and Adelhelm P., "Boehm Titration Revisited (Part I): Practical Aspects for Achieving a High Precision in Quantifying Oxygen-Containing Surface Groups on Carbon Materials," *Carbon*, vol. 4, no. 2, 2018.
- Shiraishi F., and Ishimatsu T., "Toluene removal from indoor air using a miniaturized photocatalytic air purifier including a preceding adsorption/desorption unit," *Chemical Engineering Science*, vol. 64, no. 10, pp. 2466-2472, 2009.
- Singh S. P., DePaoli D. W., Begovich J. M., Ashworth R. A., and Heyse E. C., "Review of methods for removing VOCs (volatile organic compounds) from the environment," 1987.

## Bibliography

- Sircar S., "Pressure swing adsorption," *Industrial & Engineering Chemistry Research*, Editorial Material vol. 41, no. 6, pp. 1389-1392, 2002.
- Stahlbush J. R., and Strom R. M., "A decomposition mechanism for cation exchange resins," *Reactive Polymers*, vol. 13, no. 3, pp. 233-240, 1990.
- Standardization I. O. f., "ISO 9277:2010, Determination of the specific surface area of solids by gas adsorption - BET method," 2010.
- Suidan M., "Role of dissolved oxygen on the adsorptive capacity of activated carbon for synthetic and natural organic matter," 1991.
- Suzuki M., *Adsorption Engineering*, Tokyo. Chemical Engineering Monographs, Elsevier Science Publishers, Amsterdam and New York, 1989.
- Suzuki M., Mistic D. M., Koyama O., and Kawazoe K., "Study of thermal regeneration of spent activated carbons: Thermogravimetric measurement of various single component organics loaded on activated carbons," *Chemical Engineering Science*, vol. 33, no. 3, pp. 271-279, 1978.
- Thomas W. J. and Crittenden B., "7 - Selected adsorption processes," in *Adsorption Technology & Design*, W. J. Thomas and B. Crittenden, Eds. Oxford: Butterworth-Heinemann, pp. 187-239, 1998.
- Thomas W. J., and Crittenden B., "5 - Processes and cycles," in *Adsorption Technology & Design*, W. J. Thomas and B. Crittenden, eds., Oxford: Butterworth-Heinemann, pp. 96-134, 1998.
- TOSOH Zeolite [Online]. Available: <https://www.tosoh.com/our-products/advanced-materials/zeolites-for-catalysts>.
- Tsuji M., Koriyama C., Ishihara Y., Vogel C. F. A., and Kawamoto T., "Association between bisphenol A diglycidyl ether-specific IgG in serum and food sensitization in young children," *European Journal of Medical Research*, vol. 23, no. 1, pp. 61, 2018.



## Bibliography

- U.S. EPA. "Volatile Organic Compound Rules," <https://www.epa.gov/sips-in/article-8-volatile-organic-compound-rules>.
- United States Patent US 2018/0125886, "High-performance adsorbents based on activated carbon having high meso- and macroporosity", 2018.
- Urano K., Yamamoto E., and Takeda H., "Regeneration Rates of Granular Activated Carbons Containing Adsorbed Organic Matter," *Industrial and Engineering Chemistry Process Design and Development*, vol. 21, no. 1, pp. 180-185, 1982.
- Vega E., Mugica V., Carmona R. O., and Valencia E., "Hydrocarbon source apportionment in Mexico City using the chemical mass balance receptor model," *Atmospheric Environment*, vol. 34, no. 24, pp. 4121-4129, 2000.
- Vidic R. D., and Suidan M. T., "Role of dissolved oxygen on the adsorptive capacity of activated carbon for synthetic and natural organic matter," *Environmental Science & Technology*, vol. 25, no. 9, pp. 1612-1618, 1991.
- Vidic R. D., Suidan M. T., and Brenner R. C., "Impact of oxygen mediated oxidative coupling on adsorption kinetics," *Water Research*, vol. 28, no. 2, pp. 263-268, 1994.
- Vidic R. D., Suidan M. T., Sorial G. A., and Brenner R. C., "Effect of molecular oxygen on adsorptive capacity and extraction efficiency of granulated activated carbon for three ortho-substituted phenols," *Journal of Hazardous Materials*, vol. 38, no. 3, pp. 373-388, 1994.
- Vidic R. D., Suidan M. T., Traegner U. K., and Nakhla G. F., "Adsorption isotherms: illusive capacity and role of oxygen," *Water Research*, vol. 24, no. 10, pp. 1187-1195, 1990.
- Vidic R. D., Tessmer C. H., and Uranowski L. J., "Impact of surface properties of activated carbons on oxidative coupling of phenolic compounds," *Carbon*, vol. 35, no. 9, pp. 1349-1359, 1997.
- Volatile organic compound emissions by source, <https://www.canada.ca/en/environment-climate-change/services/environmental-indicators/air-pollutant-emissions.html#VOCs>.

## Bibliography

- Wang L. K., Pereira N. C., and Hung Y.-T., Handbook of environmental engineering, Totowa, N.J.: Humana Press, 2004.
- Wypych G., "21 - Solvent Recycling, Removal, and Degradation" in Handbook of Solvents (Third Edition), Chemical Technology Publishing, vol. 2, pp. 1635-1727, 2019.
- Yaws C. L., "Chapter 2 - Physical Properties – Inorganic Compounds," The Yaws Handbook of Physical Properties for Hydrocarbons and Chemicals (Second Edition), C. L. Yaws, ed., pp. 684-810, Boston: Gulf Professional Publishing, 2015.
- Yokosuka Y., Oki K., Nishikiori H., Tatsumi Y., Tanaka N., and Fujii T., "Photocatalytic degradation of trichloroethylene using N-doped TiO<sub>2</sub> prepared by a simple sol-gel process," Research on Chemical Intermediates, vol. 35, no. 1, pp. 43-53, 2009.
- Yonge D. R., Keinath T. M., Poznanska K., and Jiang Z. P., "Single-solute irreversible adsorption on granular activated carbon," Environmental Science & Technology, vol. 19, no. 8, pp. 690-694, 1985.
- Yuan B., Shao M., Lu S., and Wang B., "Source profiles of volatile organic compounds associated with solvent use in Beijing, China," Atmospheric Environment, vol. 44, no. 15, pp. 1919-1926, 2010.
- Yun J. H., Choi D. K., and Moon H., "Benzene adsorption and hot purge regeneration in activated carbon beds," Chemical Engineering Science, vol. 55, no. 23, pp. 5857-5872, 2000.
- Zeid N. A., Nakhla G., Farooq S., and Osei-Twum E., "Activated carbon adsorption in oxidizing environments," Water Research, vol. 29, no. 2, pp. 653-660, 1995.
- Zhang X., Gao B., Creamer A., Cao C., and Li Y., "Adsorption of VOCs onto engineered carbon materials: A review," Journal of Hazardous Materials, vol. 338, 2017.
- Zogorski J. S., Algeier G. D., and Mullins R. L., Removal of Chloroform from Drinking Water, Final report to Kentucky Water Resources Research Institute, 1978.

## **APPENDIX A: SUPPLEMENTARY INFORMATION**

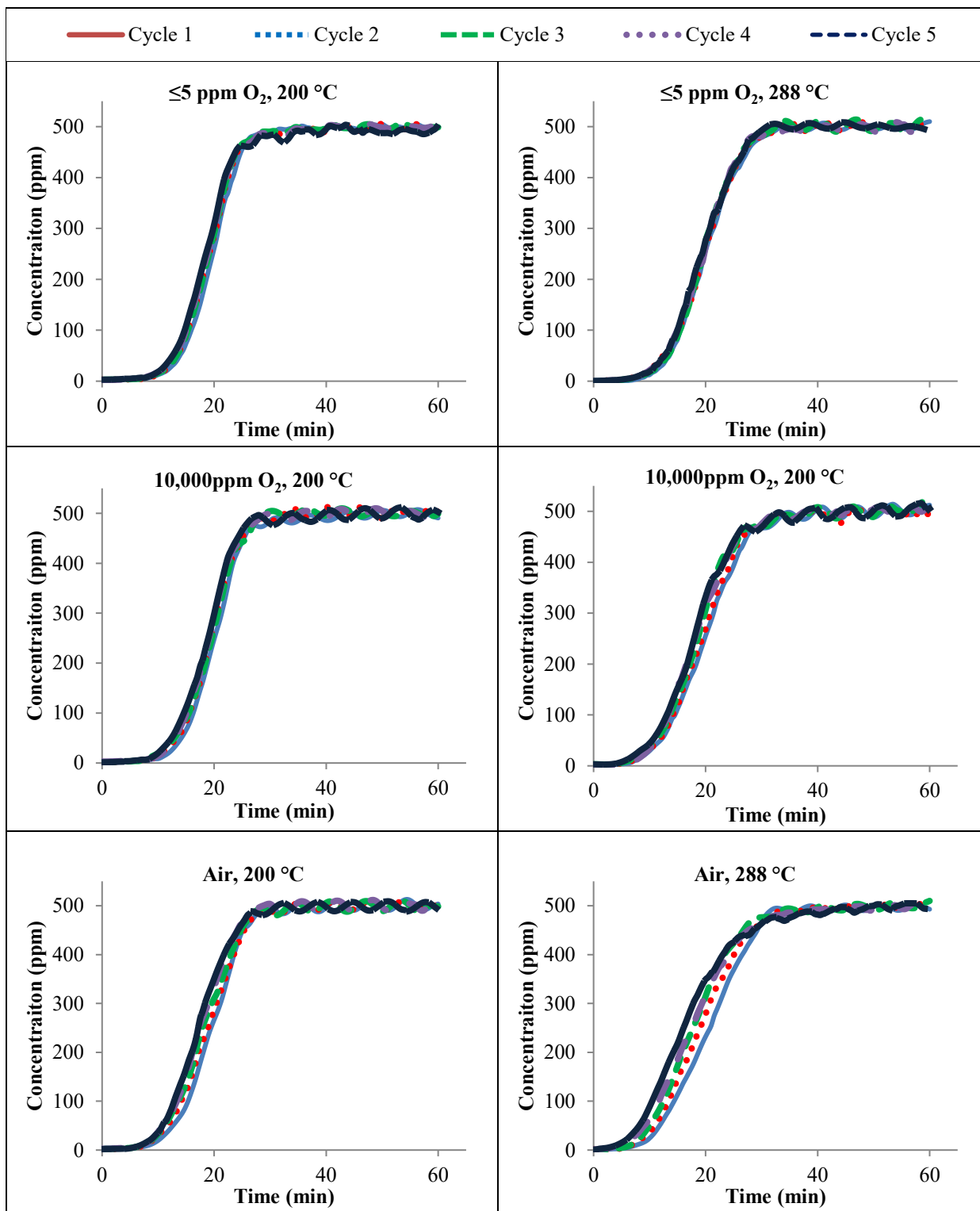


Figure A-1. Adsorption breakthrough curves for TMB on G-70R samples desorbed at 200/288°C with different oxygen impurities

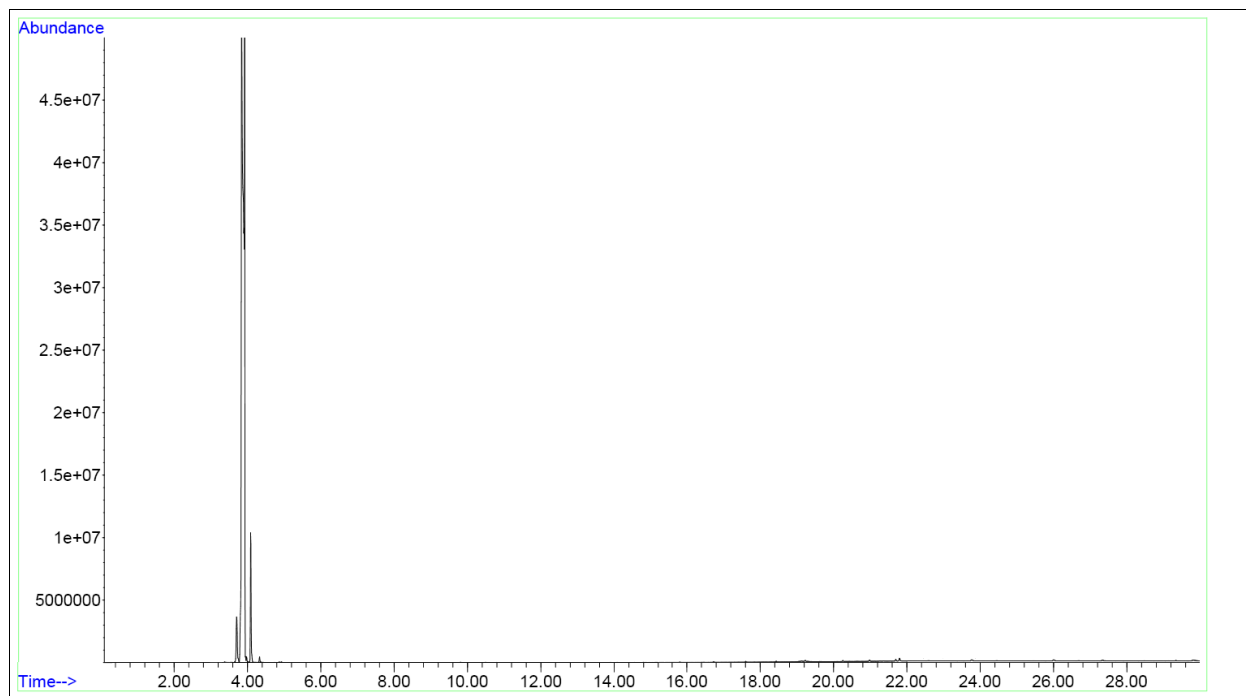


Figure A-2. Chromatogram of 98% purity TMB (Y-axis is truncated to zoom the spectra)